FACIES AND MORPHOLOGY OF PLEISTOCENE TRAVERTINE MOUNDS AT LYMAN LAKE, ARIZONA

_____

A Thesis

Presented to the Faculty of the

Department of Earth and Atmospheric Sciences

University of Houston

_____

In Partial Fulfillment

of the Requirements for the Degree

Master of Science

_____

By

Christopher Wayne Trantham

December, 2015

FACIES AND MORPHOLOGY OF PLEISTOCENE TRAVERTINE MOUNDS AT LYMAN LAKE, ARIZONA

Christopher Wayne Trantham

APPROVED:

Dr. Henry Chafetz, Chairman

Dr. Ian Evans

Dr. Jie Zhou

Dean, College of Natural Siences and Mathematics

ACKNOWLEDGMENTS

My sincere thanks to Dr. Henry Chafetz, Ph.D., for his guidance and support throughout the course my time at University of Houston. My appreciation goes to Dr. Ian Evans, Ph.D., and Dr. Jie Zhou, Ph.D., for reviewing my thesis and helping me in my journey. I would also like to thank my family for their patience and assistance.

FACIES AND MORPHOLOGY OF PLEISTOCENE TRAVERTINE MOUNDS AT LYMAN LAKE, ARIZONA

_____

An Abstract of a Thesis

Presented to

the Faculty of the

Department of Earth and Atmospheric Sciences

University of Houston

_____

In Partial Fulfillment

of the Requirements for the Degree

Master of Science

_____

By

Christopher Wayne Trantham

December, 2015

ABSTRACT

Travertine mounds in eastern Arizona formed around central vents and range from <10 m to 50 m in diameter and between 0.5-60 m thick. The travertine mounds are primarily composed of laterally extensive sheets of rhythmically alternating bacterial shrubs and intraclastic layers dipping 1-3° radially away from their vent. Individual laminations of bacterial shrubs may be 0.2-2.5 cm thick, and compose layers 3-50 cm thick extending laterally for 10-70 m. Intramicrite layers 5-40 cm thick and 30-70 m long contain well-rounded to angular allochems 0.02-70 mm long. Oncoids 1-15 mm in diameter occur in lenses 3-8 cm thick and 0.5-10 m long. Carbonate rafts suspended in micrite filled pool deposits are 4-9 cm long, whereas small rafts 0.5-4 cm long occur within bacterial shrub layers. Grass molds are 1-4 mm in diameter and 1-3 cm long, whereas reeds are 0.5-2 cm in diameter and 4-15 cm long. Individual mounds contain various scales of morphological components such as vents, distal edge high angle smooth slopes, and stacked smooth slope dams. High angle slopes are concave downward structures 2-6 m long and 0.5-1.5 m thick, composed of 0.5-5 cm laminae of ray-crystal crusts that abruptly dip 30-45°. Stacked ray-crystal slopes are column 1.5-2 m tall composed of stacked layers of individual crystalline crusts 12-20 cm wide and 3-6 cm thick. These structures represent the distal edge of mounds where water flowed into the surrounding area. Vents are composed of dense ray-crystals layers that change dip dramatically as the layers transition from the vertical walls to the surrounding vent rim. Facies analysis of Mound-A indicates that the mound was deposited over six stages of deposition and composed of seven morphological features.

Table Of Contents

CHAPTER 1: INTRODUCTION TO THE PROJECT AND FIELD AREA

1.1 Introduction

The objective of this study is to accurately describe the constituents and facies distribution of travertine mounds located in Lyman Lake, Arizona. One of the earliest descriptions of travertine defined it as a "deposit from the water of springs or streams holding calcium bicarbonate in solution" (Emig, 1917, p.10). The principal reaction that forms travertine is loss of carbon dioxide gas from a calcium bicarbonate solution leading to calcium carbonate deposition. Travertine is the result of disequilibrium in carbon dioxide between saturated water and the ambient atmosphere (Florsheim et al., 2013). Thus, in order to reach equilibrium, the water expels dissolved carbon dioxide by degassing into the atmosphere, consequently causing supersaturation of the water with respect to calcium bicarbonate and inducing carbonate precipitation (Chafetz et al., 1991). Travertine springs may host many forms of biota, ranging from vascular plants to a wide diversity of micro-organisms, which also play a part in the precipitation of carbonate by the photosynthetic removal of carbon dioxide (Fouke et al., 2003).

Historically, travertine has been used as a building material, the use of which originates with the Roman Empire. The namesake of travertine is derived from the Italian town of Tivoli, originally *Tivertino* in Latin, which supplied the majority of travertine used by the Roman Empire (Chafetz and Folk, 1984). However, there has been a major re-evaluation of travertine's economic potential as a result of the discovery of large hydrocarbon deposits within travertine located in the Itaboraí Basin of offshore Brazil

(Sant' Anna et al., 2004). Hence, whereas travertine has played an important role in the history of mankind, there has been little attention given to its attributes as a reservoir rock, regarding the spatial distribution and morphology of travertine deposits.

In order to efficiently develop travertine hydrocarbon reservoirs, a model must be developed using accessible outcrop analogues. It is the purpose of this study to provide a focused analysis of the spatial distribution, morphology, and characteristics of travertine mound accumulations. In addition, this study characterizes in detail the architectural components, depositional fabrics, constituents, and draws interpretations of environmental conditions at the time of formation. It is hoped that, the results of this study may assist in the creation of a predictive travertine model, leading to a better understanding of hydrocarbon-bearing travertine deposits.

1.2 Study Area Location and Description

1.2.1 Location of Study Area

An extensive ancient travertine deposit called the Springerville Travertine Complex is located in eastern Arizona, between the towns of Springerville and St. Johns in southeastern Apache County (Sirrine, 1958). This study focuses on the main concentration of travertine north of Lyman Lake Dam and Reservoir (Figure 1). Lyman Lake is an artificial lake that empties into the northerly flowing Little Colorado River which cuts through the travertine deposits adjacent to the lake. There is active travertine deposition at Salado Springs, located adjacent to the Little Colorado River.

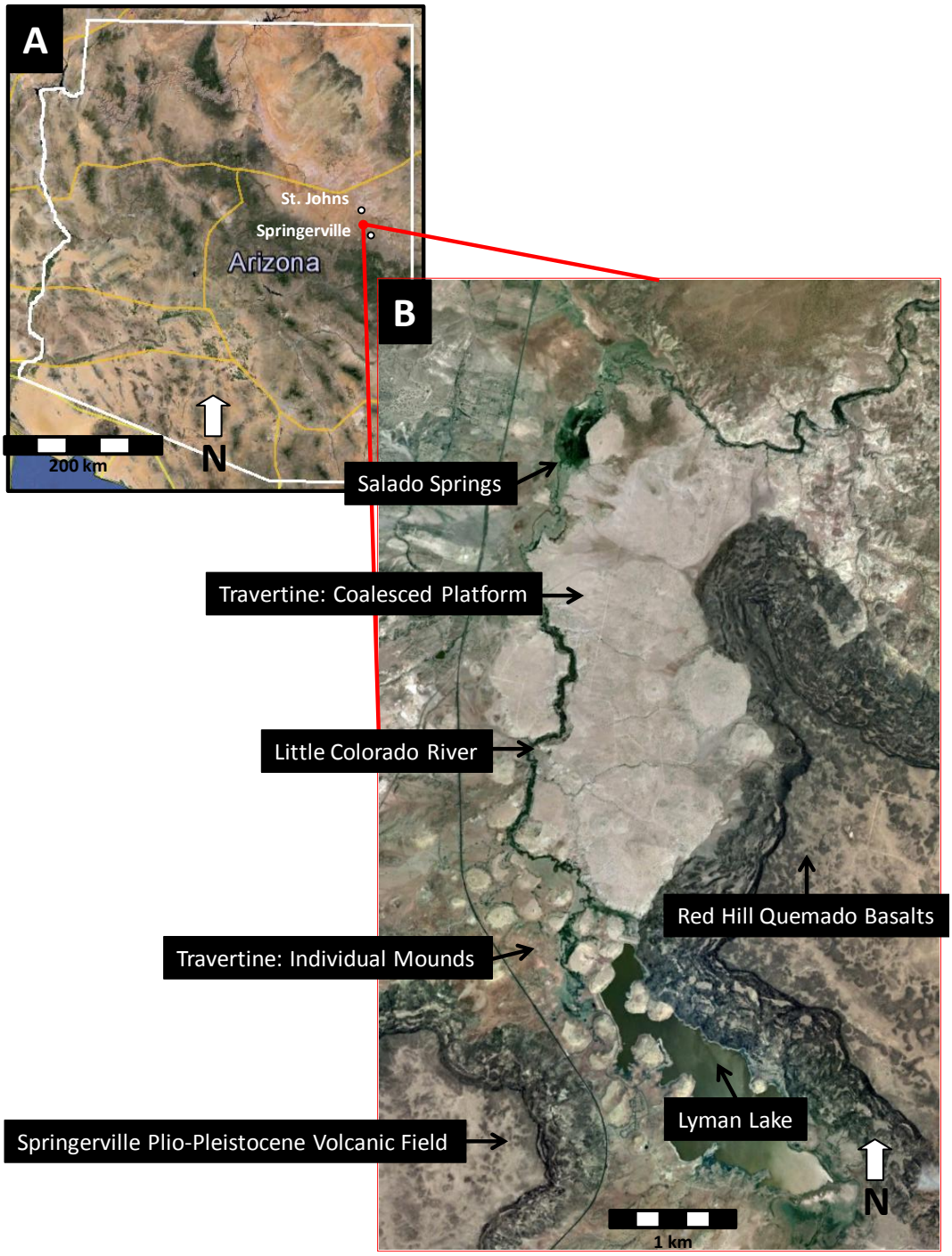

Figure 1: Satellite view showing location of field site. (A) State of Arizona. White dots are the towns of Springerville and St. Johns. Red dot is the study area at Lyman Lake State Park. (B) Close satellite view of travertine complex adjacent to Lyman Lake State Park (modified from Google Maps, 2010).

The Springerville-St. Johns Travertine Complex is one of the largest accumulations in the western United States, consisting of more than 70 travertine mounds covering over 33 km^2 (Sirrine, 1958). Most studies on the morphology of Lyman Lake travertine have been cursory, primarily focusing on CO_2 sequestration within the Springerville-St. Johns CO_2 reservoir (Rauzi, 1999; Moore et al., 2003, 2005; Gilfillan et al., 2008). Additionally, Embid (2009) utilized U/Th dating of travertine for a paleo-geomorphology study in regards to incision of the Little Colorado river. Therefore, this will be the first detailed study focusing on the internal morphology and facies of the travertine mounds at Lyman Lake, Arizona.

1.3 Regional Geologic Setting and History

1.3.1 Regional Geologic Setting

The Springerville Travertine Complex is situated at the intersection of two adjoining regional provinces, located on the southeastern edge of the Colorado Plateau and the southwestern end of the Jimez Linement (Figure 2) (Condit et al., 1989). The Jimez Lineament is an 800 km long, 50 km wide, northeast trending zone of volcanic basalts and faults that has been active over the past 4.5 Ma (Aldrich and Laughlin, 1984). The southwestern edge of the Colorado Plateau province is bounded by a 320 km long escarpment called the Mogollon Rim (Sirrine, 1958). The Springerville-St. Johns area is located on the southeastern margin of Holbrook Basin, the southwestern-most of a series

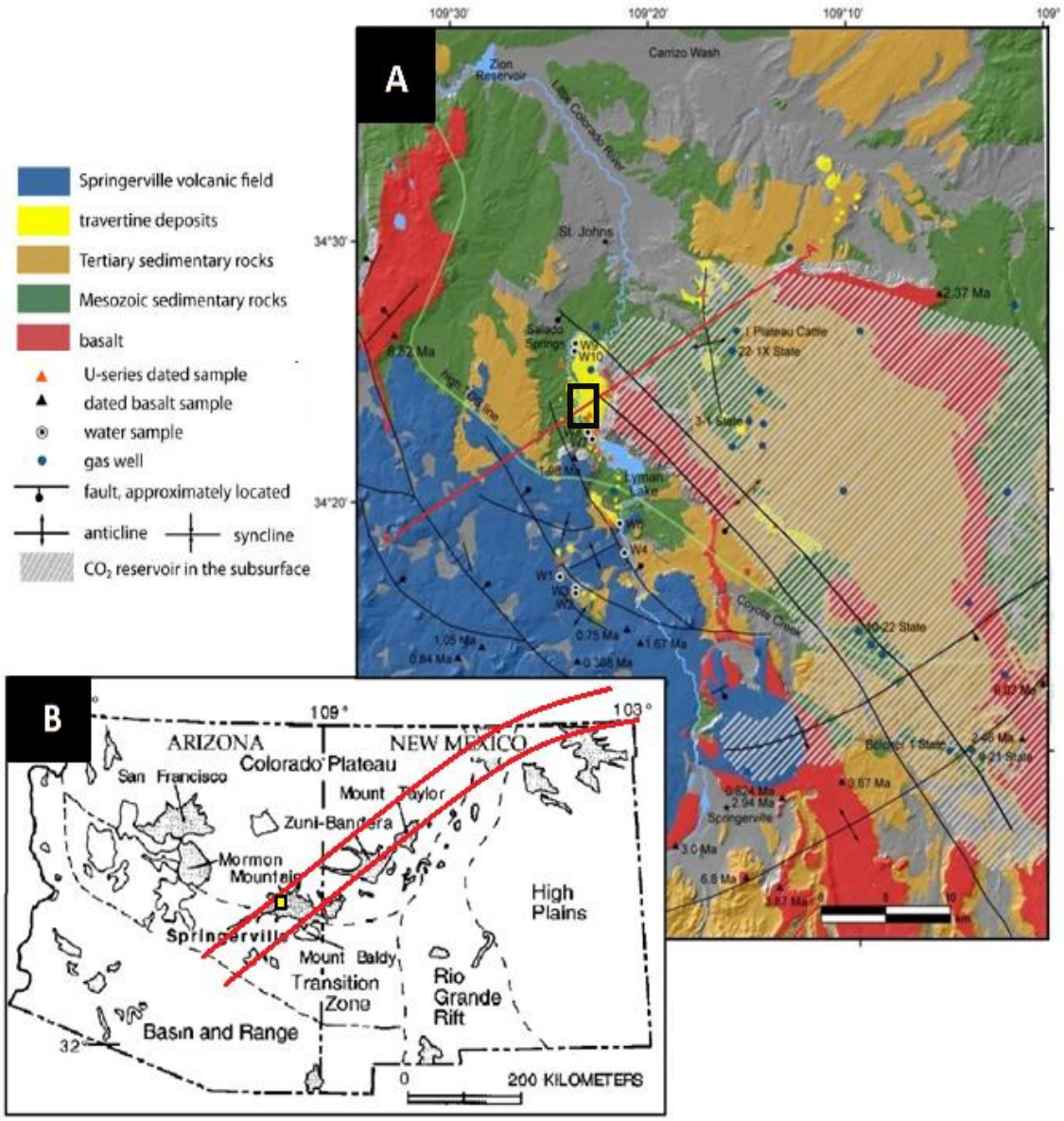

Figure 2: (A) Generalized local geologic setting of the Springerville area. The red line A-A' represents the cross section in Figure 4. Black box indicates location of study area (modified from Embid, 2009). (B) Inset is a regional geologic setting indicating physiographic provinces and volcanic fields. The Jemez Lineament is indicated by red lines. Yellow box outlined in black indicates location of study area (modified from Condit, 1996).

of seven large basins along the southwestern edge of the Colorado Plateau (Sirrine, 1958). Holbrook Basin is regionally bounded on the east by the Zuni Basin, and to the south by the Mogollon Rim (Sirrine, 1958). The Springerville Travertine Complex is located at the northeastern end of the Springerville-St. Johns Dome, one of the largest CO_2 reservoirs in the southwestern United States (Allis et al., 2001). Lyman Lake is located between two Cenozoic volcanic fields, to the east is the Springerville Plio-Pleistocene volcanic deposit, whereas to the west lies the Mio-Pleistocene Red Hill Quemado, both composed of relic volcanoes and basalt flows (Figure 3) (Sirrine, 1958).

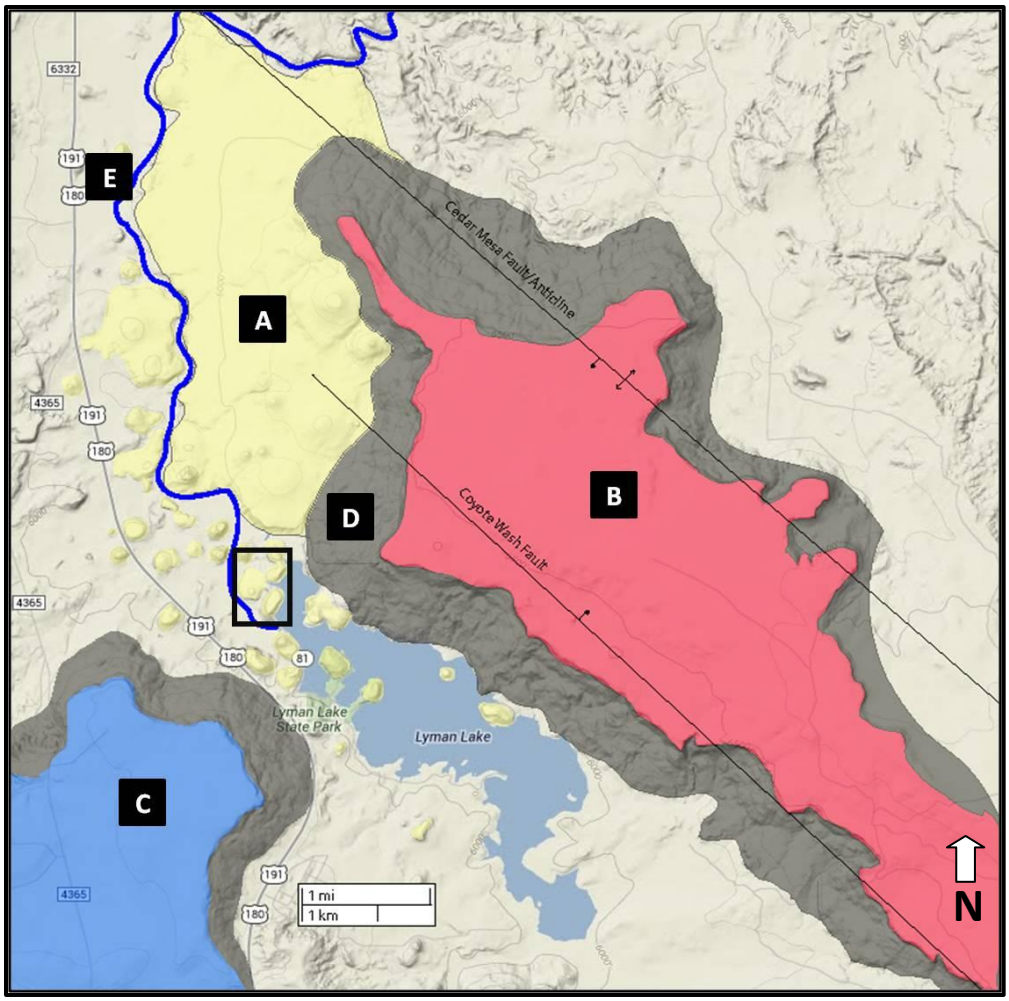

Figure 3: Geologic map of the area surrounding Lyman Lake. Yellow (A) – Travertine mounds and platform; Red (B) – Red Hill Quemado Formation; Blue (C) – Springerville-Plio-Pleistocene Volcanic Field; Brown (D) – Debris cover eroded from volcanic basalts; Dark Blue (E) – Little Colorado River; Black Box – Location of Figure 4 satellite photo (modified from Google Maps, 2010).

1.3.2 Regional Geologic History

A granite Precambrian bedrock is overlain by Paleozoic, Mesozoic, and Tertiary strata, however little is known of the Precambrian history within the region. During the Cambrian, seas encroached upon the Defiance Uplift, located in the northeastern corner of Arizona, and deposited sediment during the late Cambrian and early Ordovician that was later eroded during the Silurian and Devonian (Kelley, 1955). Down warping in northern and central New Mexico during the Pennsylvanian and Permian caused an encroachment of the sea from the east; however Pennsylvanian sediments did not extend into the Springerville-St. Johns area. Three northwest-trending uplifts developed during the Pennsylvanian and were mantled with continental sediments during the Early Permian with basins of deposition adjoining them on the southwest (Kelley, 1955). The sea began to encroach the study area in the Permian Period during the early Guadalupe times, depositing calcareous shale (Supai Formation), sandstone (Glorieta Sandstone), and finally limestone (San Andres Limestone) (Kelley, 1955). However, this region was slightly uplifted and erosion took place, forming a hiatus that cuts into the Late Permian marine limestone (McKee, 1954).

By the early Triassic, the Colorado Plateau was a westward sloping feature that extended into an epicontinental sea on the west. The sea transgressed and regressed depositing lagoonal claystone, mudstone, and limestone (Moenkopi Formation). This was limited to the northern half of Arizona by the post-Permian uplift of the Navajo Highlands in the south. The Colorado Plateau began to tilt towards the west and northwest during the Jurassic, with the Springerville-St. Johns area located at the

southern edge of the Jurassic basin of deposition and the surrounding area was dominated by playa lakes and aeolian sandstones. There was little deposition in northern Arizona during the Early Cretaceous due to regional uplift of the Mogollon Rim. Additionally, there was uplift to the east in New Mexico, causing little deposition in northern Arizona as Jurassic rocks in the Holbrook Basin were stripped by erosion. The Cretaceous is characterized by a series of transgressions and regressions depositing sandstones and shales. However, the epicontinental sea was forced to retreat in the late Cretaceous when the rate of accumulation exceeded basin subsidence. The Laramide Orogeny caused uplift of Paleozoic and Mesozoic sections during the Late Cretaceous and caused extreme erosion and an angular unconformity between the Cretaceous and Tertiary (Embid, 2009). Compression during the Laramide Orogeny caused regional reverse faulting, along with monoclinal folding of Paleozoic and Mesozoic strata, resulting in the formation of the Springerville-St. Johns Dome (Embid, 2009). Late Laramide uplift of the Mongollon Rim created the Baca Basin with its axis running east-west through the Springerville area, in which thick deposits of coarse conglomerates and aeolian sandstones were deposited during the Tertiary (Potochnik, 1989).

Regional magmatism first began during the Tertiary approximately 40-24 mya, yet the majority of volcanic activity occurred from the Miocene to Quaternary (Cather et al., 1994). Basin and Range extension began at 24.8 mya during the Oligocene, causing old reverse faults from the Laramide Orogeny to reactivate as normal faults (Faulds et al., 2001). Intense erosion occurred during the late Oligocene to early Miocene, creating an angular unconformity due to major uplift in the area which caused valleys to fill with

sediment from the erosion (Sirrine, 1958). A series of recent volcanic episodes began during the mid-Miocene and continued from 9-6 mya with the deposition of the White Mountain-Baldy Complex (Aldrich and Laughlin, 1984). Following the mid-Miocene volcanism another period of incision occurred, smaller in scale than the erosion during the Late Oligocene to Early Miocene. This period of incision was interrupted by the deposition of the Chinle Formation (Sirrine, 1958). During the deposition of the Chinle Formation there was also coeval volcanism that occurred around 4 mya, resulting in the deposition of the Red Hill Quemado Formation (Cather and McIntosh, 1994). The Pleistocene Red Hill Quemado was deposited in two distinct episodes of volcanism, occurring from 7.9-5.2 mya and 2.5-0.07 mya, thus overlapping both the White Mountain and Springerville Plio-Pleistocene (Cather et al., 1994). The most recent episode of volcanism occurred from 2.1-0.3 mya with the deposition of the Springerville Plio-Pleistocene Volcanics, with a volcanic eruption recurrence rate of approximately every 3000 years (Crumpler et al., 1994). Volcanism during the Pliocene and Pleistocene migrated laterally, with the youngest activity occurring in the north.

The travertine deposits surrounding Lyman Lake are Quaternary deposits, U/Th dating of the Springerville travertines constrained major accumulation periods to 350-300 kya, 280-200 kya, and 100-36 kya, with a calculated average depositional rate of 0.93 m/ky at the northern edge of the coalesced platform (Embid, 2009). In addition, U/Th dating suggests that travertine deposition experienced episodic pulses lasting approximately 70 ky, which coincides with wetter and cooler climatic shifts, along with hiatuses lasting approximately 25-60 ky, correlating with warm interglacial periods

(Embid, 2009). Therefore, rather than prolonged and sustained spring deposition, the discontinuity in the U/Th ages of travertine indicates periodic cycles of deposition, depending on climatic conditions.

1.3.3 Springerville-St. Johns CO_2 Gas Reservoir

The Springerville-St. Johns Travertine Complex is located at the northeastern end of the Springerville-St. Johns Dome, a 445 billion m^3 natural helium and carbon dioxide reservoir straddling the Arizona-New Mexico border, spanning an area of 1813 km^2 (Figure 4) (Rauzi, 1999). The Springerville-St. Johns Reservoir is a northwest-plunging faulted asymmetric anticline, called the Cedar Wash anticline which is faulted into segments at depth (Cather and McIntosh, 1994). The Springerville-St. Johns Dome concentrates CO_2 to the northwest portion of the reservoir beneath the Lyman Lake area, explaining the locality of travertine concentration (Moore et al., 2003). The reservoir is bounded by the Coyote Wash fault zone to the west and the Salt Lake fault zone to the southeast (Figure 4). The Coyote Wash fault is part of a discontinuous system of northwest-trending faults superimposed upon the anticlinal fold (Rauzi, 1999). The northwest trending Coyote Wash fault parallels the axis of the Cedar Wash anticline, both intersect the northeast-trending Salt Lake fault zone, which is where CO_2 gas is most heavily concentrated (Embid, 2009). The eastern flank of the anticline is segmented by the northwest trending Cedar Mesa fault, and the Buttes Monocline fault, thus causing pockets of high-pressure gas that are located anomalously high within the subsurface

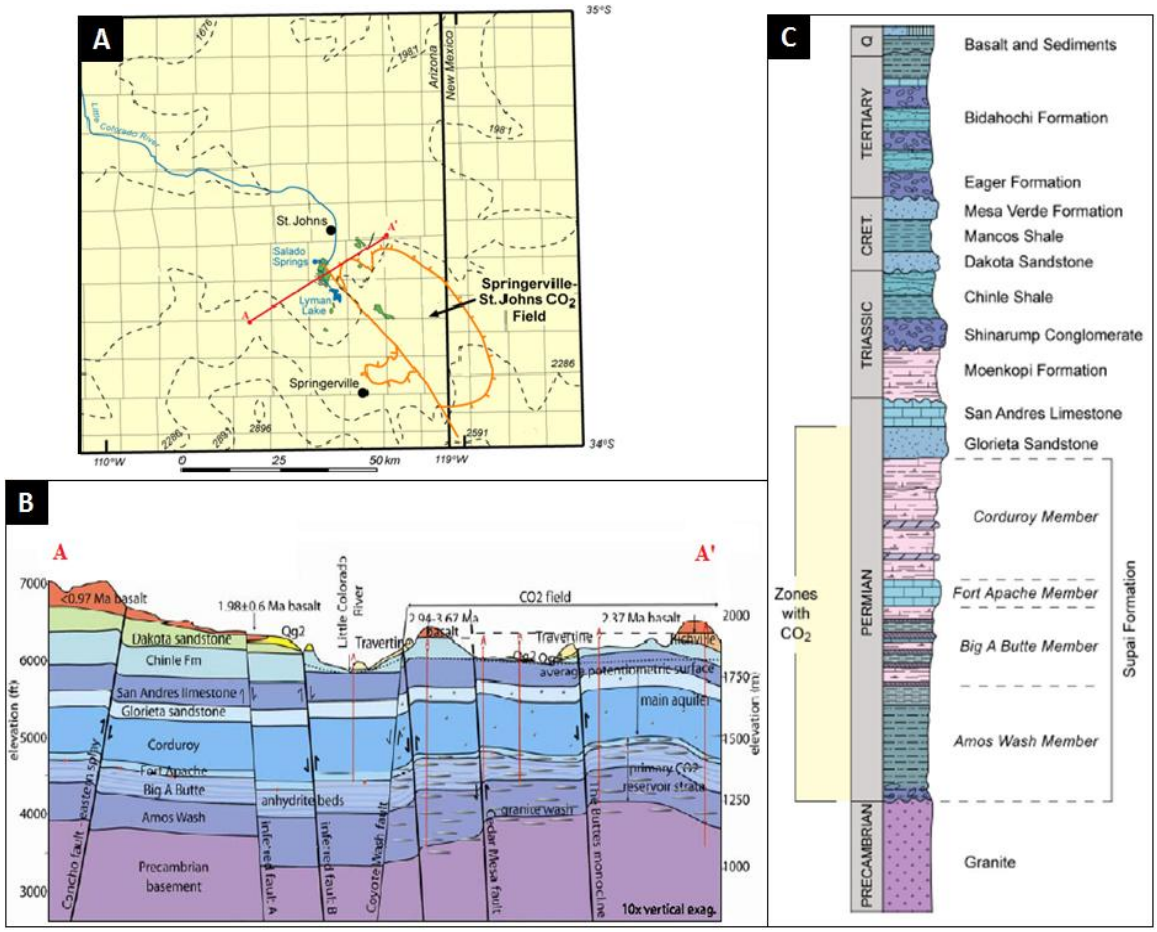

Figure 4: (A) Location of Springerville-St. Johns CO_2 field (modified from Moore, 2005). (B) Generalized cross-section of regional faults and the Springerville-St. Johns Reservoir along red line labled A-A' (modified from Embid, 2009). (C) Generalized stratigraphic section of the Springerville-St. Johns area showing zones of CO_2 (modified from Rauzi, 1999).

(Moore et al., 2005). Thus, the potentiometric surface of the reservoir is uneven, with higher-pressure fluids forced up along faults to higher elevations.

The CO_2 reservoir is sealed by Triassic anhydrite and mudstone (Figure 4). The Permian shale of the Supai Formation act as the reservoir rocks containing gas in a free state. Additionally, carbonated waters are found in the overlying Glorieta Sandstone and San Andres Limestone (Rauzi, 1999). Consequently, variations in the permeability and

porosity of reservoir rocks, along with seal effectiveness, results in fluctuations of the volume of gas, depth of producing zones, and ground water flow rates (Rauzi, 1999). The structure of the Springerville-St. Johns Dome is a product of distinct intervals of both extensional and compressional stresses. During the Laramide Orogeny, compression warped Paleozoic and Mesozoic strata (Rauzi, 1999). The Laramide Orogeny also caused reverse faulting to segment the anticline, which were then reactivated during the Tertiary as normal faults (Karlstrom et al., 2007).

Furthermore, isotopic data of δ^3He and δ^4He from the Springerville-St. Johns Dome is unusually high, ranging from 0.51-1.08 R_a (Razui, 2003; Gilfillan et al., 2008). An abnormally high proportion of ^3He relative to ^4He is indicative of mantle derived fluids (Piperov et al., 1988). The ratio of $^3He/^4He$ indicates that approximately 7% of the helium is derived from the asthenosphere (Embid, 2009). Additionally, $CO_2/^3He$ and $\delta^{13}C$ data suggests that 2-6% of CO_2 is derived from the asthenosphere (Crossey et al., 2009). Carbon dioxide is a common constituent of magma and during vertical migration the decreasing pressure causes outgassing. Ascending gas-rich fluids traveled along deep regional faults, eventually accumulating within the anticlinal structural trap. Therefore, accumulation of CO_2 within the reservoir is due in part to the rise from depth of CO_2-rich fluids due to periods of mantle degassing.

1.3.4 Artesian Spring Waters and Groundwater

In order for travertine mounds to form and grow, in addition to supersaturation of the water, groundwater must be under enough pressure for the water to reach the surface, at least approaching a hydrostatic pressure of 7 kg/cm^{-2} at ground level (Jones and Renaut, 1995). Pressurized groundwater is typically the result of artesian systems, in which the groundwater is contained within an aquifer under positive pressure (Pentecost, 2010). The height of a travertine mound is controlled by the pressure of the hydrostatic head and the point at which a hydrostatic equilibrium is reached (Moore et al., 2005). As mound height builds, the rate of flow and hydrostatic head decrease, leading to the eventual abandonment for a lower elevation. Therefore, due to the large scale of the Lyman Lake travertine deposits, it is likely that they were the result of an elevated hydrostatic head (Embid, 2009). A high hydrostatic head may result from an increase in the volume of subsurface groundwater and/or gas (Moore et al., 2005). An increase in the flux of recharging groundwater volume would likely result from climatic fluctuations into wetter climates. Furthermore, the disparity in mound size between modern and ancient springs suggests that CO_2 partial pressures were likely higher in the past. The larger size of ancient mounds, when compared with the modern Salado Spring deposits, may have been caused by an increase in the CO_2 gas volume migrating into the reservoir. This may be the result of seismic activity or a volcanic-related influx of CO_2 (Moore et al., 2005).

The level of CO_2 saturation in groundwater is critical to the formation of travertine. Within the Springerville-St. Johns region, faults play a crucial role in keeping the groundwater from being diluted by meteoric recharge (Moore et al., 2005). The

Coyote Wash fault, which bounds southwestern edge of the CO_2 reservoir, obstructs groundwater beneath the western Springerville Pliocene Volcanic Field from mixing and diluting the highly-saturated groundwater to the east (Moore et al., 2005). The Cedar Mesa fault creates an abrupt boundary west of which subsurface waters are no longer saturated with carbonate, termed the "badwater line" (Stone, 1979; Embid, 2009). Therefore, the badwater line which roughly coincides with the Coyote Wash fault, defines the southwest limit of CO_2-rich groundwater.

1.3.5 Salado Springs

Within the Springerville-St. Johns area there currently is the active formation of travertine in a modern spring system called Salado Springs. It is located adjacent to the Little Colorado River at the northern edge of the coalesced-travertine platform, downstream from Lyman Lake (Figure 1). Salado Springs is a cluster of small mounds, which pale in comparison to the size of the Plio-Pleistocene travertine deposits. The spring mounds in Salado Springs are 2 m in diameter and 0.3 m tall, discharging spring water into a surrounding marsh (Sirrine, 1958). Similar to the ancient travertine deposits, Salado Springs form cisterns rimmed by an elevated mound, being almost always filled with water and sporadically overflowing into the adjacent marsh. Despite the modern springs being much smaller in scale than the ancient-mound deposits, they are similar in morphology and may be used as an analog. Whereas modern springs expel cool water, it is inferred by Embid (2009) that the thermogenic-CO_2 origin of the Springerville-St. Johns Reservoir would suggest a shift in temperature from the ancient to modern deposits. A thermogenic-CO_2 origin would also explain the dissimilarity in scale between

modern and ancient springs, due to a thermogenic source typically displaying a higher dissolved-CO_2 volume in comparison to metogene deposits (Pentecost, 2010).

1.4 Field Location Details

The Lyman Lake Travertine deposit is a cluster of travertine mounds consisting of more than 20 individual mounds at the south end and a 6.4 x 3.2 km platform consisting of approximately 12 coalesced mounds to the north of Lyman Lake Dam and Reservoir (Figures 1 and 3). The focus of this study will be on well preserved individual mounds located adjacent to the northern end of Lyman Lake Dam and Reservoir.

These massive mound deposits are composed of sub-horizontal sheets of travertine, with a dip of just a few degrees, radially extending away from a central vent and thinning distally (Figure 5). The central vents are commonly circular, with some oblate forms. Vent depths range from 1-20 m deep and are commonly filled with alluvium. Individual travertine mounds vary from <10 m to 350 m in diameter and range from 10-60 m in thickness. Individual mounds display a low relief slope, composed primarily of sub-horizontally laminated layers forming a smooth face and typically displaying a broad circular plan view. Therefore, travertine deposits at Lyman Lake are morphologically classified as low-relief cone mounds (Chafetz and Folk, 1984). These pancake-like mounds are composed of sub-horizontal layers ranging in thickness from 3-50 cm, being composed of dense, white to beige travertine, with multiple laminae 0.2-2.5 cm thick. Weathered travertine is gray with a pock-marked/elephant skin surface

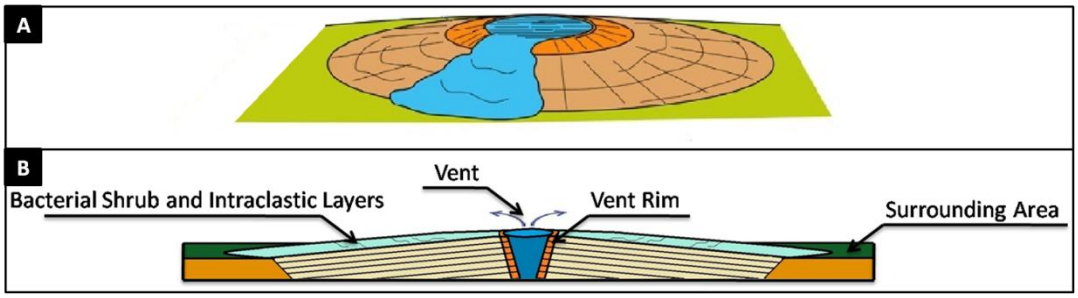

Figure 5: Conceptual depiction of mounds that formed at Lyman Lake. Mounds in the area are composed of sub-horizontal beds radially extending from a central vent, with spring water emptying into the surrounding area. (A) Oblique aerial view of a conceptual travertine mound; Dark Orange – Vent rim; Light Tan – Surrounding sub-horizontal layers; Blue – Emerging spring water (modified from Linares and Rodriguez, 2011). (B) Cross-sectional view of a conceptual travertine mound.

weathering, whereas fresher surfaces are yellow to white, with little preservation of internal features.

The symmetry and the thickness of travertine sheets around the orifice are likely due to relatively uniform precipitation along the subhorizontal surface (Kerr and Turner, 1996). However, the orifice shape is fundamental in determining mound geometry due to the formation of dam-like rims at the orifice. The vent orifice, similar in shape to a cauldron of water, develops rims around the edges which build so that overflowing water is approximately equal around the orifice, ensuring the regular mound form (Figure 5) (Fouke et al., 2000). Furthermore, both mound slope and overall geometry are likely the result of variations in surface topography, flow rate, hydraulic head, vegetation, and the degree of carbonate saturation at the vent. For example, carbonate supersaturation will cause rapid deposition near the vent orifice, resulting in a steep mound, with a self-sealing nature. However, waters with lesser degrees of carbonate saturation are likely to precipitate travertine at increasing distances away from the vent, resulting in a broader geometric profile. These mounds are unique not only because of their size but because of

their smooth, broad slopes composed of sub-horizontally laminated travertine. Unlike most global travertine mounds which display extensive to moderate terracing, these mounds feature very little terracing on small or large scales (Ford and Pedley, 1996).

The mounds are the erosional remnants of much larger deposits, due to the Little Colorado River eroding portions of individual deposits. For instance, the river separates several travertine deposits, but similar bed thickness and slope indicate that this was once one large mound that was segmented by river erosion. Many deposits are so heavily weathered that all that remains is a capping layer of travertine overlying the non-resistant conglomerates and sandstones of the Chinle Formation. Many less eroded mounds exist throughout the study area and vent locations may sometimes be determined, many displaying collapsed vents filled with sediment. However, many other mounds are so highly eroded and covered by alluvium that they preserve very little morphological information.

1.4.1 Northern Coalesced Platform

The large, 6.4 x 3.2 km, platform of travertine to the north of Lyman Lake is composed of approximately 12 coalesced and overlapping mounds (Figure 1). The top of the platform is relatively flat, with scattered vents dotting the landscape that are heavily covered by alluvium. The Little Colorado River cuts through the western edge of the platform, isolating some deposits from the main portion of the platform. The tallest mound is 200 m above Lyman Lake and over 100 m in diameter. The platform thickens to the north, with a thickness of 30 m on the southern edge and a thickness of 50 m on the

northern edge. This likely represents a waning of the hydraulic head during the migration of travertine deposition (Embid, 2009). Only the highest mound, located at the northern edge of the platform, below the Springerville Plio-Pleistocene Volcanic basalt flow, displays any appreciable outcrop exposure. However, some of the mounds on the platform have partially preserved vents with the rest of the mound covered by alluvium. For example, one heavily eroded mound has a vent exposure almost completely filled with alluvium, being only 1 m deep whereas having a diameter of 50 m. In contrast, an adjacent mound 60 m to the east, also heavily covered by alluvium, displays a 25 m deep, oval shaped vent that is 22 m long and 8 m wide.

1.4.2 Individual Mounds

1.4.2.1 Mound-A

Mound-A presents a unique opportunity to study the internal geometry and facies in a cross-sectional view of the mound. The mound is 350 m long and 150 m wide, the top is situated 35 m above Lyman Lake, with the eastern edge being highly weathered and covered by alluvium. However, the western edge of the mound was cut in order to build a service road that provides access to Lyman Lake Dam (Figure 6). The majority of the outcrop adjacent to the road is well-preserved, however there is extensive slumping in the middle and topmost portions of the exposure.

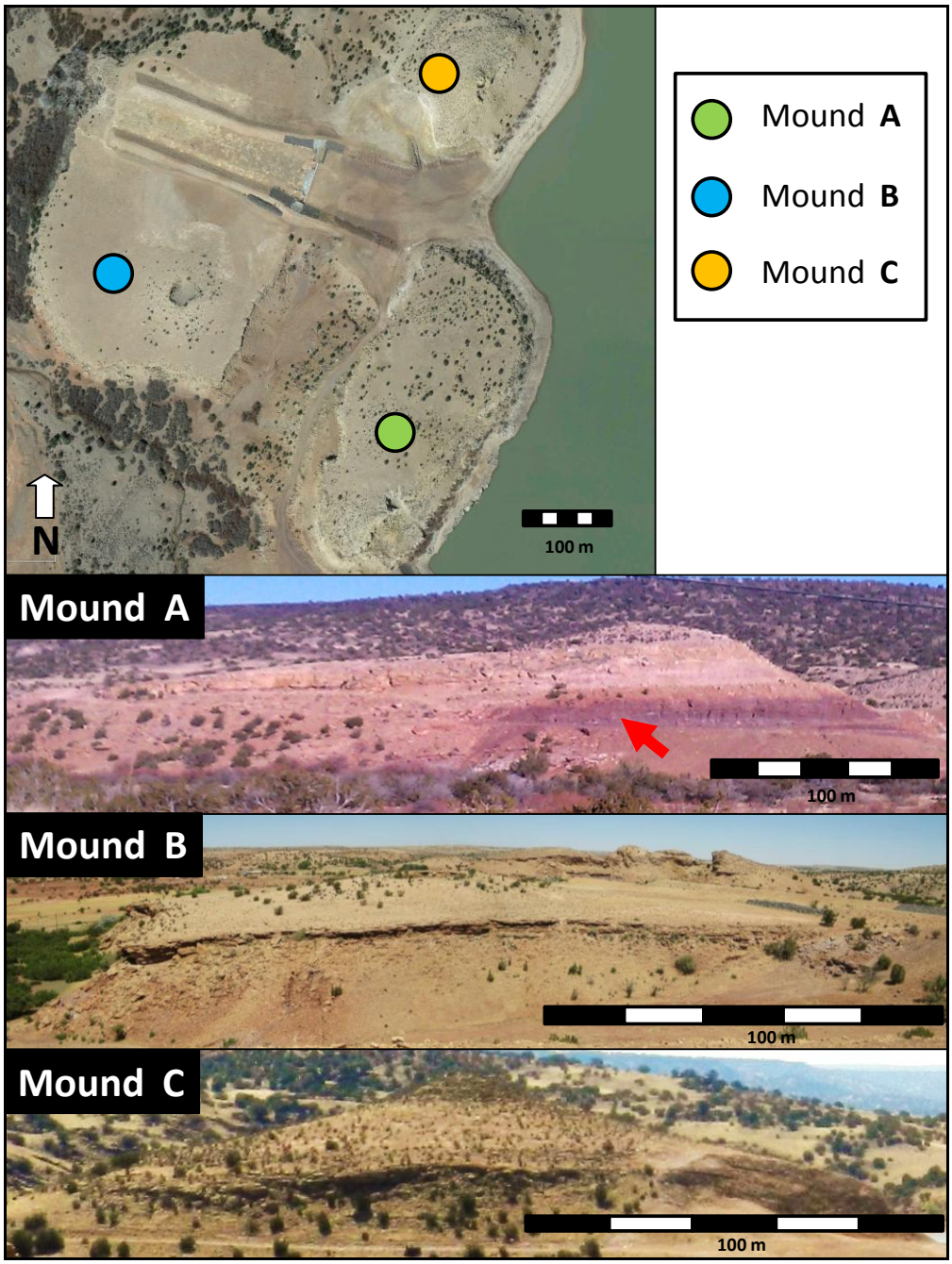

Figure 6: Aerial photo showing location of individual mounds chosen in this study (Google Maps, 2013). Mound-A – Profile of eastern edge of Mound-A, red arrow indicates service road. Mound-B – View of southeastern edge of the mound. Mound-C – Profile of northern edge of Mound-C.

Mound-A is composed primarily of sub-horizontally-bedded intraclastic and bacterial-shrub layers, ranging from 3-50 cm thick. The upper surface of this mound is heavily weathered and covered by alluvium. There is a raised portion located at the southern end of the deposit, formed from the partially eroded central vent. The vent is an erosional remnant and does not have a vent wall. The vent outcrop is a semi-circle 20 m in diameter and 4-7 m high, composed of layers immediately adjacent to the vent. The adjacent layers to the vent wall steeply dip away then level into the sub-horizontal layers that form the rest of the mound. Likely, the vent was composed of an elevated cistern on top of a mound, where steeply dipping surfaces composed the elevated portion and dramatically changed distally into sub-horizontal layers.

1.4.2.2 Mound-B

Mound-B is located adjacent to the northern edge of Lyman Lake, on the eastern side of the Lyman Lake Dam (Figure 6). The western side of this mound was cleared during construction of the dam, exposing an 8 m thick section of cross-bedded conglomerates and calcareous silt that underlie the travertine mound. The mound is 150 m long and 80 m wide, the top is 25 m above Lyman Lake. There is an asymmetric preservation of this mound deposit, with the majority of the deposit extending to the north.

This mound is heavily weathered and covered by alluvium, yet displays cross-sectional exposure of a vent cistern that faces Lyman Lake. The exposed vent consists of vertically-oriented layers that dramatically flare outward from the vent center changing

orientation to sub-horizontal layering. The partially exposed vent is 6 m deep and filled with alluvium. Similar to other mounds in the area, the bulk of this mound is composed of low-relief, well-bedded layers gently dipping away from the central vent. Weathering of the mound has created benches of heavily weathered travertine layers ringing the mound surface in a step-like fashion, with areas between benches covered by alluvium.

1.4.2.3 Mound-C

Mound-C is located west of Mound-A, just south of the Lyman Lake Dam (Figure 6). Despite being heavily weathered, this mound displays the typical broad form of travertine deposits throughout the region. The mound is 280 m in diameter, forming a symmetric deposit and exposing an outcrop of an approximately constant thickness of 1.5 m at the distal edges. The central vent is 32 m in diameter, 3 m deep, and filled with alluvium. Beds around the vent display a similar relationship to the exposed vent as do those of Mound-B. Successive layers of travertine are oriented vertically around the vent, dramatically changing dip to form the continuous sub-horizontal layers, which comprise the bulk of the mound.

CHAPTER 2: INTRODUCTION TO TRAVERTINE

2.1 Overview of Travertine

Travertine is a type of carbonate deposit formed either from hot or cool water that is saturated with $CaCO_3$. Dissolved $CaCO_3$, or 'calcium carbonate' is produced by dissolved CO_2, or 'carbonic acid', attacking Ca-rich rocks and incorporating calcium into solution (Pentecost, 2005; Jones and Renaut, 2010). Groundwater may become saturated with CO_2 either derived from a near-surface 'metogene' source or deep-seated 'thermogenic' source.

The Lyman Lake travertines were formed from groundwater saturated with thermally-generated CO_2 that has been trapped within the Springerville-St. John's Dome (Embid, 2009). The high-subsurface pressures cause CO_2 to become more soluble, allowing circulating groundwater to dissolve large amounts of limestone. Yet alone, even large amounts of dissolved CO_2 are not sufficient to produce travertine, instead a carbonate rock is required as a source of Ca^{2+} in order to precipitate $CaCO_3$. In the Springerville-St. Johns travertine complex, calcium is derived by the dissolution of Permian Fort Apache and San Andres limestones, located beneath the sealing anhydrite and mudstones of the CO_2 reservoir (Rauzi, 1999).

Furthermore, water that becomes saturated with $CaCO_3$ may either be derived from deep-seated or shallow meteoric sources. Not only does travertine formation require CO_2 saturated water, but also a pathway to reach the surface, such as faults. These faults may act as high-permeability conduits that carry carbonate-saturated waters to the

surface, resulting in travertine deposition to be concentrated along the exposed surface of fault traces (Mudd, 1999; Guo and Chafetz, 2012). In the case of the Lyman Lake travertines, CO_2-rich fluids escape from the Springerville-St. Johns Reservoir, traveling along major faults, such as the Cedar Mesa fault, and resulting in carbonate-rich springs at the surface (Embid, 2009).

Therefore, travertine is a byproduct of CO_2-saturated waters dissolving Ca-rich rocks yielding $CaCO_3$ saturated fluid, which then travels upward along faults and eventually emerging at the surface, resulting in the precipitation of travertine through a combination of biotic and abiotic mechanisms.

2.2 Travertine Precipitation and Deposition

As $CaCO_3$-saturated groundwater emerges at the surface, travertine may precipitate either through abiotic or biotic processes, yet is governed by the same reaction (*Eq. 1*).

$$(Eq.\ 1)\quad Ca^{2+} + 2(HCO_3)^- \rightleftharpoons CaCO_3 + CO_2 + H_2O$$

An abiotic 'degassing' of CO_2 occurs when saturated groundwater comes in contact with the atmosphere, resulting from the disequilibrium between the CO_2 concentrations of the air and the emerging spring water, causes an increase in $CaCO_3$ saturation and resulting in the precipitation of carbonate (Chafetz et al., 1991). However, water must be super-saturated in regard to calcite to overcome inhibitors to precipitation (Zhang et al., 2001).

Abiotic precipitation of carbonate may occur through several mechanisms, which are a function of the stability of saturated CO_2, which is dependent upon several variables such as flow hydrodynamics, temperature, and water chemistry (Zhang et al., 2001). A higher concentration of saturated $CaCO_3$ will increase precipitation because of a more vigorous degassing as a result of the greater disequilibrium between the CO_2 concentrations of the atmosphere and water. Therefore, the higher the concentration of dissolved HCO_3^- that is retained in solution, the greater amount of $CaCO_3$ that can be precipitated during degassing (Chafetz et al., 1991). Furthermore, at higher temperatures CO_2 becomes less soluble in water; thus emerging hot waters will contain less CO_2 in comparison to the more soluble ambient water temperatures. Intensive abiotic precipitation also occurs at sites where there are sudden hydrological changes caused by an increase in slope, such as vent rims, waterfalls, or terraces. Hydrological changes, such as an increase in flow rate, can induce carbonate precipitation through three mechanisms which increase CO_2 degassing, the 'aeration effect', the 'low pressure effect', and 'jet-flow effect' (Chen et al., 2004). All of these effects increase the exposure of water to air, increasing the degree of degassing (Chen et al., 2004). Firstly, the 'aeration effect' occurs when turbulence causes bubbles and air entrainment. Secondly, the 'low pressure effect' occurs when high velocity water causes a decrease in the static water pressure. Furthermore, according to Henry's Law, dissolved gasses are more easily released at lower pressure, resulting in an additional increase at the air-water interface for gas-bubble release. Finally, the 'jet-flow effect' occurs when turbulence breaks water into spray and droplets, further increasing the exposed air-water interface.

It has long been recognized that modern springs precipitating travertines are associated with organisms (Weed, 1890). The presence of organisms and the impact of biotic processes are controlled by many variables such as water composition, temperature, pH, oxygen saturation, flow velocity, salinity, and light intensity (Fouke et al., 2000). However, water chemistry is the most important factor in determining the habitability of spring water (Chafetz and Folk, 1984). A major influential component of spring water chemistry is dissolved sulfur, which can poison the water, limiting biotic growth of higher taxa. Modern spring systems with high-sulfur concentrations are dominated by certain bacterial growth, the only taxa able to survive the harsh-chemical conditions (Chafetz and Folk, 1984; Chafetz and Guidry, 1999). However, at agitated sites, H_2S gas readily escapes by degassing, allowing for biotic growth (Chen et al., 2004). As hot spring water emerges, water flows downstream and decreases in temperature, becoming more habitable to higher taxa allowing biotic processes to become more prevalent downstream (Fouke et al., 2003). A wide range of organisms are known to colonize spring systems and their distribution is determined by their ability to survive within certain environmental thresholds. Therefore, organisms occur in a predictable distribution as water temperature and chemistry change downstream from the hot spring. Bacteria including cyanobacteria and archaea will be the first to colonize, followed by higher taxa of plants (Fouke et al., 2003). Only heterotrophic bacteria and archaea can survive in the extreme conditions of hyperthermal-spring waters (>75°C) (Pentecost, 2010). In hot-water springs (>25°C) flora is limited to bacteria at the vent and other prokaryotes downstream (Folk, 1994; Fouke et al., 2003). By comparison, in cool-water springs (<25°C) there is less environmental stress, allowing for a diverse range of

eukaryotes, such as moss, algae, grass, and reeds (Guo and Riding, 1998; Fouke et al., 2000).

Organisms play both an indirect (physical) and direct (chemical) role in calcite precipitation. Organisms colonizing spring systems may serve an indirect role with no biochemical processes, simply providing a substrate for carbonate precipitation. Plants can influence travertine fabric by providing nucleation sites for carbonate encrustation around plant parts which subsequently decay, resulting in their preservation as stalk molds (Mudd, 1999). The presence of large plants may become obstacles to flow, causing water to increase in turbulence, and leading to increased CO_2 degassing. Plants can have a major impact on spring deposition if encrusted buildups become large enough to influence water flow, and over time contribute to the large-scale morphology of the deposit (Guo and Riding, 1998). In addition, the orientation of plant molds may be used to predict the direction of water flow in a paleospring system (Drysdale et al., 2003). One direct role of organisms in carbonate precipitation is attributed to an unbalance caused by the removal of CO_2 by photosynthesis, causing a micro-environmental gradient in alkalinity which leads to a supersaturation of calcite and carbonate precipitation (Riding, 2000). However, the slowest rate of degassing is still far greater than the photosynthetic removal of CO_2, indicating that biotically-induced precipitation will dominate mainly when spring waters are at or near equilibrium with the atmosphere and degassing effects are minor (Pentecost, 2005). Furthermore, photosynthesis is less effective in highly alkaline environments, where the gradient caused by CO_2 removal is not significant enough to result in supersaturation (Riding, 2000).

Bacteria play a fundamental role in the direct precipitation of calcite by altering the surrounding microenvironment through their metabolic processes. Metabolic activity, which occurs on the bacterial surface of the EPS (Extracellular Polymeric Substance), raises alkalinity and creates a gradient due to the photosynthetic uptake of CO_2 and/or HCO^{3-} (Folk, 1993). Bacterial metabolic processes act as a catalyst for carbonate precipitation by providing diffusion limited, negatively charged, sites that attract positively charged calcium ions and induces $CaCO_3$ precipitation (Pentecost, 1985). Yet the presence of bacteria does not ensure carbonate precipitation; metabolic activity is fundamentally required in order to alter the microenvironment (Buczynski and Chafetz, 1991).

The carbonate precipitation that occurs along a travertine mound can be generally divided into three stages: initial vent degassing, intermediate stage, and distal equilibrium (Chafetz and Folk, 1984). The most calcite-saturated spring water emerges from the vent; where abiotic calcite precipitation from initial degassing is most prevalent in respect to the entire spring system (Pentecost, 1995). However, this may not always be the case as in slightly charged springs in which biotic processes may dominate the entire system. Within the transition zone, water discharged from the vent flows downstream and undergoes further losses of CO_2 from degassing and photosynthesis, resulting in additional carbonate precipitation, and an increasing pH downstream. Finally, the remaining dissolved CO_2 within water flowing from the transition zone will eventually reach equilibrium with the atmosphere, allowing biologic processes to dominate the removal of CO_2 and resultant carbonate precipitation. Therefore, abiotic processes are

most prevalent within close proximity of emerging waters where the waters are degassing, whereas organic processes become increasingly prevalent downstream. However, temperature may not always decrease downslope-water temperature may increase distally by external solar heating, especially where water flows in thin laminar sheets over a sloping-mound deposit (Chafetz and Lawrence, 1994). The evaporation of spring waters can induce precipitation by reducing the water volume and increasing the dissolved ion concentration, causing the water to become supersaturated with respect to calcite (Chen et al., 2004). However, a strong influence of evaporation is usually limited to playa lakes, where water experiences an unusually long stagnation under high temperatures.

2.3 Classification of Travertine

The classification of travertine springs is a complex issue due to the wide variety of depositional and biological systems (Veysey et al., 2008). Spring system morphology is the combined product of hydraulic mechanics and geomorphology, allowing for a diverse range of spring systems (Jones and Renaut, 2010). Therefore, it is difficult to develop a classification system that incorporates the variability of travertine systems. Many similar components of travertine systems can vary vastly in scale and impact upon morphology, yet have the same fundamental elements and formative processes (Ordonez et al., 1986). Furthermore, because spring systems are dynamic, changes at a small scale may influence large scale morphology as the system evolves over time. For example, the processes controlling the precipitation of travertine are identical for both large dams and micro-terraces, resulting in identical fundamental elements composing the structures.

Thus, whereas processes and elements of formation are similar, the magnitude of impact on the entire spring system differs vastly. Although an interestingly unique feature of travertine systems, this multi-scaled nature creates a problem when devising a classification system that can encompass all of the scales and global variability of travertine systems.

There is no single classification that covers the diversity of spring deposits in modern and ancient systems. Several classification systems have been proposed for cool-water-spring deposits, however comparatively few systems exist for hot-water springs. There are a variety of classifications based on features such as water source, water temperature, and constituent type. For example, modern spring systems are commonly classified based on the water temperature of emerging waters (Pentecost, 2010). This type of classification distinguishes hot-water springs (>25°C) from cold-water springs (<25°C) (Pentecost, 2010). Existing classifications tend to treat the cold-water and hot-water deposits as separate entities, even though they commonly overlap in sites where hot water cools as it flows downstream (Jones and Renaut, 2010). Furthermore, travertine has been classified based on the origin of the CO_2, which saturates the groundwater (Pentecost and Viles, 1994; Pentecost, 1995; Viles and Pentecost, 2007). This classification distinguishes between CO_2 that originates either from the soil (meteogene) or from deep-thermal processes (thermogene). Whereas classification based on temperature or CO_2 source is independent of scale and a viable method for the classification of modern springs, it is difficult to apply to ancient travertine deposits. Additionally, another problem is that some classification systems are solely suited for the

spring from which they were formulated, such as the hot-water springs of Angel Terrace in Yellowstone National Park, studied by Fouke (2000). Classification schemes devised specifically for a study area are apt for local differentiation, but not applicable when considering the global diversity of travertine systems. Nevertheless, the classification of a particular locale helps in the understanding of the full range in variability of that particular system. Therefore, the aforementioned classification systems are not practical when applied to the global variety of modern and ancient systems.

Therefore, the best classification system is based on overall geomorphology of the spring system, because morphology can be applied to both ancient and modern systems, whilst still covering a range of varying spring conditions. However, an important consideration must be made due to the possibility of gradation between spring types at a single locality. Nevertheless, Riding (2000) suggested that purely descriptive definitions, irrespective of their origin, may be too broad for a classification system. Therefore, a simple classification of travertine systems is needed that can encompass both modern-and ancient-spring systems.

Chafetz and Folk (1984) identified five basic-large-scale forms that can be closely related: 1) cascade/waterfall, 2) lake-fill/lacustrine, 3) fissure ridge, 4) terraced mound, and 5) sloping mound. The strength of this classification system is its basis on a purely morphological description of travertine deposits, allowing it to be applied to both modern and ancient deposits, while remaining independent of scale. Furthermore, this scheme can be applied irrespective of water temperature, facies, flora, or mineralogy because it is based on the large scale morphology of the deposits.

1) Waterfall/cascade deposits are the most distinctive from the other classes proposed by Chafetz and Folk (1984). They form at sites of increased agitation where water flows over a dam, resulting in carbonate precipitation from turbulent waters. The aggradation of dam construction experiences episodic erosion by periodic floods. These deposits are common sites for the growth of attached algae and mosses which further increase carbonate encrustation (Pentecost, 1991). However, bacteria are less common in these deposits, likely due to the cool, non-sulfuric nature of the waters that produce these waterfall/cascade deposits (Chafetz and Folk, 1984). Algae and mosses struggle with competing rates of growth against carbonate encrustation, preserving hollow tubes after decay of the plant matter (Chen et al., 2004). Waterfall/cascade deposits are composed of highly irregularly laminated travertine which is porous on both large and small scales.

2) The largest deposit within this classification, shallow lake-fill/lacustrine deposits are laterally extensive, commonly tens of meters thick (Chafetz and Folk, 1984). Lacustrine travertine deposits may either form in ambient-temperature waters or hot waters. Sub-aqueous mounds are commonly scattered in lacustrine travertine deposits, forming at sites of emerging water, undergoing abandonment and migration as emerging waters shift in location (Ford and Pedley, 1992). Hot-water lake deposits are composed of a series of horizontally stratified travertine, punctuated by comparatively thin, gently sloping soil horizons representing erosional periods (Chafetz and Folk, 1984). The horizontally stratified travertine composing lacustrine deposits consist of thin layers of horizontally laminated carbonate mud interspersed with layers of bacterial shrubs. The soil horizons are likely due to the breaking of dams that contained the lakes, causing

water level to drop and resulting in erosion. Commonly, benches of travertine have paludal deposits at the top, due to a last stage of vertical aggradation. Yet these marsh deposits are thin and have a low-preservation potential due to their erodible nature and position adjacent to erosional soil horizons. The sub-horizontally stratified layers are commonly onlapping sloping erosional surfaces. Therefore, these lake deposits were able to remain relatively shallow because travertine accumulation was able to keep pace with the aggrading dams that contained the lake. Cold-water lakes are similar to warm-water lakes, yet are dominantly composed of massive deposits of micrite and lack the pervasive stratification of hot water lake-fill deposits.

3) A fissure ridge is a linear deposit generated from a central fissure, with sloping layers away from the central fissure (Chafetz and Folk, 1984). It is formed when carbonate-saturated waters are brought to the surface by a fault or linear fracture with precipitation occurring along the surface trace of the structure. A fissure ridge is composed of thin layers continuous from the crest down the sloping sides and conforming to the surface morphology (Hancock et al., 1999). The deposit can be highly porous, being composed of encrusted plants and irregular inorganic crusts, somewhat similar to a waterfall/cascade deposit. Fissure ridges can be similar to terraced mounds, sometimes displaying microterraces on the sloping surface (Renaut et al., 2002).

4) Terraced mounds are composed of a series of terraced ledges consisting of rimstone dams surrounding a flat-floored shallow pool (Chafetz and Folk, 1984). Similar to sloping mounds, these mounds can display a considerable depositional relief with a step-like pattern of terraces. Dams are composed of a raised rim of dense ray-crystal

travertine around the edge of a pool and are formed by turbulent flow over the dam inducing carbonate precipitation (Hammer et al., 2010). The rimstone dams surround shallow pools that receive overflowing water from the terraces above. The dams and pools grow at approximately equal rates (Chafetz and Folk, 1984). On the floor of terrace pools water turbulence is low, allowing shrubs to be a major component with associated bacterial oncoids and pisoids. Terraced mounds are occasionally associated with smooth sloping mounds, showing that these categories can occur with each other.

5) Sloping mounds/fans/cones display laminated beds that dip away from a central elevated area (Chafetz and Folk, 1984). Sloping mounds are typically symmetric with a central vent supplying water. However, fans may be produced when deposited on a gently dipping slope (Ford and Pedley, 1996). In addition, there are dipping erosional surfaces similar to those present in shallow-lake fill, yet not as pronounced and they are parallel with adjacent beds. These likely resulted from periods of non-deposition where spring waters either ceased flowing or shifted to another, steeper, portion of the mound. In contrast with the uniformly laminated strata of hot-water lake deposits, individual laminations may pinch out laterally within sloping mounds. Sloping mound deposits are primarily composed of oncoids and intraclasts, with minor shrub components that occur more frequently distally on lower slopes.

There have been many other attempts at a classification system for travertine deposits. For example, Ford and Pedly (1996) proposed single unified-classification scheme, which unified hot-and-cold water systems, dividing travertine into ‘cool’, ‘thermal’ and ‘saline’. Cool water travertines consisted of braided fluvial, barrage fluvial,

perched springline (sloping fan system), lacustrine, and paludal. Hot-water travertines were divided into fissure ridges and terrace mounds. Saline travertines included evaporative lacustrine/hyperalkaline deposits composed of large mounds within standing bodies of water. However, this system has not been widely adopted and will not be used in this study.

2.4 Travertine Constituents

Many factors control the formation of travertine constituents, such as hydrodynamics (laminar or turbulent flow), kinetics of growth inhibitors, temperature, and ion transport mechanisms. The constituents of travertine provide insights into the depositional environment and the processes operating during deposition. Therefore, proper identification and interpretation of travertine constituents leads to a more accurate interpretation of paleoenvironmental conditions.

2.4.1 Travertine Shrubs

The term ‘shrub’ was first used by Kitano (1963) to describe structures in Japanese travertines and subsequently popularized by Chafetz and Folk (1984) in their extensive and important studies of central Italian travertines. The latter were first to recognize the significance of shrub structures and demonstrate their association with bacterial colonies. Furthermore, Chafetz and Guidry (1999) went on to distinguish three types of shrubs: 1) bacterial, 2) crystal, and 3) ray-crystal. The three types of shrubs

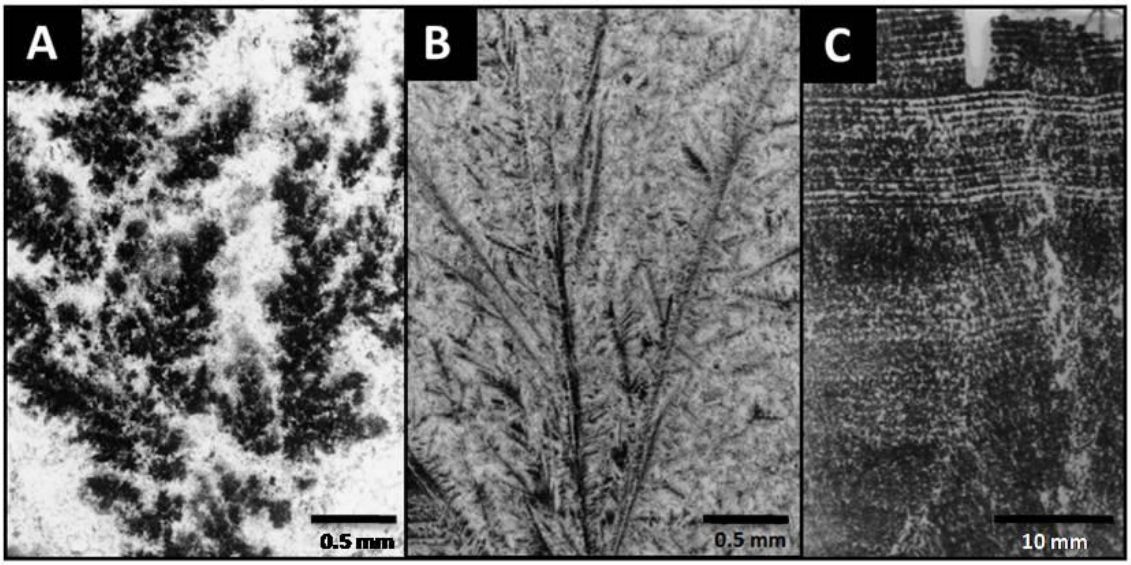

Figure 8: Photomicrographs of (A) bacterial shrubs, (B) crystal shrubs, and (C) ray-crystal shrubs (modified from Chafetz and Guidry, 1999).

represent members recording the relative contributions between biotic and abiotic precipitation (Figure 8) (Chafetz and Guidry, 1999). Bacterial shrubs are dominantly biotically mediated, whereas ray-crystal shrubs are formed by dominantly abiotic processes. However, bacteria play a fundamental role in the formation of all three shrub types, acting as a catalyst and nucleation site for the precipitation of calcite or aragonite (Chafetz and Guidry, 1999). Therefore, the relative influence of bacterial processes on abiotic processes results in a gradation in morphology between shrub types. All shrub types display bacterial fossils under SEM that are either rod and/or prolate spheroid forms less than 1 μm in length (Allen and Albert, 2000). After death, many of the encrusted bacteria fossils burst and subsequently decompose, generating microporosity. Bacterial shrubs display an arborescent branching form, crystal shrubs form branching geometric patterns, and ray-crystal crusts are composed of sweeping crystalline fans. Travertine shrubs conform to the surface topography of the depositional surface, and thus

shrubs orient their structures with the long axis at right angles to the growth surface and may range from horizontal to vertical orientation with regard to a horizontal surface. In modern springs, young crusts at the surface are commonly soft and brittle; however, lithification occurs quickly, resulting in resilient deposits. Because all shrub types are bacterially mediated to some degree, they are typically limited to hot-water, sulfuric spring environments where bacteria have little competition from other organisms and may thrive unimpeded.

1) Bacterial shrubs form preferentially in quiescent terrace pools or along travertine slopes and may also coat grains in higher energy water, forming oncoids. Bacterial shrubs are generally <5 cm high, forming an upward-expanding, irregular dendritic morphology of branches extending from a central region. The branches of bacterial shrubs consist of separate aggregations of micrite clumps, called 'leaves', which precipitated around bacterial colonies (Chafetz and Guidry, 1999). These 'leaves' are dominantly composed of micrite and are commonly encased within single crystals of clear calcite; microspar may also be present within the leaf interior. Bacterial-shrub layers are commonly laterally continuous up to tens of meters and can display a wide range in the packing density of adjacent shrubs along a single layer. Bacterial shrubs commonly display cyclic repetition of laminations, reflecting seasonal growth cycles. Bacteria experience the most growth during the warm growing season, resulting in thick shrub layers. However, during colder seasons, bacterial growth is limited, resulting in thin layers of silt-sized, bacterially induced micritic peloids (Chafetz and Folk, 1984). Finely laminated sediment made of transported, silt-sized bacterial peloids, commonly in

layers 2-6 mm thick, underlie and overlie each shrub layer and have been mechanically deposited at times when shrubs were not growing. Thick layers of shrubs, separated from each other by the thin bands of micritic peloids, comprise a complete repeated shrub sequence.

2) Crystal shrubs represent an intermediate state between the other two shrub types where abiotic processes are becoming increasingly dominant despite being bacterially mediated (Chafetz and Guidry, 1999). Crystal shrubs are similar in size and distribution to bacterial shrubs, yet they are composed of well-formed geometric crystals that result in a straighter, elongate, well-defined morphology. Crystal shrubs display a central, dominant, straight stalk commonly with straight branches extending outwards (Chafetz and Folk, 1984). Similar to bacterial shrubs, the leaves of crystal shrubs are composed of bacterial clumps encased in an increasingly well-formed calcite crystal.

3) Ray-crystal crusts are abiotically precipitated, forming in environments such as rimstone dams and orifice rims where there is high hydraulic flow and supersaturation of carbonate (Chafetz and Folk, 1984). Ray-crystal crusts represent almost exclusively abiotic precipitation with very little bacterial influence. On the outcrop scale, ray-crystal crusts gradate into the laterally extensive bacterial shrub layers. Chafetz and Folk (1984) proposed two forms of ray-crystals, 'thicker radial crusts' where individual layers of crystals were 2-8 cm thick and 'fine ray-crystal fans' measuring approximately 1 mm in thickness. Ray-crystals are composed of coarse blades of radial calcite oriented perpendicular to the surface of deposition and displaying sweeping extinction under crossed polarized light (Folk et al., 1985). The coarse blades extend from layered patches

of bacterial micritic peloids that are aligned perpendicular to the growth direction of calcite crystals. Under SEM the fine crystal fan is composed of strings of diamond-shaped plates approximately 3 µm long and 1 µm wide with a high degree of intercrystalline porosity (Folk et al., 1985).

2.4.2 Coated Grains

Coated grains are classified based on origin and characterized by a nucleus encased by cortical laminae. Coated grains are unattached forms of mobile travertine formed either by abioitic or biotic processes within flowing-water conditions (Tucker and Wright, 1990). Abiogenic coated grains are termed ooids or pisoids whereas biologic coated grains are oncoids (Pentecost, 2005). Three types of coated grains have been identified based on the cortex texture: 1) concentrically laminated (Folk and Chafetz, 1983), 2) stromatolitic mammilated (Guo, 1993), and 3) radial shrub (Folk and Chafetz 1984).

1) Concentrically laminated grains are inorganic coated grains with a concentrically laminated cortex, typically forming in turbulent circulating waters such as a vent orifice (Figure 9B) (Folk and Chafetz, 1984). 2) Coated grains with a stromatolitic mammillated cortex are classified as a type of oncoid and are likely formed by cyanobacteria (Kosun et al., 2005). 3) Oncoids are a biogenic-radial-shrub-coated grains with radially laminated, shrubby laminae, which form by the seasonal lamination of bacterial growth (Figure 9A) (Folk and Chafetz, 1984). As with bacterial shrubs, oncoids experience greatest growth during warmer seasons due to the increase in light conditions

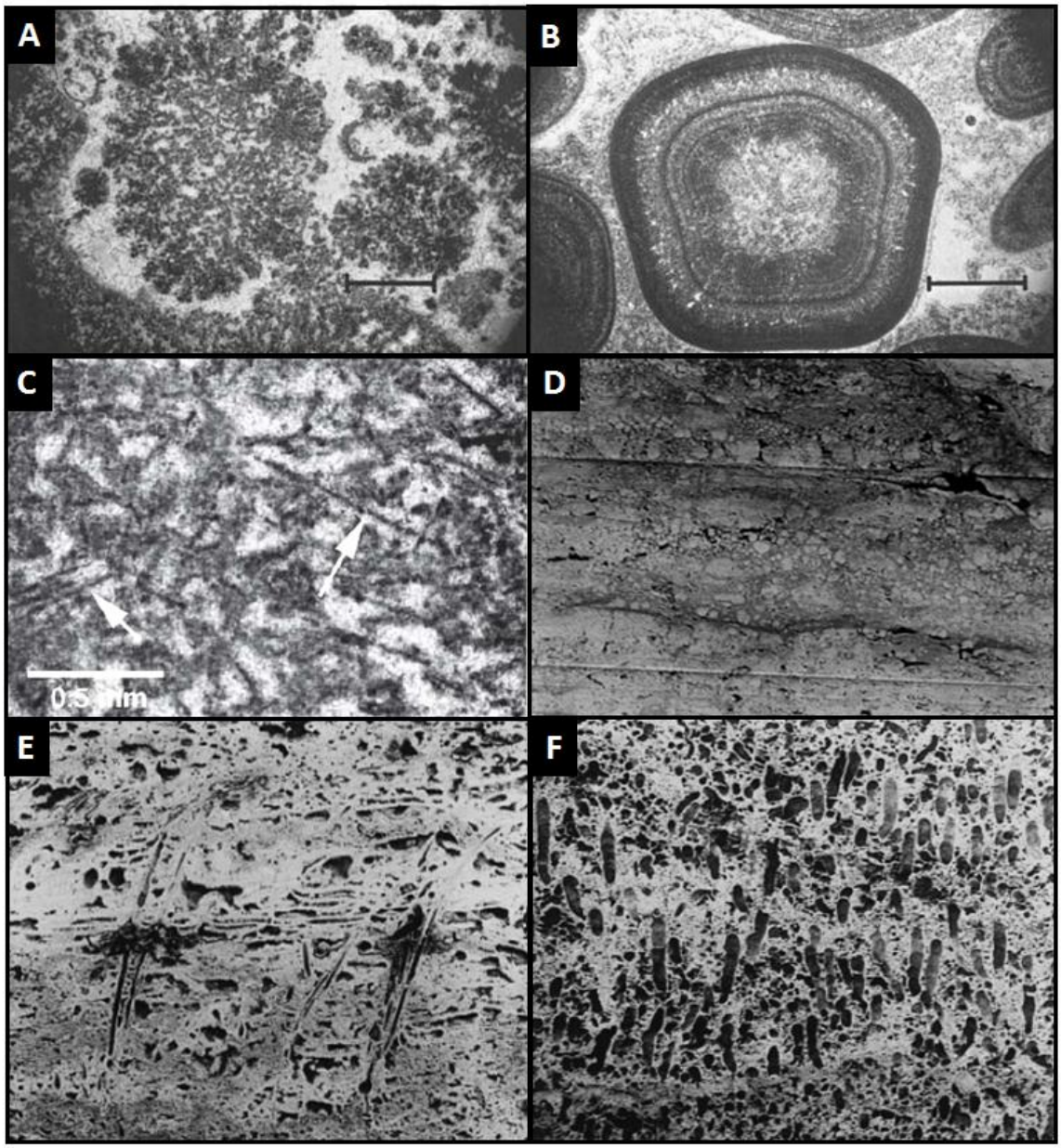

Figure 9: Constituents commonly found in travertine deposits. (A) Photomicrograph showing oncoids, a radial shrub coated grain. Scale equal to 1 mm (Folk and Chafetz, 1983). (B) Photomicrograph showing concentrically laminated coated grains. Scale equal to 1 mm (Folk and Chafetz, 1983). (C) Photomicrograph showing rafts (Chafetz and Guidry, 2003). (D) Outcrop showing intraclasts. Width of view 16 cm (Guo and Riding, 1998). (E) Slab showing reed molds. Width of view 12.5 cm (Guo and Riding, 1992). (F) Slab showing lithified bubbles. Width of view 20 cm (Guo and Riding, 1992).

(Pedley, 1992). Oncoids typically form in small terrace pools located upon steep slopes or wide pools. They may range greatly in size and consist of a nucleus covered by a cortex of concentric carbonate that is approximately even in thickness (Guo and Riding, 1998). The cortex is normally spherical and composed of irregular laminae that may overlap, its shape ultimately determined by the strength and regularity of hydraulic flow. All oncoids are generally mobile to some extent, ensuring that growth occurs over the entire surface, however under lower flow conditions oncoids may be incorporated into the substrate or become oblate spheroids (Pedley, 1990). Oncoids may display 'basal rings' where growth occurs preferentially on one side due to the oncoid remaining in place long enough to develop a crust preferentially on the exposed surface (Pentecost, 2010). The nucleus is typically micritic, but may be composed of plant fragments which may also result in an oblate spheroid (Pedley, 1990). Thus, oncoids grow through a series of overlapping cortical layers resulting in an overall rounded morphology.

2.4.3 Paper-Thin Rafts

Paper-thin rafts, also known as 'floe', 'hot water ice', or 'calcite ice', are formed in stagnant and slow moving waters typically in terrace pools and depressions (Figure 9C) (Folk et al., 1985). Rafts form on the water surface, supported by surface tension and resulting from carbonate precipitation from degassing of CO_2. Commonly <1 mm in thickness, rafts are composed of spar crystals growing downward from the water surface, resulting in a flat upper surface and a dentate lower surface (Chafetz et al., 1991). Rafts commonly display a bipartite structure from the upward growth of spar, resulting from capillarity action causing precipitating waters to creep along the raft surface. As

precipitation on the raft continues, it thickens until it is too heavy and sinks to the bottom of the pool where rafts may settle at variable angles (Chafetz et al., 1991). Furthermore, disturbance at the water surface may cause rafts to break which results in their transportation and deposition.

2.4.4 Intraclasts

Intraclasts are also a common constituent of travertine mounds, resulting from the erosion of previously formed travertine (Carthew and Drysdale, 2003). Intraclasts are typically angular to subangular and may be derived from a wide range of originating material such as ray-crystal dams, bacterial shrubs, and plants (Figure 9D) (Guo and Riding, 1998). Intraclasts may be derived from preexisting structures when, for example, erosion collapses features such as dams or waterfalls. When erosion affects encrusted plant material, it results in the transportation of phytoclasts. Intraclasts form during periods of elevated flow rates, typically due to periodic surges in spring water expulsion or heavy rain (Arenas et al., 2000). The intraclasts derived from erosion are then washed downslope, accumulating in depressions, ponds, or barriers to flow such as dams or reed buildups.

2.4.5 Micrite

Micrite typically accumulates in quiet pools adjacent to barriers of flow such as dams, resulting in thick accumulations of laterally extensive calcareous silt and mud. Micrite is an important constituent of travertine systems, especially in shallow cool water lake deposits. Micritic travertine is the most prevalent lithofacies of the pre-Quaternary

travertines within the Itaborai Basin of southeast Brazil (Sant'Anna et al., 2004). Micrite is defined as fine-grained calcite <4 μm in diameter, normally displaying equant and anhedral crystals (Folk, 1959). Most likely, micrite is derived from the clastic working of the primary building blocks of travertine, diffuse mats and clumps of bacteria which are lithified during the early precipitation of sparry calcite (Chafetz and Folk, 1984). Therefore, it is most likely that micrite is an admixture of fine-grained authigenic precipitate combined with mechanically reworked clastics. However, Riding (2000) suggested several other mechanisms for the formation of micrite such as calcification of dead microorganisms and the induced precipitation from whitings.

2.4.6 Reed and Grass Travertine

Higher taxa of plants, such as reeds and grasses, are common at the distal edges of spring systems where water has cooled sufficiently to be a habitable environment for higher organisms (Guo and Riding, 1998). Reeds and grasses typically occur in paludal or shallow depressions where water accumulates, and are typically associated with rafts. Travertine encrustation of plants from degassing and photosynthesis results in a travertine fabric rich in molds of plant parts (Figure 9E). Reeds and grasses are typically encrusted by micritic carbonate, yielding cylindrical molds 0.5-4 cm wide (Pentecot, 2005). Secondary-radial-calcite growth is typical within molds, displaying crystals 20-150 mm long. Aggregations of encrusted plants may obstruct water flow, diverting spring water.

2.4.7 Lithified Bubbles

Coated-gas bubbles are common in slow moving waters such as terrace pools and shallow depressions. They form from photosynthetic activity within the sediment that releases oxygen bubbles. As the oxygen bubbles rise, they become trapped by rafts, plants, or bacterial shrubs, then rapidly become encased in carbonate (Figure 9F) (Chafetz et al., 1991). The imbalance in P_{CO2} between the adjacent water and the oxygen bubbles causes degassing of CO_2 from surrounding water into the bubble, resulting in high supersaturation and thus encrustation (Chafetz et al., 1991). Encrusted bubbles typically preserve as spherical to oblate moldic porosity that ranges in size from a millimeter to centimeters (Guo and Riding, 1998). Aggregations of several lithified bubbles may cause an interconnected, tabular appearance. Similar in structure to rafts, lithified bubbles have an inner micritic layer and an outer sheath of euhedral crystals that was in contact with the water. Bimineralogical structure is caused by a variation in the supersaturation level of the water (Chafetz et al., 1991).

2.5 Travertine Facies and Depositional Environments

Travertine spring systems display a wide array of depositional environments that give rise to many different lithofacies, although all are composed of carbonate. Facies are the total characteristic nature of sediment or rock, allowing it to be associated with a particular depositional environment (Guo and Riding, 1998). However, travertine springs may consist of a range of intergrading facies with allochthonous and autochthonous deposits being closely associated, resulting in complex morphologies that defy simple

classification. Despite the wide variety of travertine systems, several studies have identified and named travertine facies and their depositional environments. However, there has been little focus on hot-water spring facies and no unifying classification system has been universally adopted for either cool or hot water-springs. Unfortunately, the most comprehensive facies classifications have focused on cold-water spring systems, assuming additional applications to hot-water springs. These studies classified travertine facies based on the processes involved in their formation, role of organisms, sedimentological criteria, and petrographic features.

Ford and Pedley (1996) proposed a classification scheme for cool and hot water travertines, based on analogies with Dunham's (1962) carbonate classification. Lithological associations were based on fabric type and constituents that divided travertine facies into allochthonous and autochthonous deposits. The allochthonous deposits were further subdivided into microdetrital and macrodetrital travertine. The microdetrital class is analogous to Dunham's (1962) lime-mudstone and consists of micrite, peloids, sapropelic (organic-rich), and lithoclastic (inorganic) travertine. The macrodetrital subdivision, analogous to wackestone, packstones, and grainstones, is composed of oncoids, cyanoliths, intraclasts, phytoclasts, and lithoclasts. The autochthonous deposit consists of phytoherm travertine, which is analogous to boundstones. The phytoherm travertine is subdivided into stromatolith-like bacterioherms (sheets of micrite and peloids), microherm (shrubby framework of bacterial colonies), and framestones (framework of macrophytic coated organisms with mixed micritic and

sparry calcite fringes). However, this scheme was developed from cool-water travertines and assumed to subsequently apply to hot-water deposits.

Pentecost and Viles (1994) proposed a revised classification that divided travertine deposits into eleven categories subdivided into large scale and small scale features which are further classified into autochthonous and allochthonous sub-groups. The large scale autochthonous classes included: springs (fissure ridge/mounds), rivers (cascade/barrage/crust), lake (crust), marsh (paludal). The large scale allochthonous deposits included one class, clastics, which includes lakes, valley fills, bars, and alluvial cones. The small scale autochthonous classes included microbial (oncoids/bacterial shrubs/algal tufts/laminated crusts/stromatolites), bryophyte (moss and hepatics), and inorganic (foam rock/carbonate rafts/ sinter/pisoids) travertine. The small scale autochthonous includes one class, clastics, consisting of intraclasts and peloids.

Another system proposed by Guo and Riding (1998) and employed by Ozkul et al., (2002) focuses on the medium scale, dividing their study area into depositional regimes: slope system, depressional system, and mound system. Each depositional regime that represented separate depositional environments was subdivided into facies types which were composed of several lithotypes. The lithotypes proposed were crystalline crust, shrub, pisoid, paper-thin raft, coated bubble, reed, lithoclast-breccia, and paleosols. The slope depositional system is subdivided into terrace slope facies, smooth slope facies, and waterfall facies. The terrace slope facies is further subdivided into terrace walls or rims composed of crystalline crusts and terrace pools composed of shrub, pisoid, micrite, raft, and coated bubble lithotypes. The smooth slope facies has no

subdivisions and consists of sheets of crystalline crust. The depressional depositional system is divided into shrub flat facies (shrub, pisoid, lithoclast, and bubble lithotypes) and marsh-pool facies (lithoclast and reed lithotypes). However, the mound-depositional system is only composed of reed-mound facies, composed of reed and lithoclast lithotypes.

The classification scheme proposed by Chafetz and Folk (1984) describes the morphology of large scale deposits and the small-scale constituents that compose travertine. Although not explicitly called facies, each constituent may be regarded to represent a particular depositional environment because of the unique conditions specific to each constituent. However, constituents may occur together and are not mutually exclusive. Therefore, since the architectural elements of travertine systems have been adequately described by Chafetz and Folk (1984) and there has been little consensus on the classification of travertine morphology and facies, this study proposes lithofacies classification system be based jointly on travertine constituents and depositional environment.

CHAPTER 3: METHODS

3.1 Fieldwork

To assess the potential of the field area, an initial exploratory trip was conducted in May, 2012. In depth fieldwork was later conducted in June and December, 2012, each trip lasting approximately 13 days. The purpose of the exploratory trip was to inspect the potential of individual mounds for study, and collect preliminary samples. During the first trip in June, 2012, detailed fieldwork focused on Mounds-A, B, and C, as well as cursory sampling and photographing 10 other mounds in the area. Mound-A was the primary focus in December, 2012, focusing on composing stratigraphic sections and intensive sampling. An additional 5 mounds in the northern platform were also photographed, measured, and sampled during the December, 2012 trip. During these two trips, high resolution photographs were taken, samples were collected for laboratory analysis, and detailed stratigraphic sections were made for Mound-A.

Continuous stratigraphic sections were created at sufficiently large enough outcrops for Mound-A. Stratigraphic columns were not feasible for Mounds-B and C due and extensive weathering. Stratigraphic columns within a section were spaced approximately 5 m apart in order to record lateral changes within the mound. However, denser spacing was required to account for sudden changes due to morphological features. Columns were measured from ground level and heights varied from 4-6 m. The stratigraphic sections were then grouped into lithographic packages based on constituent composition and thickness. The objective of the stratigraphic sections was to collect data

about lithographic packages that could be identified within a sequence, such as constituents, layer thickness, hydraulic regime, and porosity. Stratigraphic sections were compiled for Mound-A from the western outcrop adjacent to the service road and the upper-vent exposure. In Mound-C, stratigraphic columns were developed from the eastern-vent exposure and adjacent outcrop.

Photographs were taken with a 12.1 MP, P500 Nikon camera at varying distances. Distant photographs encompassing the entire mound were taken at multiple angles to show the large-scale morphology. Medium-scale photographs were taken 2-8 m away to show trends in the morphology of bedding and lateral relationship of layers. Small features were closely photographed in order to display individual constituents and bedding. For close photographs, diluted hydrochloric acid or water was commonly used to accentuate constituents.

Samples were collected from every surveyed mound within the field area. The stratigraphic sections were heavily sampled, with a maximum of 1-1.5 m of lateral variation away from the line of section and sampling approximately every 10-20 cm vertically. Additionally, prominent and distinguishable laterally continuous layers were sampled at multiple intervals with a lateral spacing of approximately 2-3 m. In other mounds, extensive weathering constrained sampling within the well preserved parts of the travertine system. Sample sizes range from 3-40 cm in length, many composed of multiple constituent layers. Most samples were obtained with a 16 oz rock hammer, however, many samples composed of dense crystalline crust required the additional use

of a chisel. After samples were taken, they were labeled accordingly and a picture was taken of the sample at the *in situ* location.

3.2 Laboratory Work

All samples collected were cut into slabs for the macroscopic study of constituents and fabric. Cut samples were then wetted with diluted hydrochloric acid and photographed with a scale bar. During the first trip in June, 2012, a total of 127 samples were taken: 63 samples from Mound-A, 12 samples from Mound-B, 14 samples from Mound-C, and 28 samples from five other mounds. A total of 107 samples were collected during the second trip in December, 2012: 46 from Mound-A, 41 from Mound-C, and 20 from mounds composing the northern platform. Samples chosen to be made into thin sections covered the range of observed constituents in hand samples and locations. Of the 100 total thin sections, 70 were taken from Mound-A samples, 6 from Mound-B samples, 8 from Mound-C samples, and 16 from other mounds. In order to accurately distinguish the porosity, thin sections were impregnated with a blue epoxy. The blue epoxy allowed for the distinction between natural porosity and the inadvertent porosity created by thin-section preparation.

A scanning electron microscope (SEM) was used on collected samples, utilizing a JEOL JSM6330F SEM. The SEM also gave a more detailed view of the crystalline habit of constituents. This aided in the interpretation between abiotic and biotic origin of travertine samples. Samples prepared for SEM analysis were chosen to cover the full range of constituents. Freshly broken samples were used and were not etched. Samples

were mounted on a graphite disk with a 2.5 cm diameter, coated in carbon, and the edges were bound using carbon conductive adhesive tape to reduce electron scattering.

CHAPTER 4: DATA AND INTERPRETATION

Travertine deposits within the study area are the remnants of broad, low relief features, similar in appearance to a shield or dome. Travertine was precipitated from carbonate-rich waters expelled outward from vent openings. The gently sloping mound deposits consist of well-bedded layers mainly composed of bacterial shrubs and intraclasts. In association with these layers are other constituents such as oncoids, reed/grass molds, and rafts. The beds which compose the mounds dip radially outward from the high areas of the mounds where the vents were located.

4.1 Individual Mounds

4.1.1 Mound-A

Similar to other mounds in the study area, Mound-A is a low-relief sloping mound with a pancake-like morphology. A road cut through the western edge of the mound exposes relatively fresh rock in comparison to other mounds in the study area (Figure 6). Mound-A is composed of gently dipping travertine layers overlying the Chinle Formation. The Chinle Formation is mainly obscured by alluvium, however a 14 m outcrop of cross-bedded sandy siltstone is exposed at the southwestern edge of the mound. The Chinle Formation becomes increasingly obscured by alluvium to the north and consists of conglomerates at the northernmost exposure. The top of the mound surface is covered in yellow alluvium with sparse brush and grass growth. The travertine deposit is 340 m long and 160 m wide, and is 7 m thick on the southern edge of the exposure and thins to 1.5 m in the north. The northern portion of the deposit extends

down-slope for 260 m from the vent, with a 24 m loss in elevation. There is a raised domal portion on top of the southwestern edge of the deposit, formed by the eroded vent. The vent forms a semi-circular exposure 20 m in diameter and 4-7 m high. The mound is composed of gently sloping, laterally continuous interbedded shrub and intraclastic layers overlying the Chinle Formation. Mound-A also includes a range of morphological features such as stacked smooth slope columns, reed buildups, and distal edge smooth slopes. Interbedded bacterial shrubs and intraclastic layers occur in a repeated pattern, ranging from 5-30 cm in thickness. The upper 1-2.5 m of the western road cut in Mound-A is heavily obscured by alluvium and debris. The heavily weathered portions of Mound-A display exposed surfaces that are gray to dark tan and fresh surfaces that are tan to pale-yellow. Exposed surfaces in outcrop of bacterial-shrub samples are creamy white to light tan, intraclasts are pale red to dark tan, and micrite is dark brown to tan.

4.1.2 Mound-B

The travertine base of Mound-B is 15 m above lake level and overlies 4.5 m of the exposed Chinle Formation, which dips to the northwest at this location. The Chinle Formation is composed of cross-stratified sandstone and conglomerate. Travertine directly overlying the Chinle Formation is silty and composed primarily of intramicrites. The mound is heavily weathered, and the exposed surfaces are tan to gray, whereas fresh surfaces are tan to yellow. Despite being heavily weathered and covered by alluvium, the eastern outcrop of this travertine mound displays an cross-sectional view of its vent morphology. The outcrop exposing the vent and surrounding layer is located on the southwestern edge of the mound, adjacent to Lyman Lake. This exposure is 9 m thick at

the vent center and radially thins to 1 m at the distal edges of the mound. Vertical beds make up the vent walls, changing dip at the vent rim and transitioning into sub-horizontal layers that dip at 1-3° extending outward from the vent. The vertical walls of the vent are 3-3.5 m tall and the diameter at the top of the vent is 5.5 m, narrowing to 2.3 m wide at the base of the exposure. The vertical vent walls are composed of dense ray-crystal crystals oriented perpendicular to the bedding plane and laminae cross-cutting crystals oriented parallel. The laterally extensive sub-horizontal layers adjacent to the vent are composed of interbedded intraclasts and shrubs that are 0.1-0.5 m thick and continuous for 50-60 m. Individual layers thin towards the top of the mound, decreasing in thickness from 30 cm at the northern edge of the mound to 7 cm near the vent exposure. Calcite veins are present preferentially between the sub-horizontal beds directly adjacent to the vertical vent wall. The ray-crystal strata of the vent walls have very little calcite veins except for a crosscutting web of calcite veins towards the base of the exposure. Calcite veins are 1-6 cm thick and composed of white to translucent gray, large calcite crystals oriented perpendicular to the bedding plane.

4.1.3 Mound-C

Mound-C is a flat, pancake-shaped mound with a vent near the center of the deposit and caps 13 m of the exposed Chinle Formation sandstone. The mound is 12 m thick at the vent rim and thins to 1-3 m thick at the edges. The vent is 10 m in diameter and 2.5 m deep, and is partially filled with alluvium. This vent displays similar morphology to Mound-B, and is similarly composed of a circular vertical wall that dips steeply at the crest, becoming sub-horizontal as the beds extend outward. The mound is

heavily weathered, exposed surfaces are red-brown to gray and fresh surfaces are red-tan to pale yellow. Similar to other mounds, this mound is composed mainly of interbedded bacterial shrubs and intraclastic layers. However, in comparison to other mounds, Mound-B is composed of thicker intramicrites with thinner bacterial shrubs. The intraclastic layers are 3-40 cm thick, whereas shrub layers are 3-50 m thick. Intramicrite layers are composed of angular to subangular grains that are 0.5-70 mm long and suspended in a red-tan micrite. In addition, this mound contains an abundance of phytoclastic reed molds within intramicrite layers.

4.2 Constituents

The mounds within the study area contain a wide range of allochemical constituents such as bacterial shrubs, intraclasts, rafts, oncoids, reed/grass molds, and ray-crystal fans/crusts. All layers of constituents are well-layered and gently dip downslope, away from the vent.

4.2.1 Ray-Crystal Fans/Crusts

Ray-crystals are not extensively abundant, yet are an important component of mounds, composing two major morphological features. In Mound-A, ray-crystals are present formations as stacked smooth slopes or distal edge smooth slopes. The aggrading stacked slopes may range in size from small features 5-15 cm tall to larger stacked columns 1.5-2 m tall. The stacked smooth slopes are arranged in a column of stacked individual crystalline crusts 12-20 cm wide and 3-6 cm thick, which are composed of laminae 0.05-1 cm thick (Figure 10). The stacked smooth slope formations are up to 1.5-

2 m tall and individual layers display a marked break in slope compared to laterally adjacent beds. The distal edge smooth slopes are composed of 0.05-5 cm thick laminae of ray-crystal crusts that abruptly dip, truncating underlying beds. These large deposits can be 2-6 m wide and 0.5-1.5 m thick.

Ray-crystal crusts are composed of layers of calcite crystals that are oriented perpendicular to the depositional surface, forming dense crystal aggregates (Figure 11). Individual ray-crystal fans may amalgamate into a layer forming a crystalline crust. Amalgamated crusts are more common on high gradient slopes, whereas individual fans are more common on more gentle slopes. In hand samples, crystalline crusts are dense, layered, and white to pale yellow. Ray-crystals are 1-5 mm high, displaying a fan-shape, radiating pattern (Figure 11). In thin section, crystalline crusts display layers of elongate calcite crystals with fine laminations that cut across crystals, perpendicular to elongation

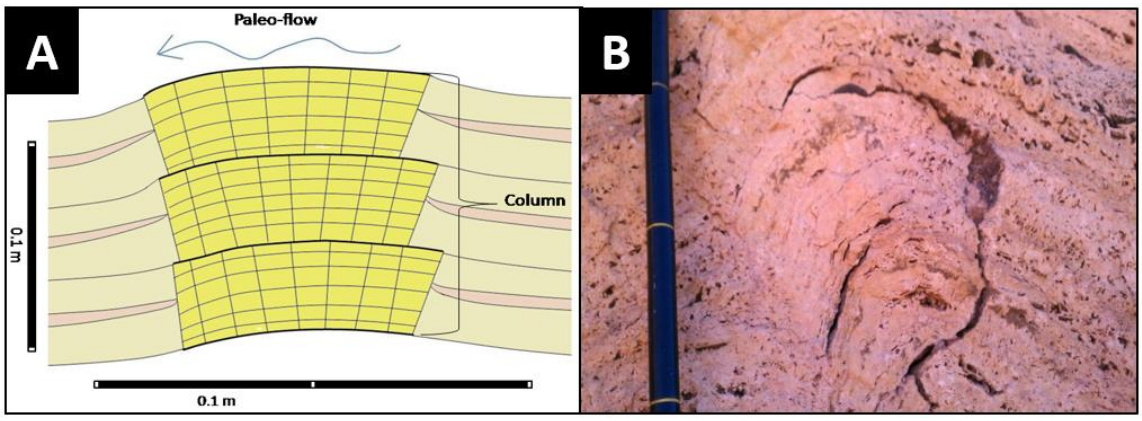

Figure 10: (A) Diagram showing relationship of stacked smooth slope dams comprising a column. Dark yellow is a ray-crystal column. Light yellow is bacterial shrub layers. Light red is intraclastic layers. Vertical lines in ray-crystal column represents direction of crystal growth. Horizontal lines represent growth laminations. Wavy blue line is the interpreted paleo-flow direction. (B) Outcrop view of stacked smooth slope dam column. Note stacked layers of ray-crystal forming a column with adjacent bacterial shrubs. Scale interval is 0.1 m.

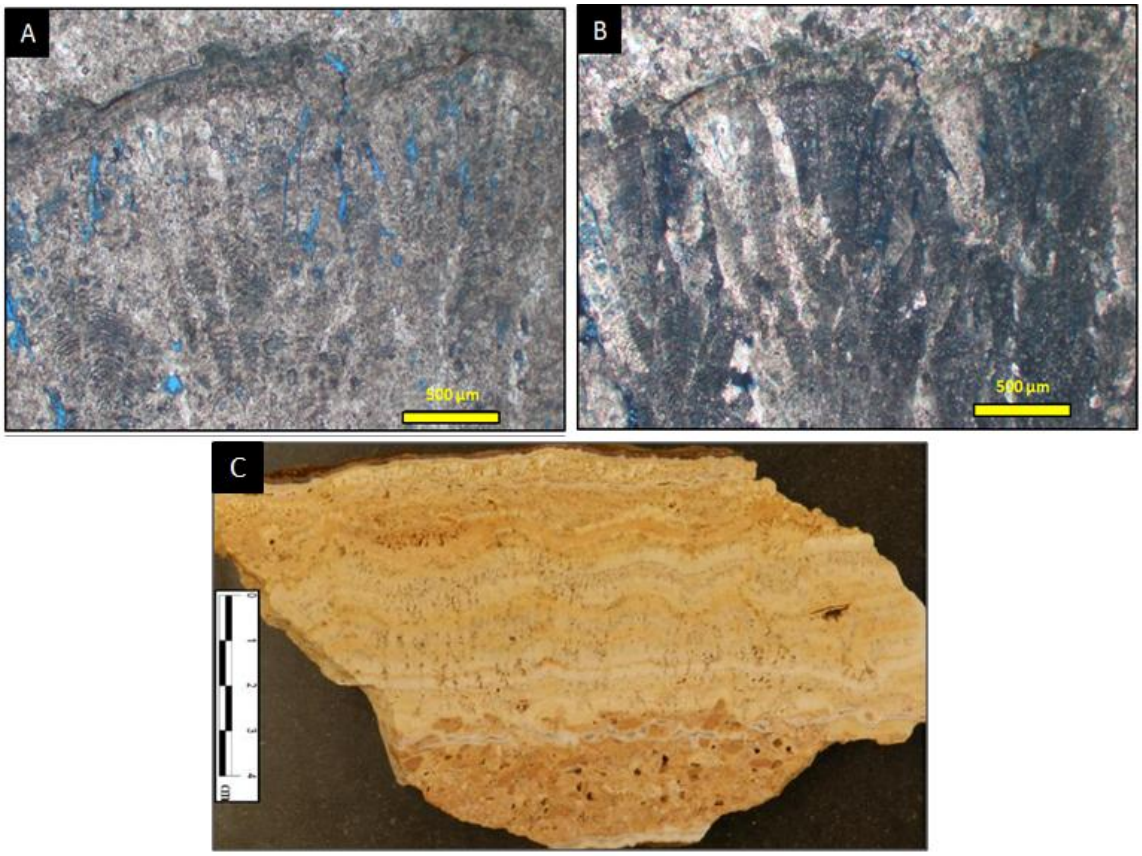

Figure 11: Photomicrograph of ray-crystals in plane light (A) and cross-polarized light (B). Note fine laminations that cut across individual crystals of calcite that display sweeping extinction. (C) Hand sample of ray-crystal overlying intra-clastic layer.

(Figure 11). The fine laminations are growth lines that are concave downward, extending away from the fan base. In thin section, the radiating calcite crystals that compose ray-crystal fans display sweeping extinction under cross-polarized light (Figure 11). Additionally, growth of adjacent ray-crystal fans can be variable. If two adjacent ray-crystal fans grow at an equal rate, growth lines are identically spaced between the two separate forms. However, if one grew at a faster rate than an adjacent crystal, the faster growing crystal will predominate and overlap the slower growing fan.

4.2.2 Bacterial Shrubs

Layers composed mainly of bacterial shrubs are the most dominant constituent of the mounds within this field area. In outcrop, layers of bacterial shrubs are laterally continuous for 10-70 m and are 3-50 cm thick. Layers of bacterial shrubs occur in packages of individual laminations that can be 0.2-2.5 cm thick. Shrubs nucleate on a substrate and form horizontal to sub-horizontal layers (Figure 12). Bacterial shrubs occur as vertically repetitious couplets of arborescent layers alternating with finely laminated micritic layers (Figure 13B). Micrite layers are typically 5-20 cm thick, interlaminated between shrub layers. The fine alternating laminae are readily observable in lightly weathered outcrops. In hand samples, bacterial shrubs appear as small bush-like growths that are light yellow to creamy white (Figure 12). Bacterial shrub layers are composed of multiple shrubs stacked in the layer, or a series of individual shrubs the thickness of the entire layer. Shrubs within a single layer are typically of the same height, whereas there may be significant variation of shrub height between different layers. Shrubs may nucleate from horizons of oncoids and envelope basal intramicrite layers (Figure 12). Individual intraclasts are commonly found suspended at the interface between shrub layers.

Figure 12: Hand sample of bacterial shrub layer overlying intramicrite layer. Brackets indicate change in constituents. (1) Platy intraclasts. (2) Smaller angular intraclasts suspended in micrite. (3) Bacterial shrub layer, note red arrow indicating where the overlying bacterial shrubs encrusted the intraclasts, suggesting a sudden shift in depositional environment. (4) Bacterial shrub layer with oncoids.

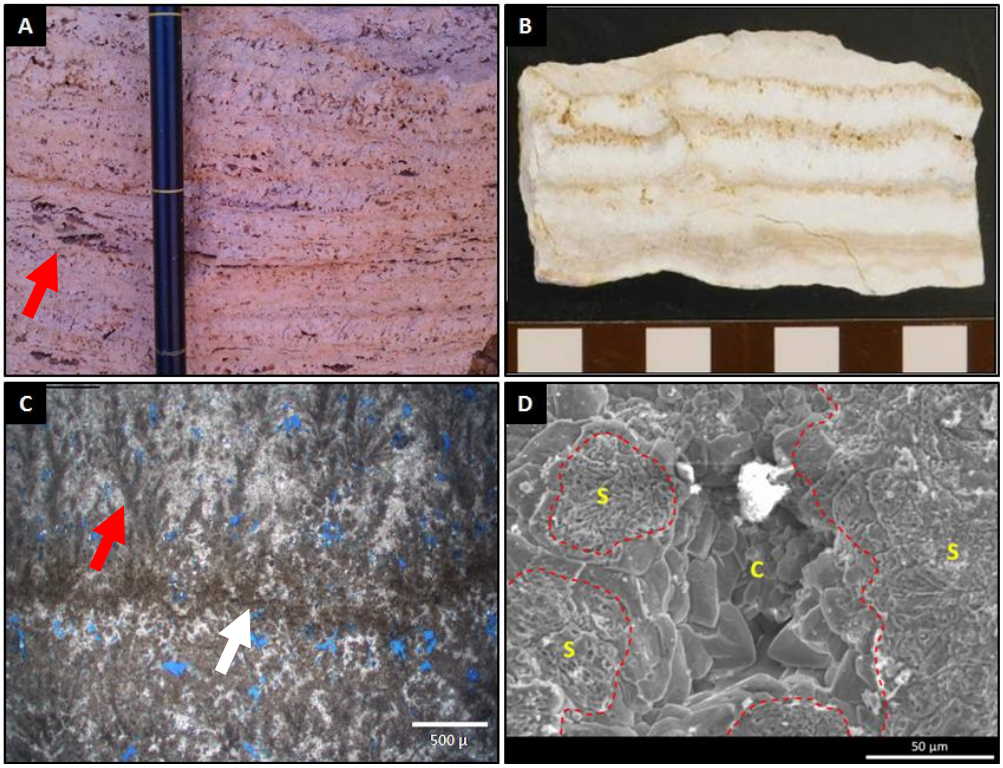

Figure 13: (A) Outcrop view of bacterial shrubs, red arrow indicates rafts. Scale at 0.1 m intervals. (B) Hand sample of bacterial shrubs. Scale at 1 cm intervals. (C) Photomicrograph of bacterial shrub layers in plane polarized light. Layers composed of bacterial shrubs (red arrow) and separated by a layer of intramicrite (white arrow). (D) SEM image of a vertical section showing microporous leaves [S] of a shrub surrounded by non-microporous spar cement [C]. The contacts between the bacterial leaves and the cement is in red dashed lines.

In thin section, arborescent-shrub growth have radiating ‘branches’ that are composed of multiple ‘leaves’, form an overall outward branching morphology of an individual shrub (Figure 13C). Each leaf is 0.03-0.5 mm long and is composed of clumps of micritic material encased in spar. In plane polarized light, the leaves of the bacterial shrubs are dark brown with no internal structure and display a wide range of shapes. The area between adjacent shrubs is either filled by spar or pore space. Due to the three-dimensional, branching nature of shrubs, individual leaves may be completely isolated by spar from the component branch. Scanning Electron Microscopy (SEM) analyses of the bacterial shrubs show that the micritic leaves contain an abundance of microporosity, whereas the surrounding spar cement does not (Figure 13D). The microporosity of bacterial shrubs is due to the initial carbonate precipitation on bacterial cells, which have since died and decayed, leaving behind extensive microporosity (Chafetz, 2013). The abiotic second generation precipitation of clear spar cement that envelops the bacterial shrubs did not contain bacteria during formation, thus leaving no microporosity (Figure 13D). Previous studies have observed that bacterial shrubs preferentially form in harsh environments that are beyond the habitable threshold of higher taxa. For example, Chafetz and Folk (1984) observed that bacterial shrubs are a common constituent within the H_2S-rich hot spring deposits of Tivoli, Italy. Petrographic and SEM analysis of spar cement from mounds at Lyman Lake found sheaths of gothic-arch calcite, an unusual crystal form in which the internal crystal lattice is arched due to the presence of sulfur (Figure 14) (Folk et al., 1985).

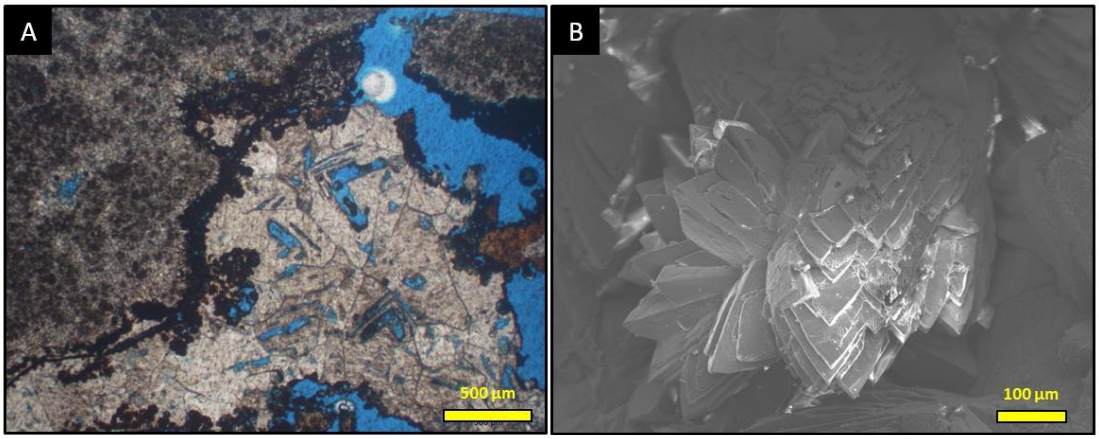

Figure 14: Gothic arch calcite crystals formed by the incorporation of sulfur into the crystal lattice. (A) Photomicrograph of gothic arch spar crystals in plane light. (B) SEM image of gothic arch crystals.

4.2.3 Oncoids

Oncoids are a less common constituent of mounds in the field area in comparison to bacterial shrubs. Oncoids are bacterially mediated coated grains, composed of a nucleus that is surrounded by cortices composed of bacterial shrubs radially oriented away from the nucleus. In select hand samples, oncoids appear concentrically laminated, alternating light yellow and tan layers (Figure 15B). Oncoids range in diameter from 1-15 mm and are spherical to discoidal, displaying a radially oriented, micro-shrub morphology with irregular shrubby profiles (Figure 15C). Oncoids typically occur in horizons between or above bacterial shrub layers, occurring in lenses 0.5-10 m long and 3-8 cm thick (Figure 15A). Oncoids may also grade laterally and vertically into intraclastic layers. In thin section, an accumulation of oncoids commonly coarsen upward and are surrounded by bacterial shrub growth. Oncoids display a range of growth forms, ranging from an incipient stage with thin cortices to well-developed gravel-sized individuals with thick cortices. The shape of oncoids is influenced by the shape of the

nucleus, the amount of hydraulic motion, and the thickness of the shrub cortical growth. For example, in environments where the oncoids are not agitated sufficiently, bacterial shrubs may preferentially grow on one side (Figure 15B). However, oncoids commonly display spherical to elliptical profiles with constant cortical thickness (Figure 15C). The nuclei of oncoids in the study area commonly consist of intraclasts, but nuclei may also be poorly defined rafts, clumps of micrite, or calcite crystals. The radiating shrubs cortices of oncoids display the same attributes as bacterial shrub layers. SEM analysis of oncoids confirms a similar microporosity to the bacterial shrubs, due to the decay of encrusted bacterial cells (Figure 15D).

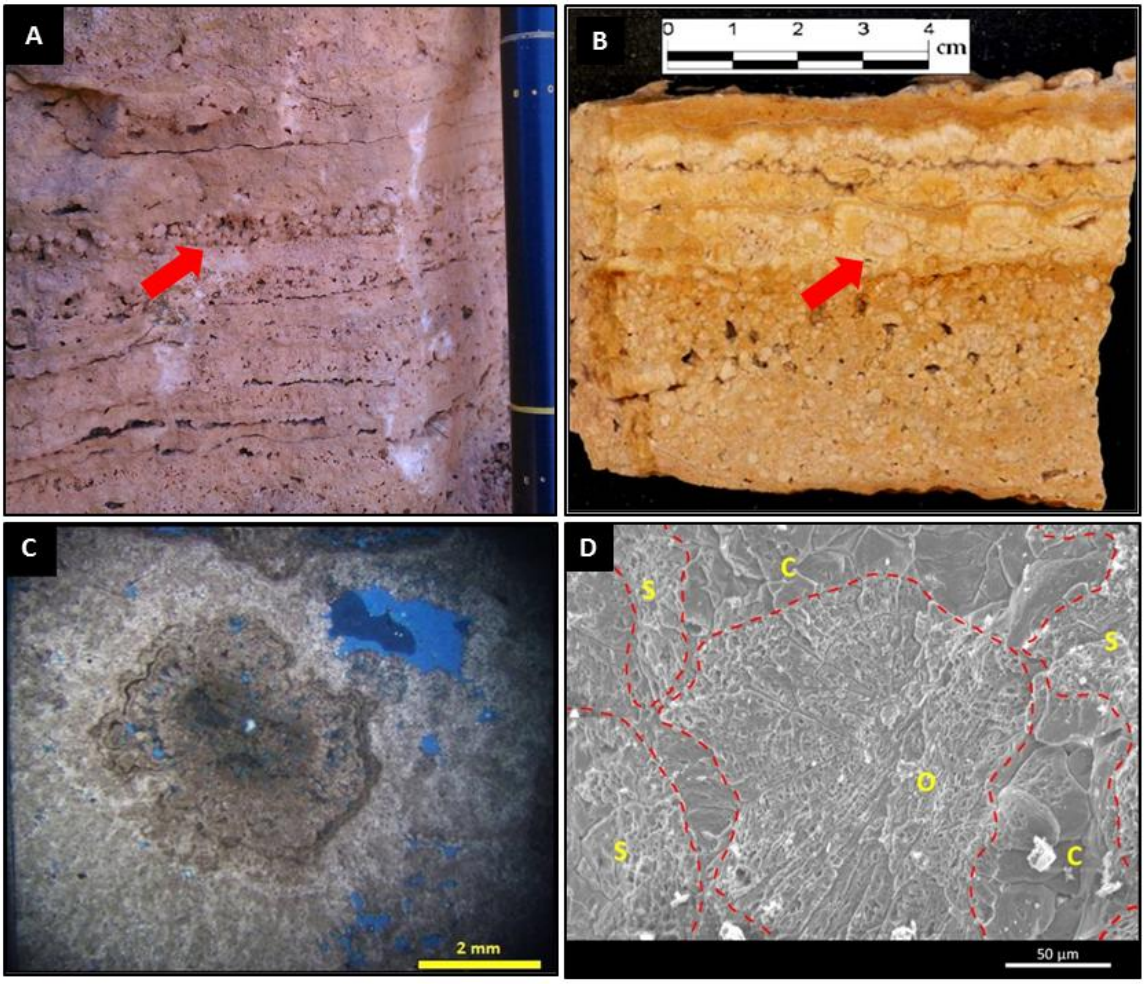

Figure 15: (A) Outcrop showing beds of oncoids indicated by red arrow. Scale interval at 0.1 m. (B) Hand sample of oncoids and shrubs, red arrow indicates an oncoid with preferential bacterial shrub growth on the top. (C) Photomicrograph in plane light showing oncoid. Note the irregular shrubby profile. (D) SEM image showing oncoid surrounded by spar cement and radial shrub growth. Note the microporosity present in the organically influenced oncoid compared to the lack of porosity in the abiotic spar cement. [O]-Oncoid [C]-Spar cement [S]-Bacterial shrub growth.

4.2.4 Rafts

Rafts are readily observable in outcrop, occurring in patches or lenses, either suspended in micrite or surrounded by bacterial shrub growth. Rafts range in length from 0.05-10 cm long and 0.1-0.8 mm in thickness. However, occurrences of rafts commonly are well sorted, displaying accumulations of similar size and thickness. Occurrences of rafts may be oriented chaotically or sub-horizontally The smaller chaotically oriented rafts are 0.5-4 cm long and commonly associated with grass molds and bacterial shrubs (Figure 16). However, larger sub-horizontally oriented rafts 4-9 cm long are commonly associated with micrite (Figure 17B). The large rafts suspended in micrite typically occur on the upstream side of pools created by dams or in wide pools on mound slopes. In thin section, rafts are composed of a central dark elongate micrite line 2-10 µm wide encrusted by calcite crystal growth 20-50 µm thick. The dark line in the center of the raft is the initial raft that rapidly developed on the water surface (Figure 16). After the raft

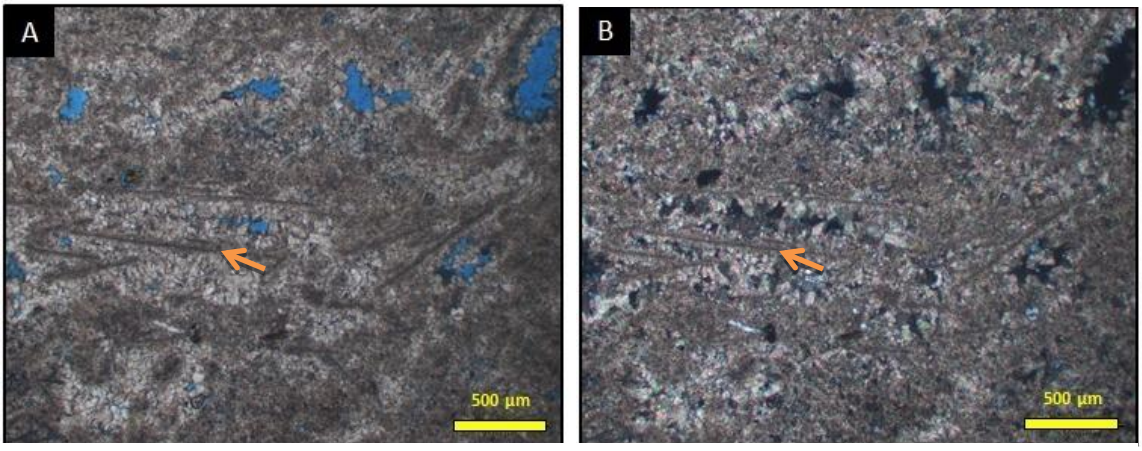

Figure 16: (A) Photomicrograph in plane light (A) and cross-polarized light (B) in same field of view showing small scale carbonate rafts. Lower portion beneath rafts are filled with spar, occluding shelter porosity. Orange arrows indicate dark central line of raft.

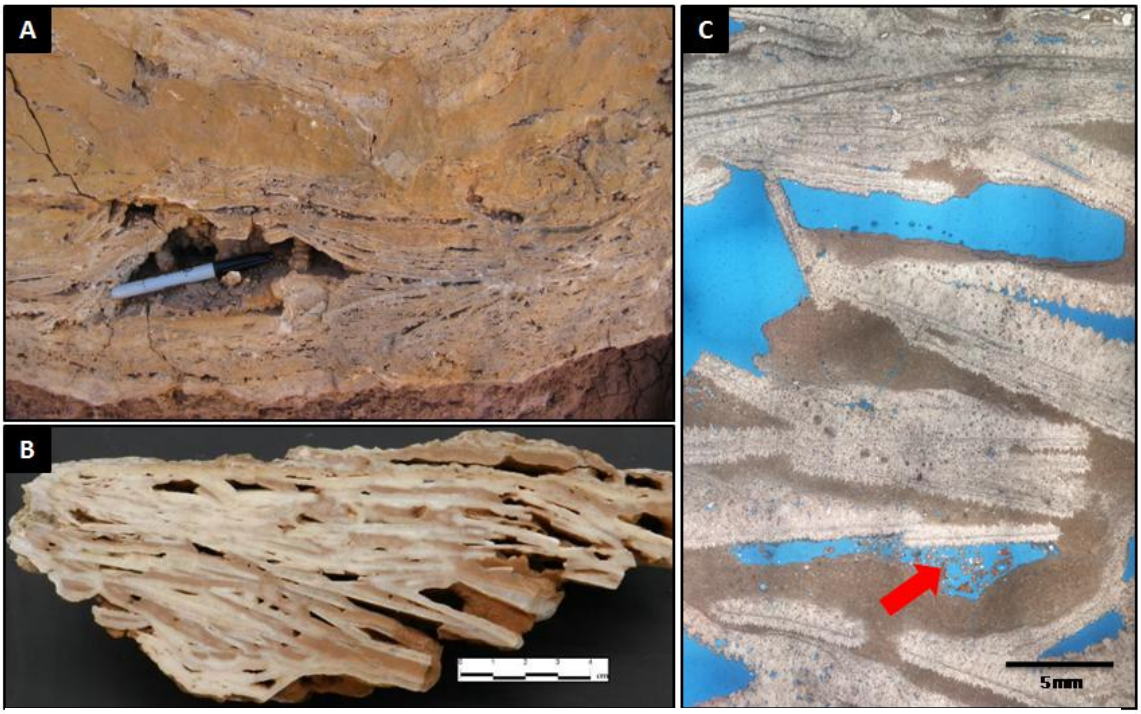

Figure 17: (A) Outcrop of micrite filled pool with large rafts. Permanent marker for scale. (B) Hand sample showing accumulation of rafts from a micrite pool. (C) Photomicrograph in plane light showing rafts suspended in micrite. Shelter porosity indicated by red arrow. Note asymmetric spar growth on raft. The thicker side formed facing downwards at the raft-water interface and the thinner side formed facing up at the air-raft interface.

grows, it will eventually sink under its own weight, settling to the bottom of the water column. Therefore, calcite encrustation on the lower surfaces of rafts is commonly thicker. However, rafts may have precipitation around the entire surface, indicating that precipitation on the raft occurred when the raft was completely submerged. Small rafts are the broken pieces of larger rafts, possibly damaged by a greater flow rate. Larger rafts were able to settle without a high flow rate disturbing them. The deposition of rafts commonly results in the creation of shelter porosity beneath them, yielding fenestral porosity that can only be filled by secondary cementation (Figure 17C). When a raft settles, the top part of the raft is covered by sediment and the raft shelters the area

underneath it from deposition, creating shelter porosity. Rafts are commonly thickened due to secondary encrustation during early diagenesis and also may be dissolved completely, leaving moldic porosity.

4.2.5 Intraclasts

Intraclasts and peloids are both included in this section, yet it is important to distinguish the difference between the two constituents. Intraclasts are formed pene-contemporaneously from erosion of rock either above or laterally adjacent to the intraclastic layer. However, peloid is a term given to a grain of an unknown micritic origin that has been obscured due to alteration. Constituents identified as peloids are likely intraclasts.

Intraclastic layers can be 3-40 cm thick, with individual grains ranging in size from 0.5-70 mm long (Figure 18). Intraclastic layers occur in laterally extensive lenses 40-70 m long, eventually pinching out distally. Intraclast layers are commonly interbedded with bacterial shrub layers and occasionally with oncoidal or micritic layers (Figure 18A). Intraclasts are angular to subangular and occur as oblate to platy fragments. In the measured sections of Mound-A, intraclastic layers display an upward trend towards thicker layers with larger grain sizes and an increased association with oncoidal layers. However, individual layers are commonly fining upward in grain size. Also, angular pieces of bacterial shrubs or ray-crystal shrubs were observed in the intraclastic layers, particularly in the basal portion (Figure 19). This erosion is caused by the high flow rate

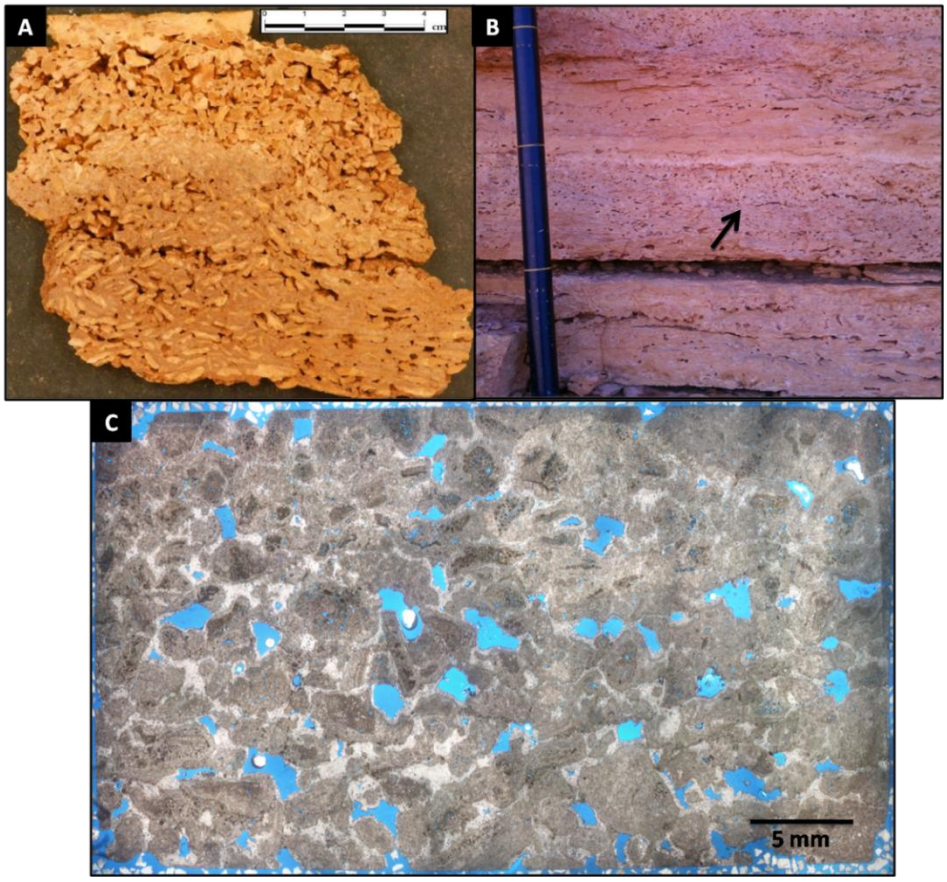

Figure 18: (A) Hand sample of intramicrite layer. (B) Outcrop of intramicrite overlain by bacterial shrubs. Scale at 0.1 m intervals. (C) Plain light photomicrograph of intramicrite.

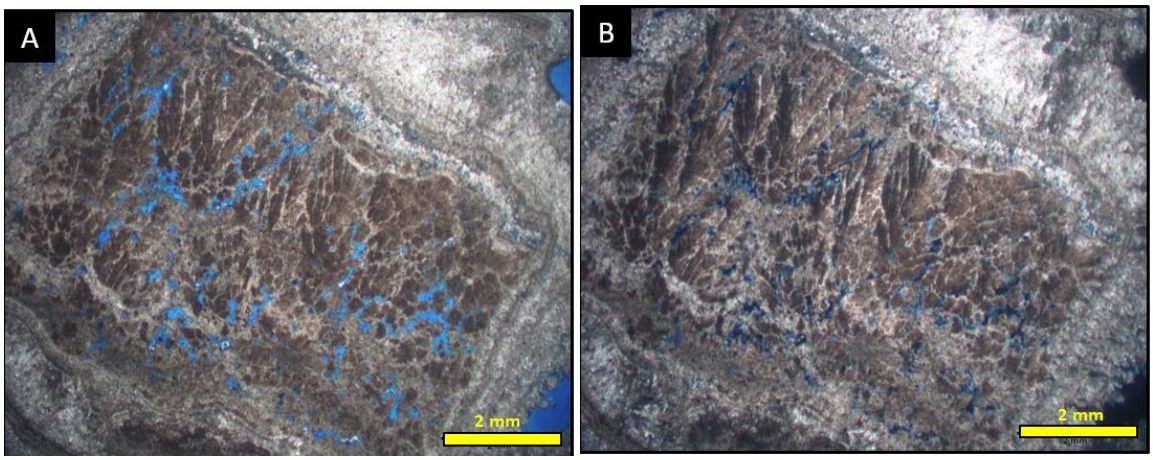

Figure 19: Photomicrograph in plane light (A) and cross-polarized light (B) of same field of view showing an intraclast derived from a ray-crystal deposit, which was coated in bacterial shrub growth.

associated with the derivation and transportation of intraclasts. Erosional boundaries are not undulatory, instead generally conforming to the attitude of the underlying layer. In addition, oncoidal layers beneath intraclasts are sometimes truncated, but more commonly exhibit a gradational boundary. Intraclasts may also be derived from the erosion and collapse of waterfalls or terraces. Intraclastic fragments are common on the distal side of dams, producing angular, platy fragments 0.5-7 cm long suspended in red-brown micrite. Spar is most commonly found in the intergranular space between intraclasts due to the high porosity created by the large well sorted grains. Spar is commonly thicker on the lower surfaces of intraclast grains, indicating precipitation under the effects of gravity in a vadose environment (Figure 18C).

Peloids, likely well rounded and micritized intraclasts, have spherical to oblate shapes, with diameters commonly ranging from 50-2000 μm. Layers of rounded intraclasts consist of a structureless clotted matrix of intraclasts suspended in spar. These intraclastic grains occur either as individuals or as aggregates. In intraclastic aggregates, individual intraclasts are observed with well-defined boundaries and are separated by micrite (Figure 20A). However, many aggregated intraclasts consist of closely spaced individual grains, causing individual boundaries to become indistinct, resulting in a clotted appearance (Figure 20B). Sparry calcite cement is common in intraclastic layers, encrusting grains in microspar. In addition, intraclasts are the most susceptible of the allochems to dissolution, re-precipitation replaces the micritic intraclasts with microspar.

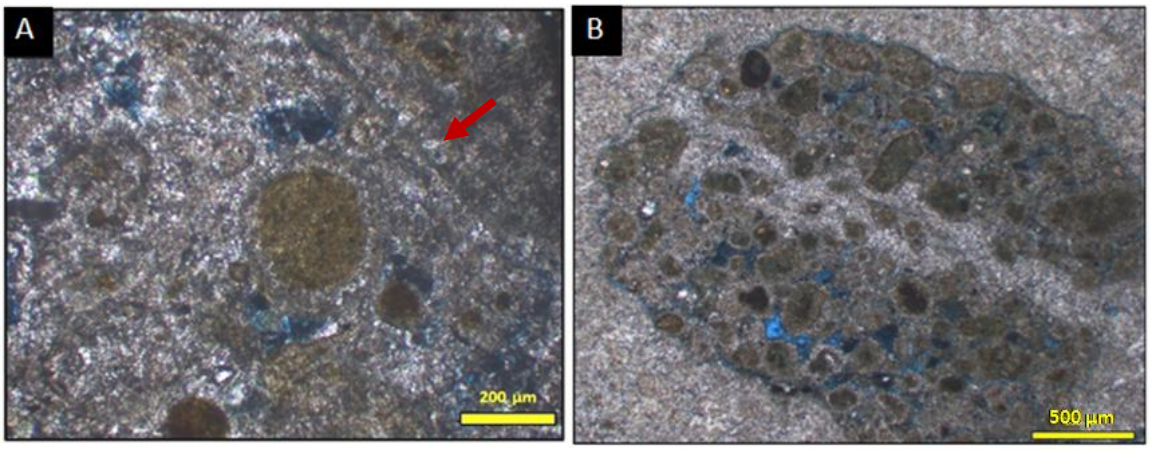

Figure 20: (A) Photomicrograph in cross-polarized showing individual rounded intraclastic allochems, raft indicated by red arrow. (B) Photomicrograph in cross-polarized light showing an aggregated intraclast with a spar vein running through the allochem.

4.6.6 Reed and Grass Travertine

Reeds and grasses in a travertine system commonly produce moldic porosity, caused by the decay of the encrusted plants. Reed molds are readily visible in outcrop and can be 4-15 cm long and 0.5-2 cm in diameter (Figure 21). However, grass molds commonly are 1-3 cm long and 1-4 mm in diameter (Figure 22A). Reeds and grass are commonly associated with each other, as well as with bacterial shrubs and rafts, generally occurring in clusters or lenses 2-4 m in length (Figure 22C). Reed molds typically display striations oriented parallel with the long-axis of the mold, presumably reed stalk impressions (Figure 21). In addition, reed molds are commonly red-tan with a creamy white ring of carbonate encrustation present around the molds (Figure 21). Reeds may occur as sparse individuals or an abundant clustering that may have obstructed water flow. The clustering and encrustation of reeds and grasses may entrap other constituents. Reeds are commonly vertically oriented or tilted downslope, whereas phytoclastic reed molds are commonly sub-horizontal and the long axis is interpreted to be aligned with the

paleo-flow direction. It is common for calcite crystals to form within the molds of reeds and grass, growing inward in typical void-fill pattern.

Figure 21: Reed mold in outcrop. Red arrows indicate reed molds. Note internal striations and coloration. Scale in centimeters.

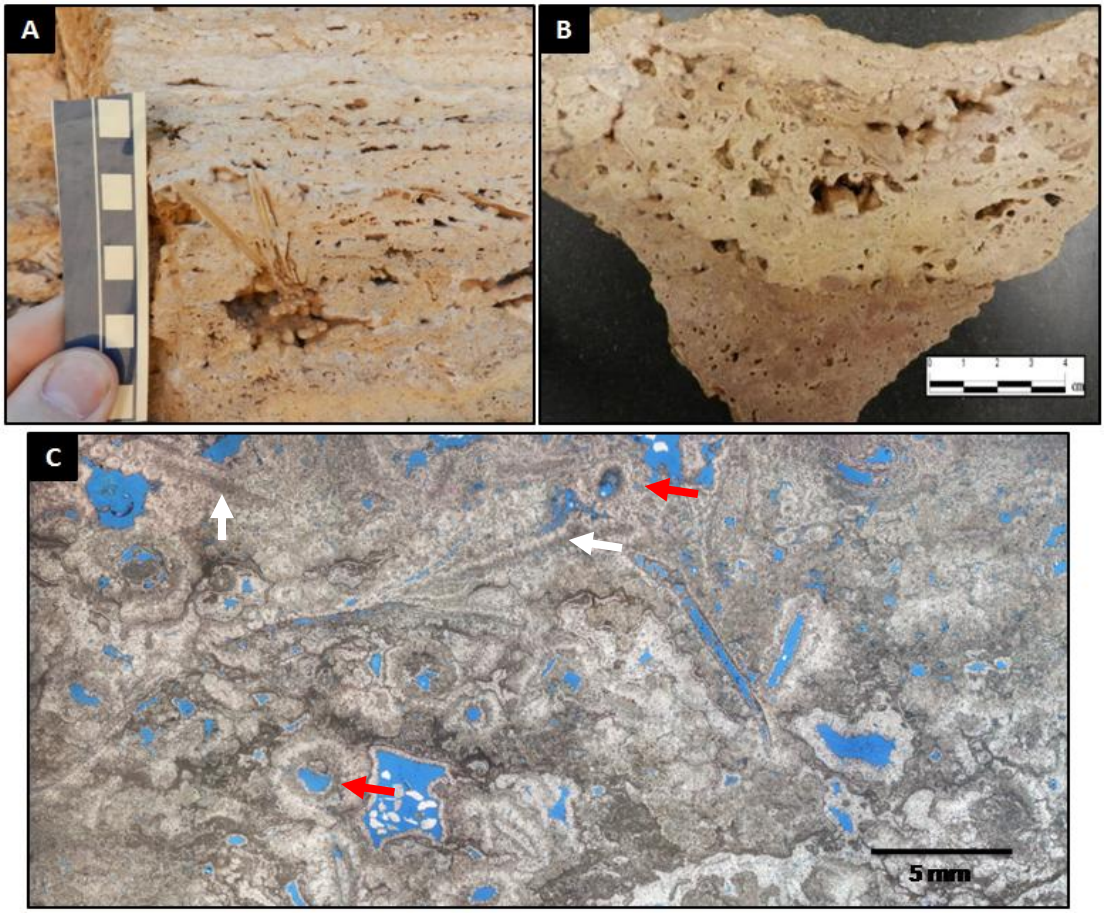

Figure 22: (A) Outcrop view of grass molds. Scale at 1 cm intervals. (B) Hand sample of grass molds overlying intraclastic layer. (C) Photomicrograph in plane light of grass molds, red arrows indicates reed molds, white arrows indicates rafts.

4.3 Mound-A: Depositional Morphologies and Facies

Facies analysis can provide clues when reconstructing the evolution and development of a mound. The road-cut through the western edge of Mound-A allows for good exposure of well-preserved samples and an extensive cross-sectional view (Figure 23). Therefore in examining Mound-A, a detailed facies study was conducted. In performing this study, measured sections were taken along the road cut, beginning at the

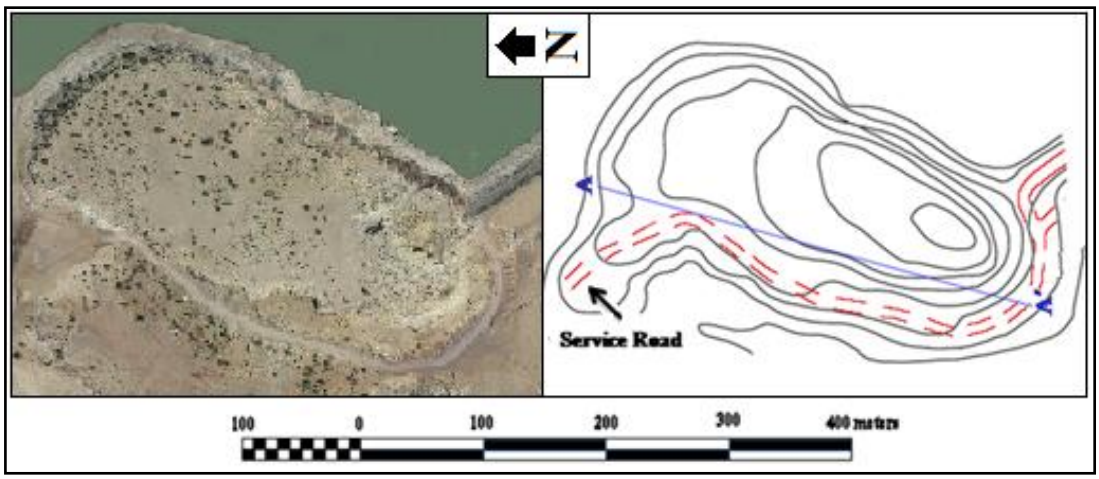

Figure 23: Mound-A aerial view and topographic map depicting line of cross section A-A' in Figures 25 and 26. Service road is marked by red dashes. Contour Interval: 20 ft (6.1 m).

southern end of the outcrop, which is most proximal to the vent, with successive sections extending to the north. The facies in this mound are the product of a radial flow of water away from the vent over a sub-horizontal mound surface. Mound-A is predominantly composed of bacterial shrubs, intraclastic layers, oncoidal layers, and ray-crystal slopes. By using mound morphology and constituents, Mound-A can be readily divided into 7 facies, comprising six periods of growth. Facies include vents, reed buildups, ray-crystal slopes, distal plaudal deposits, and bacterial shrubs interbedded with intraclastic layers.

4.3.1 Mound Vents

Vents were preserved in many mounds throughout the area, although stratigraphic sections and petrographic samples were only collected form Mound-A. Many of the mound vents were heavily weathered, yet displayed a similar morphology and anatomy. A general archetype can be constructed from the collected observations of vent exposures

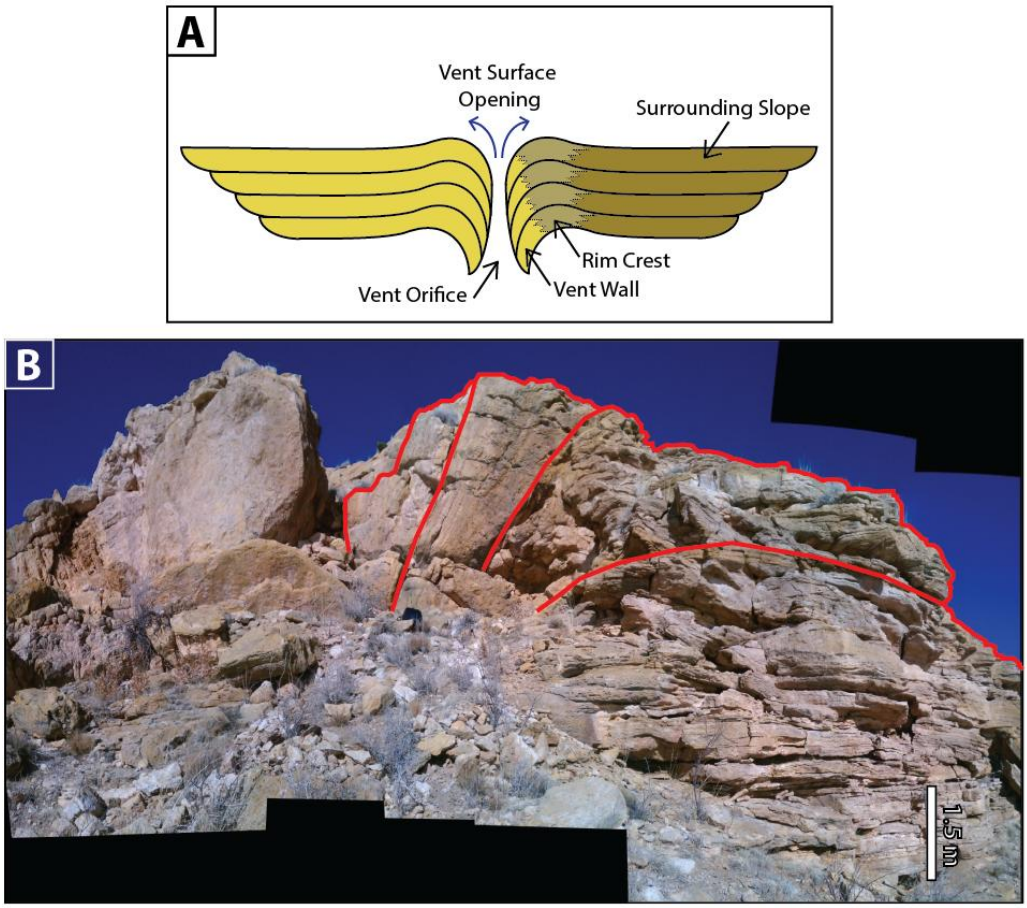

Figure 24: (A) Cross-sectional archetype for mound vents within the area. (B) Outcrop from Mound-B showing cross-section of vent, note change in dip of beds outlined in red.

within the area (Figure 24). Mound vents are sites where upwelling water collected in bowls with smooth walls, from which water overflowed onto the adjacent mound. Little is known of the original size, shape, and nature of the vent due to weathering. The vent in Mound-B is composed of multiple layers 0.1-0.4 m thick forming the vent wall and the surrounding mound (Figure 24). The vent wall is nearly vertical and the surrounding layers dip radially away from the crest. Layers at the crest of the vent, change dip in a concave downward nature as they transition from the vent wall into the surrounding

layers. The symmetry of some of the mounds may be related to the formation of dam-like rims at the orifice. These rims build so that the overflow of water is approximately equal all-round the mound, ensuring its regular form. However, it is likely that the mound outlines become irregular, presumably in response to minor differences in ground level or the overlapping of surrounding springs. The vent in Mound-A is partially eroded, therefore there is no preservation of the interior vent wall. Instead, this outcrop displays the immediately adjacent distally sloping layers adjacent to the vent wall, composed of shrub layers with interbedded intraclasts and veins of displacive spar. Microterracing was observed on Mound-B, and only located at the vent. A large displacive calcite vein is present in the vent, oriented parallel-subparallel to the bedding planes. The large calcite vein is composed of dense white botryoidal calcite crystals, and occurs as a lens extending 8 m with a variable thickness of 0.05-0.2 m. Smaller veins occur between layers and are composed of gray to white spar crystals 1-5 cm thick oriented with the bedding plane.

4.3.2 Basal Intramicrite Layer and Chinle Formation

At the southern-most portion of the western edge of Mound-A, the proximal part of the accumulation, exposed by the road-cut, there exists well layered travertine overlying a 1.5-2 m thick layer of red calcareous silt with undulatory travertine lenses 40 m long and 3-50 cm thick. The contact between the calcareous silt and the cross-bedded sandstone of the Chinle Formation is obscured by alluvium and debris. The rest of the Chinle Formation in the western outcrop is heavily covered by debris and alluvium. Nevertheless it can be observed that the Chinle Formation is present as a 2 m thick

conglomeritic deposit. The bottom layer of Mound-A, unconformably overlying the Chinle Formation, is composed of an intramicrite base that is continuous for 56 m, however, distal portions are obscured by alluvium (Figure 25). The basal intramicrite layer is undulatory with a variable thickness, thinning out distally to the north away from the vent (Figure 26). Additionally, this layer displays a decrease in grain size and an increase in the degree of sorting trending to the north. The proximal portion of the layer closer to the vent is composed of angular to subangular intraclasts 0.1-10 mm in length (Figure 27). However, the distal end of the basal layer is composed of subrounded intraclasts 0.4-8 mm in length. In addition, quartz grains and a high proportion of ray-crystal derived intraclasts are only found within the basal layer of the mound (Figure 27C).

4.3.3 Plaudal-Reed Buildups

Overlying the basal intramicrite layer in Mound-A are a series of ray-crystal dams capping the high-point of several reed buildups (Figure 25 and 26). The reed buildups and associated dams form a layer that ranges from 0.1-0.3 m thick, extending laterally for 4 m before pinching out (Figure 26). This paludal layer consists of five reed accumulations spaced 0.2-0.6 m from each other and 0.5-1.5 m high, decreasing in size downslope (Figure 28). In carbonate spring systems, plants are quickly encrusted and stabilized by the precipitation of finely crystalline carbonate, which may form in situ clumps that act as an organic baffle that traps transported phytoclastic material. The reed buildups are composed of in situ plants that are vertical or tilted to the north away from

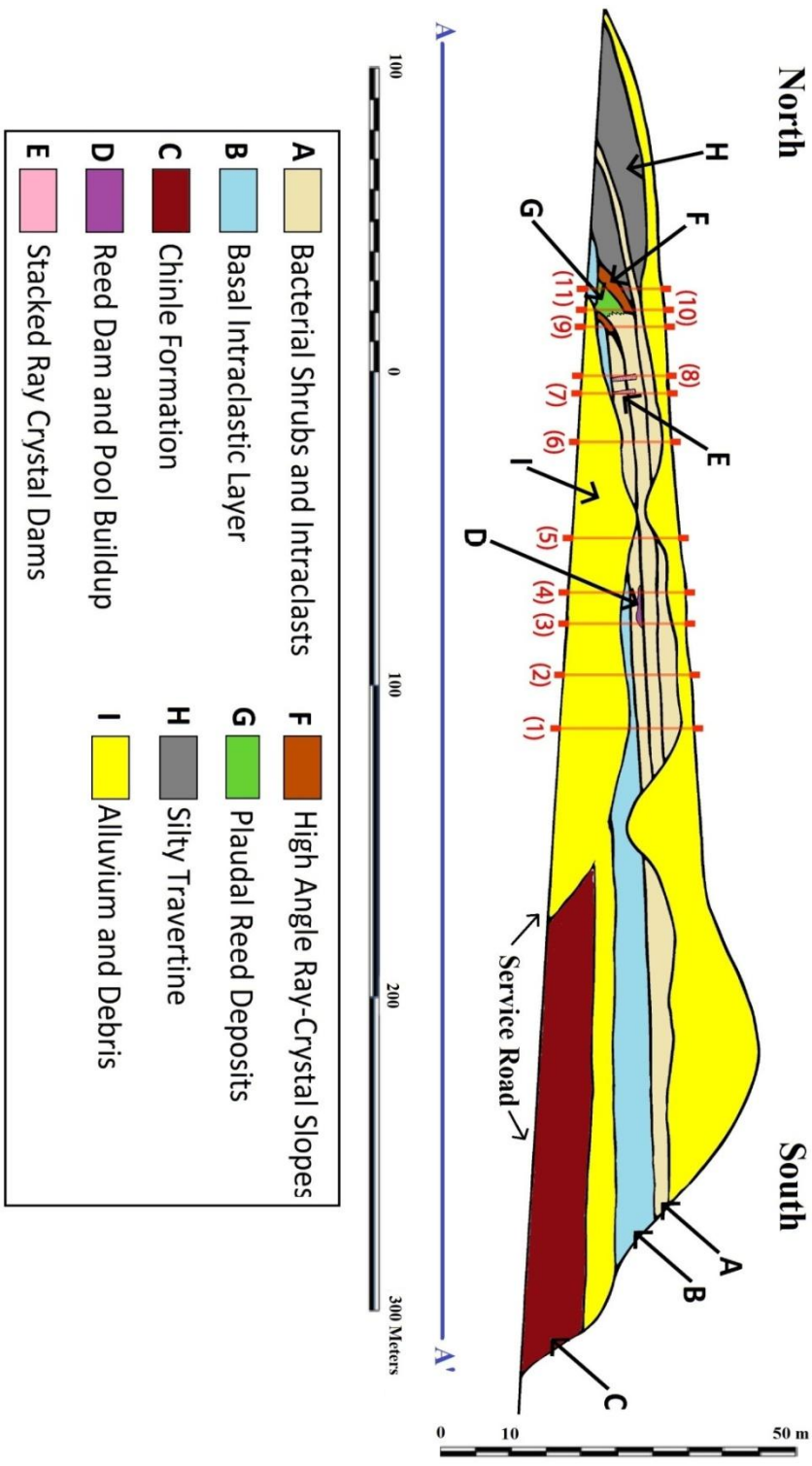

Figure 25: Mound-A cross-sectional view of the outcrop adjacent to service road. Cross-section location shown in Figure 23. Facies and features are color coded and marked with letters. Locations of stratigraphic columns shown in Figure 26 are marked in red.

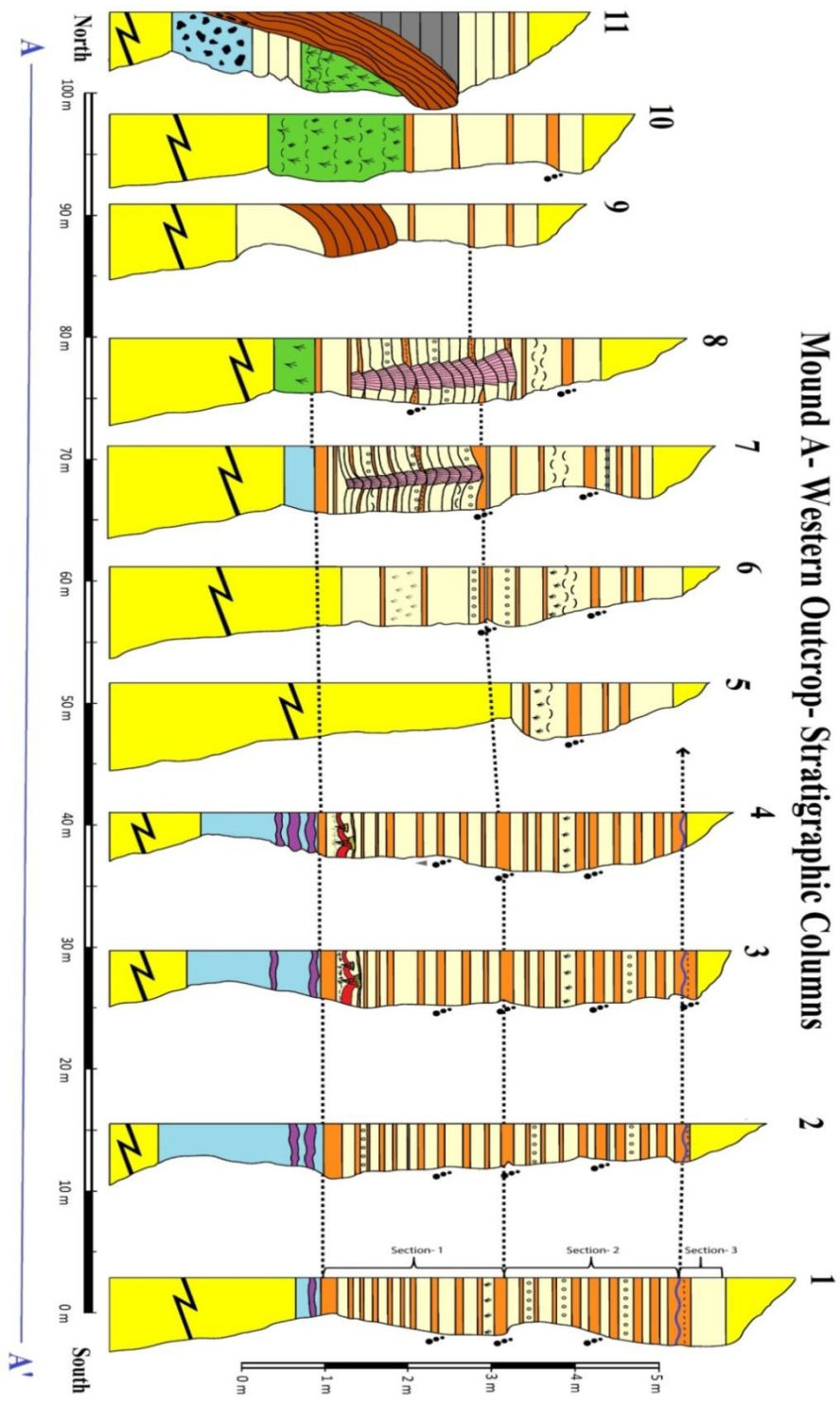

Figure 26A: Stratigraphic columns for western outcrop along road cut. Legend and locations of columns shown on Figures 25 and 27. Dashed lines indication proposed sections of interbedded bacterial shrubs and intraclastic layers, sections labeled with brackets.

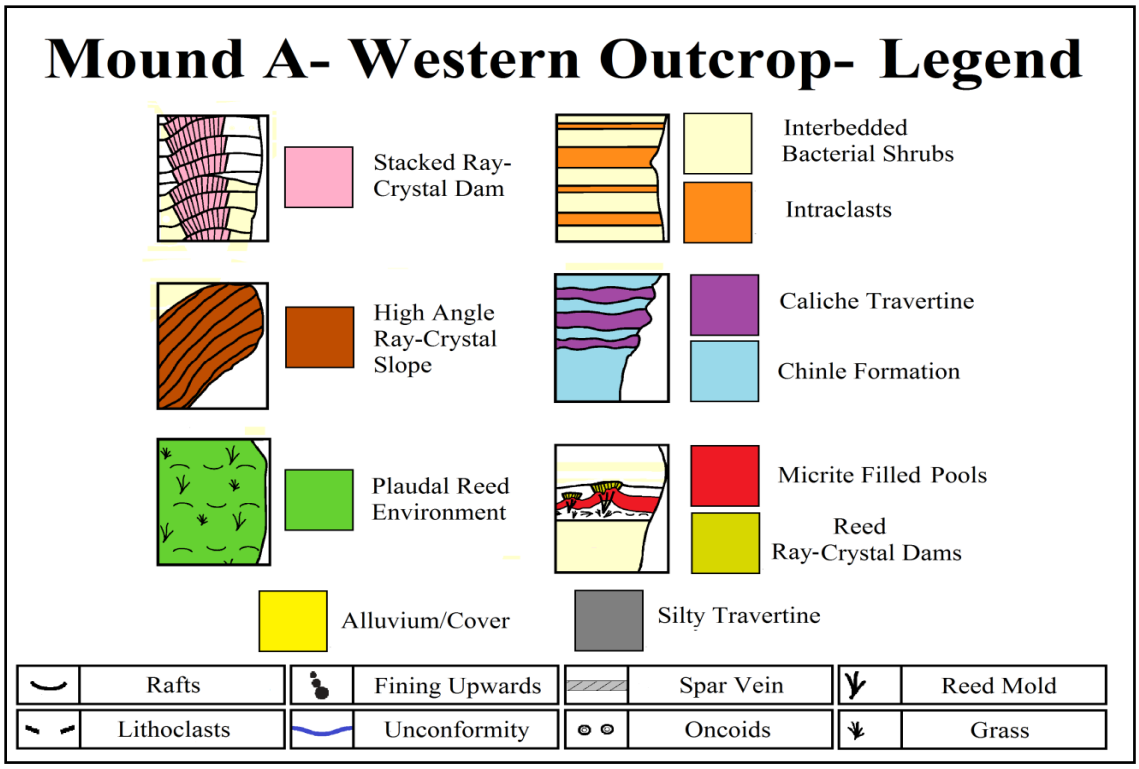

Figure 26B: Legend for Mound-A stratigraphic columns

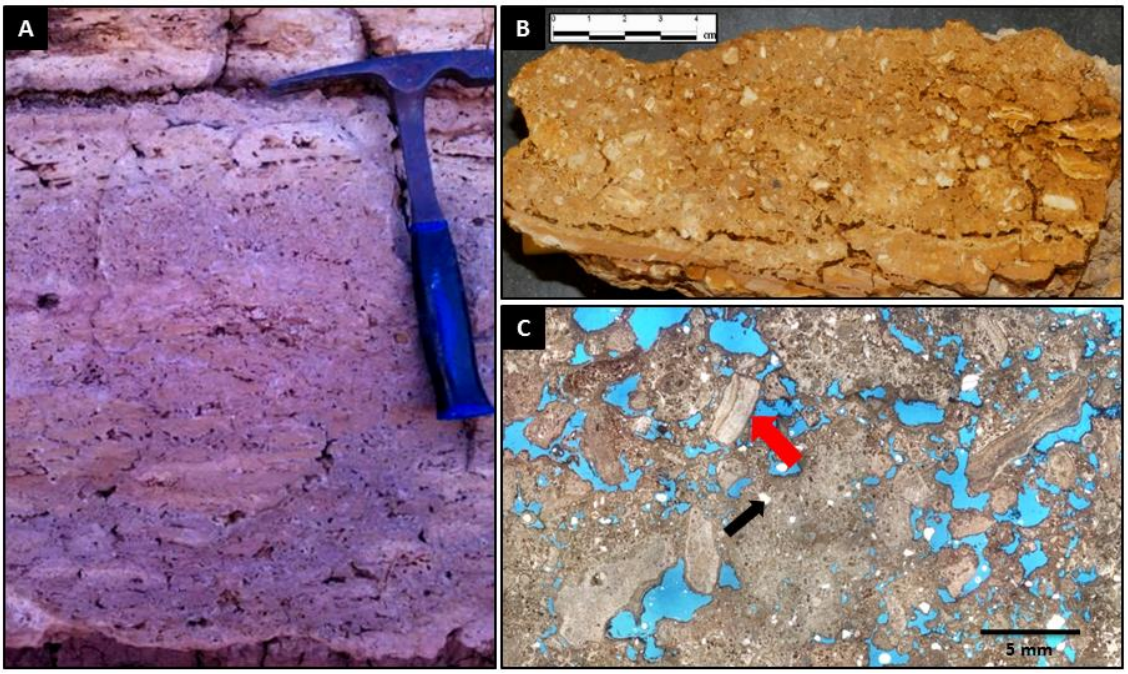

Figure 27: (A) Outcrop of basal intramicrite layer. Rock hammer for scale. (B) Hand sample from basal intramicrite layer. (C) Plain light photomicrograph from basal intramicrite layer. Red arrow indicates reworked ray-crystal intraclast. Quartz grains were only found in this layer, indicated by a black arrow.

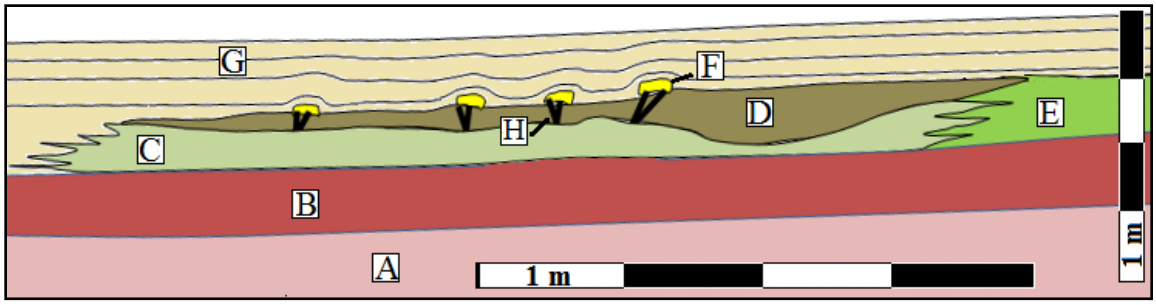

Figure 28: Schematic showing spatial relations adjacent to reed buildups. A – Chinle Formation. B – basal intramicrite layer. C – Bacterial shrub layers rich in grass molds and small rafts. D – Encrusted reed and grass molds oriented northwest-southeast. E – Pools associated with reed dams, filled with micrite and rafts. F – Ray crystal dams atop reed molds. G – Bacterial shrub layers. H – Vertically oriented reed molds acting as organic baffles. Scale bar with 1 m intervals.

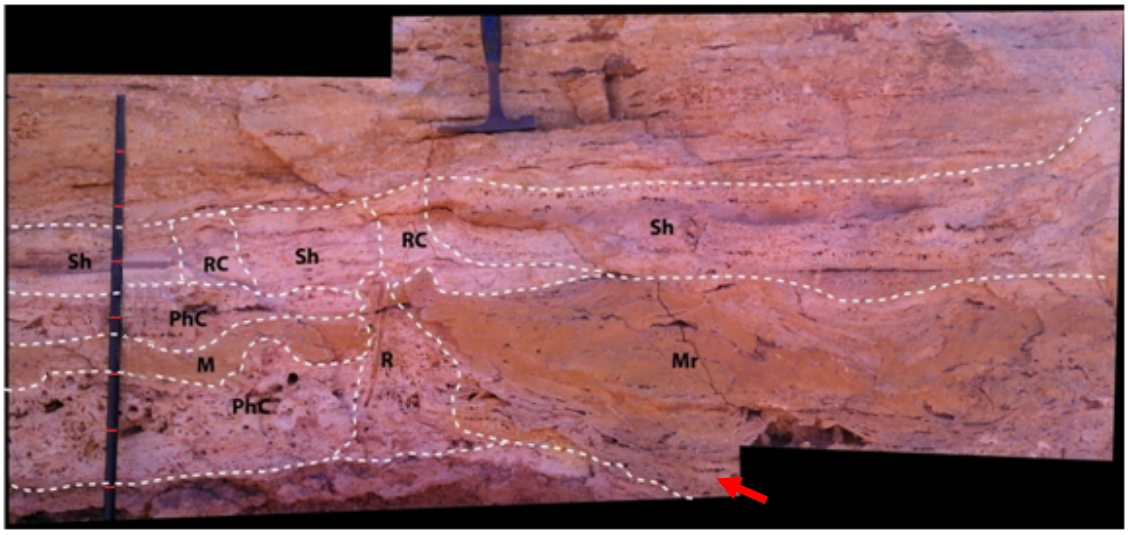

Figure 29: Outcrop photograph of reed buildup. R – Reed molds. Mr – Micrite with rafts. M – Micrite. PhC – Phytoclasts. Sh – Bacterial shrub accumulations. RC – Ray-crystal dam. Red arrow indicates rafts. Rock hammer and scale bar with 0.5 m intervals for scale.

the vent, whereas trapped phytoclastic material is oriented west-northwest east-southeast, parallel to flow from the vent of Mound-A. Additionally, overlying beds initially dip down the paleo-surface created by the dam, but become sub-horizontal after 0.1-0.2 m laterally.

Ray-crystal dams 5-10 cm tall form on top of the encrusted reed buildup and are associated with laterally adjacent bacterial shrub layers. Pools occur on the upstream side as water flow is obstructed and slowed (Figure 29). In association with the encrusted reed buildups are a series of upstream pools filled with micrite and paper-thin rafts. Pool deposits occur as asymmetrical lenses that are thickest near the reed buildups, the pool deposits ranged in size from 0.3-2.5 m long and 0.2-0.5 m thick (Figure 29). The large proximal pool accumulation contains rafts that become smaller and more chaotically

oriented away from the reed buildups with an increasing amount of associated grass molds. Rafts and fine micrite are a common component of pool accumulations, due to the quiescent hydraulic conditions that allowed for the deposition of these allochems. The pools associated with reed buildups contain the largest rafts observed in Mound-A, ranging from 3-10 cm long. Rafts are suspended in brown micrite, creating shelter and fenestral porosity.

4.3.4 Ray-Crystal Slope Facies

4.3.4.1 Stacked-Smooth-Slope Dams

There are two stacked smooth slopes located 65 m and 73 m north of the vent, respectively called the proximal and distal stacked slopes (Figure 30). The stacked smooth slopes are a series of sloping ray-crystal layers that aggraded on top of each other,

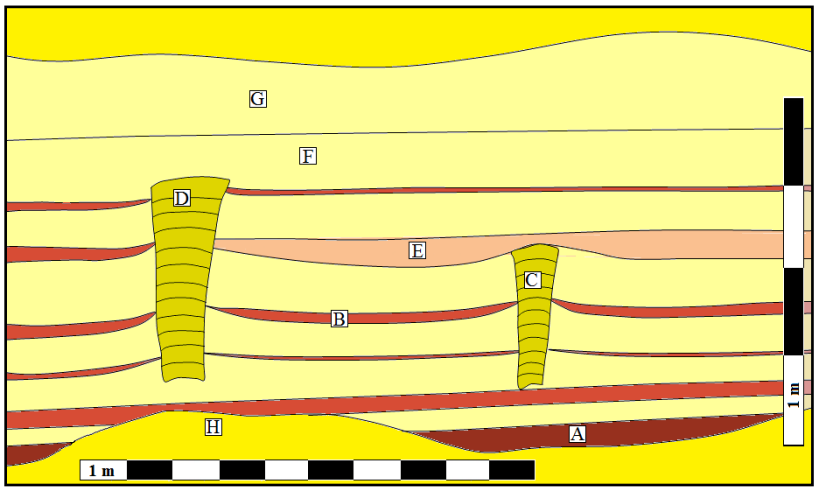

Figure 30: Schematic showing spatial relationship of stacked smooth slope columns. A – basal intramicrite layer. B – Intramicrite layers. C – Proximal ray-crystal column. D – Distal ray-crystal column. E – Intramicrite that overlies and conforms to top of proximal column. F – Bacterial shrub layers. G – Bacterial shrub layers rich in rafts. H – Alluvium cover. The stacked smooth slope columns are 8.5 m apart. Scale bar with 1 m intervals.

composed of individual ray-crystal layers 1-2 cm thick and 0.1 m long (Figures 31 and 32). The proximal stacked smooth slope column is 1.5 m high whereas the distal stacked smooth slope column is 2 m high. Both columns range in width from 0.2-0.3 m. Beds adjacent to the columns are composed of interbedded intramicrite and bacterial shrub layers, 6-30 cm and 5-20 cm thick, respectively (Figures 31 and 32). Adjacent layers thin and terminate against the stacked slope columns, but are similar in thickness and lithology on both sides of the columns. Because layers adjacent to the column cannot be traced through the dam surface, yet are similar on opposite sides, it is likely that the ray-crystal slope grew contemporaneously with the formation of adjacent layers. Beds on both sides of the slope have a similar lithology, there are some small differences in the proportion and character of allochemical constituents. Small rafts are abundant behind the stacked column, whereas intraclasts are more abundant downslope, indicating some pooling behind the stacked slope. Angular to platy intraclasts 0.5-7 cm long derived from ray-crystals are present on the downstream side and are and suspended in micrite. Above the proximal ray-crystal column is an intramicrite layer that varies in thickness and conforms to the sloped surface created by the stacked smooth slopes (Figure 30).

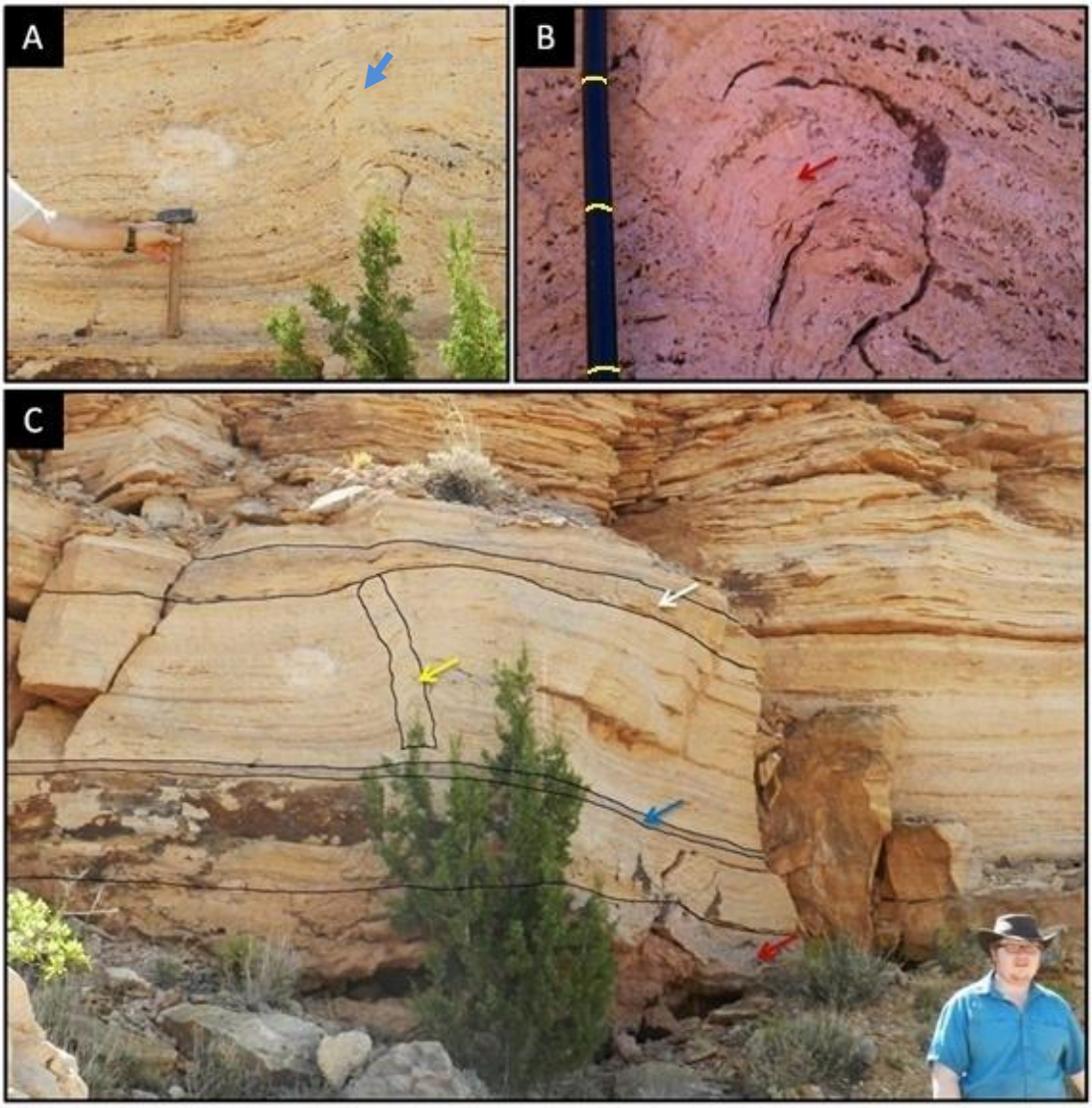

Figure 31: (A) Outcrop photograph showing the first (proximal) stacked smooth slope dam and adjacent bedding. Blue arrow indicates stacked smooth slope. Rock hammer for scale. (B) Close-up photograph of individual ray-crystal layers within the stacked column, red arrow indicates one sloping layer. Meter stick with 0.1 m intervals for scale. (C) Outcrop photograph of the proximal stacked smooth slopes, red arrow indicates basal intramicrite layer, blue arrow indicates continuous intramicrite layer, yellow arrow indicates stacked smooth slope dam, white arrow indicates micrite drape.

Figure 32: (A) Outcrop photograph of the distal stacked ray-crystal slope, white arrow indicates stacked slopes, black arrows indicate distal intraclastic layers that pinch adjacent to slopes. Scale bar with 0.5 m intervals for scale. (B) Close-up photograph of intraclastic layers that pinch adjacent to slopes, red arrow indicates intraclastic layer that abuts stacked ray-crystal smooth slope. (C) Close-up photograph of individual layers within the stacked slope. Meter stick for scale with 0.1 m intervals.

4.3.4.2 Distal-Edge High-Angle Smooth Slopes

There are two distal edge smooth slope deposits in the distal portion of the western road-cut (Figure 33). These sloping deposits are concave downward structures that display a marked break in slope, where sub-horizontal beds rapidly change attitude by steeply dipping toward the distal end of the mound. The proximal sloping deposit is located 18 m away from the distal stacked smooth slope, and is heavily weathered and largely obscured by debris. The proximal sloping deposit is 2 m thick, dips 35° downward, and overlies heavily altered, convoluted bedding. The distal sloping deposit is located 15 m away from the proximal sloping deposit. This distal slope is 1.5-2 m tall, 0.3-0.5 m wide, and abruptly dips down at an angle of 45° (Figure 34).

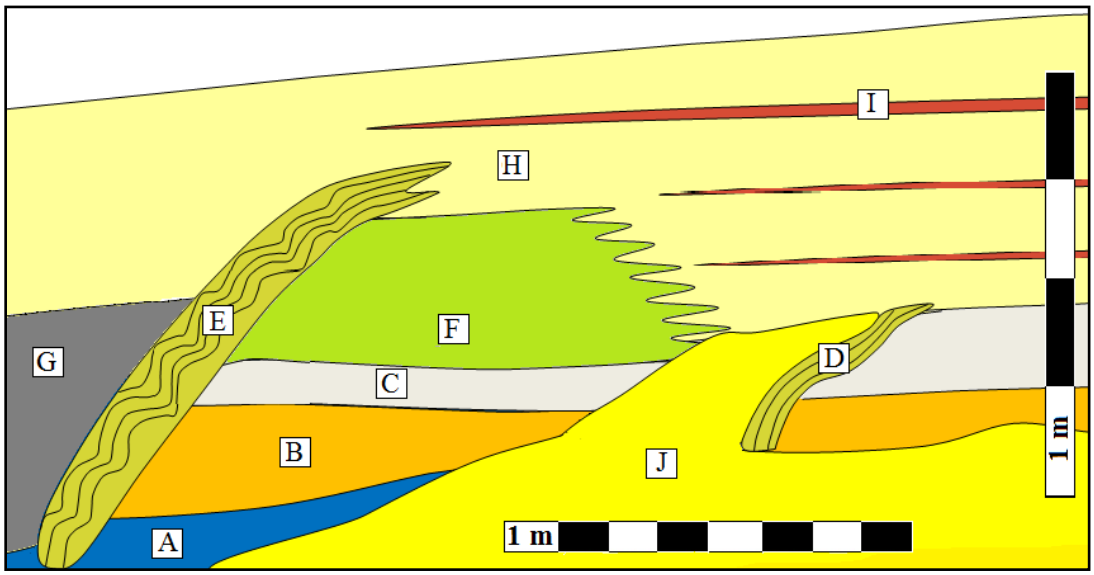

Figure 33: Schematic showing spatial relationship for distal edge smooth slopes. A – Conglomerate from the Chinle Formation. B – Calcite cemented gravel deposit, pinches out proximally. C – Highly altered bacterial shrub layers. D – First distal edge smooth slope. E – Distal edge smooth slope. F – Paludal reeds with associated grass molds and rafts. G – Silty travertine that composes the proximal edge of the mound. H – Bacterial shrub layers. I – Intraclastic layers that pinch out distally. J – Alluvium cover. Scale bar with 1 m intervals.

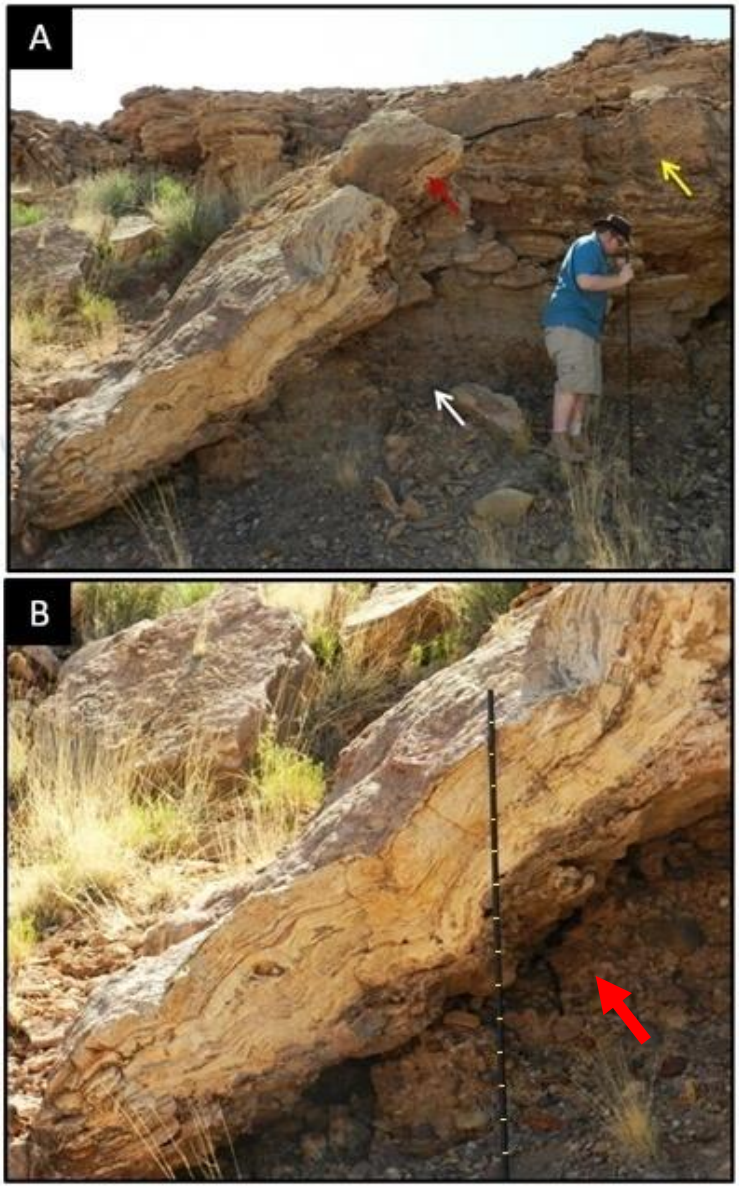

Figure 34: (A) Outcrop photograph of distal edge smooth slope, red arrow indicates ray-crystal slope deposits, yellow arrow indicates paludal reed facies, white arrow indicates conglomerate from Chinle Formation. (B) Close outcrop view of northern ray-crystal slope, red arrow indicates where gravel is incorporated into base of the smooth slope. Meter stick with 0.1 m intervals for scale.

The distal slope overlies a conglomerate deposit of the Chinle Formation, incorporating gravel in the base of the sloping deposit (Figure 34). The smooth slope consists of dense ray-crystal shrubs forming layers 0.1-0.5 m thick, oriented perpendicular to the bedding, that are finely laminated. The proximal slope is composed of multiple layers which display identical attitude with the dip of the distal smooth slope

deposit. However, the distal sloping deposit is composed of multiple scalloped laminae with a concave downward shape that eventually gradate upslope into planar laminae. The proximal side of the sloping deposits gradates laterally into continuous sub-horizontal interbedded intraclastic and bacterial shrub layers. The interbedded intraclasts and shrubs associated with the stratigraphically higher distal slope overlie those associated with the proximal slope. Overlying the distal slope is a 1.5-2 m thick layer of horizontally stratified interbedded intraclasts and shrubs that is continuous for 200 m thinning to 1 m thick at the distal end of the mound.

4.3.5 Distal Paludal Facies

Between the two distal edge smooth slopes is an area rich in bacterial shrub laminae with encrusted rafts, reeds molds, and grass molds (Figure 33). In this paludal reed deposit, 4-15 cm long reed molds are oriented vertically with some phytoclastic reed molds (Figure 35). The vertically oriented reed molds are interpreted to form in situ.

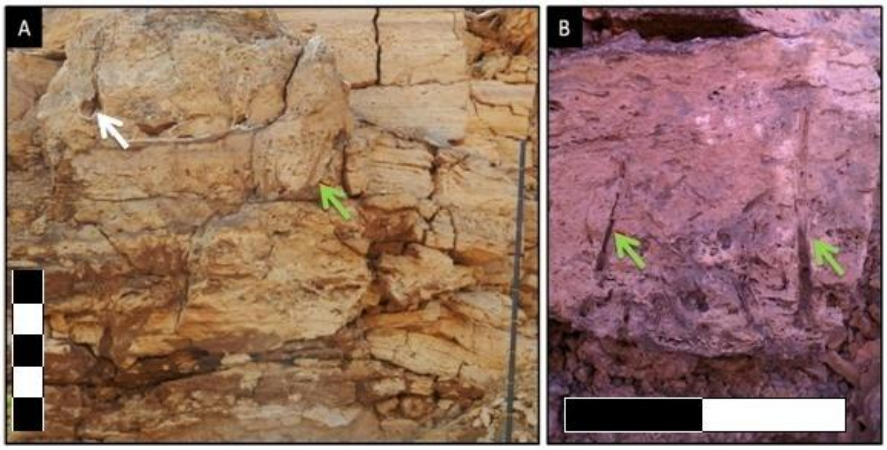

Figure 35: (A) Outcrop photograph of northern distal reed facies, reen arrow indicates reed molds, white arrow indicates solution cavity with spar fill. Scale bar at 0.1 m intervals (B) Close outcrop view of reed molds. Green arrows indicates vertical reed molds. Scale bar with 0.1 m intervals.

4.3.6 Smooth Slope--Shrub Flat

Both overlying and adjacent with the distal sloping deposits are 4-6 m thick layers of interbedded bacterial shrubs and intraclasts which can be divided into three sections indicated by the solid and dotted lines on Figures 25 and 26, respectively. The outcrop can be divided laterally into two sections of interbedded intraclasts and bacterial shrubs, each associated with an adjacent distal edge smooth slope. The third section of interbedded intraclasts and shrubs gradually dips distally and is heavily eroded. Not all layers are continuous, however, oncoidal and intraclastic layers may gradually thin, occurring as lenses. Additionally, intraclastic layers display less lateral thinning and are far longer in lateral extent than oncoidal beds.

Section-1 is 2 m thick, composed of laterally extensive interbedded shrubs and intramicrites laterally adjacent to the proximal side of the first sloping ray-crystal deposit. Interbedded bacterial shrub and intraclastic beds are continuous for 30-60 m and may be 3-50 cm thick. Layers laterally associated with the proximal edge smooth slope deposit also include the basal intramicrite layer and the lower 0.6 m of the distal ray-crystal column. Section-1 also displays a commonly repeated upward vertical sequence of layers composed of intraclasts, bacterial shrubs, then micrite. Intraclastic layers are composed of constituents that are platy to oblate and angular to subangular, being 0.05-70 mm long. Shrub layers are composed of arborescent shrub growths, with laminae 0.2-2.5 cm forming laterally continuous layers 3-50 cm thick. Overlying bacterial shrubs often encrust individual intraclasts, suggesting a sudden shift in depositional environment.

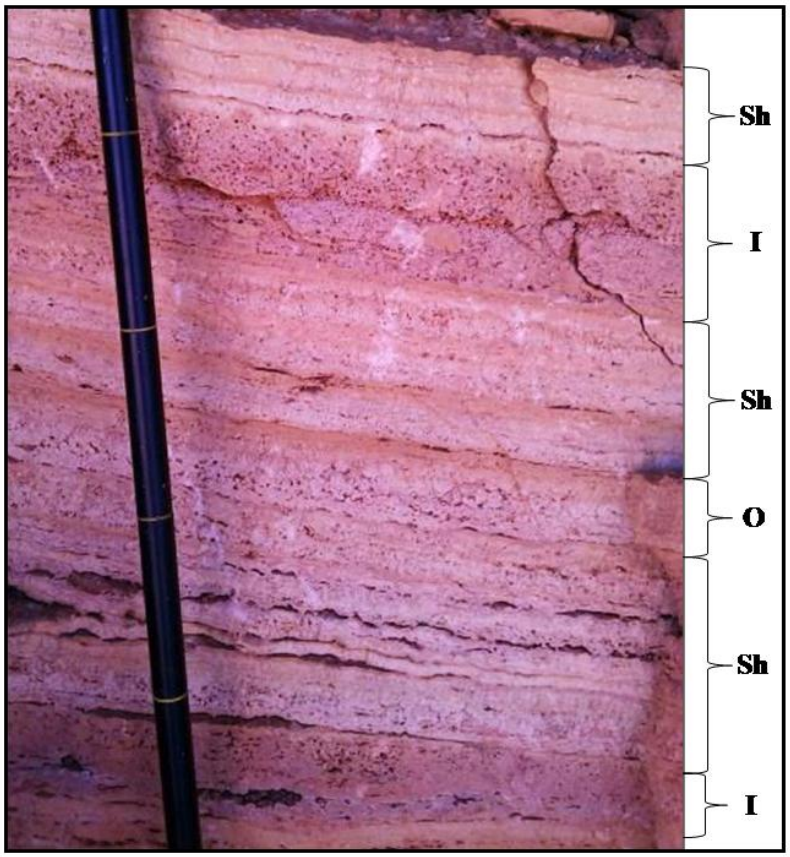

Figure 36: (A) Outcrop photograph of Section-2 with interbedded [I] intraclasts, [Sh] bacterial shrubs and [O] oncoids. This portion of outcrop has fractured from the main mound and does not accurately display slope of layers. Scale at 0.1 m intervals.

Allochems may be spherical to oblate, and some oncoids are present as well as rafts. Oncoidal layers are rare, but occasionally present as lenses within shrub layers. Micrite layers are 4-20 cm thick and often contain incipient shrub horizons.

Section-2, consists of bacterial shrub, oncoidal and intraclastic layers laterally adjacent to the proximal side of the second sloping deposit and overlies Section-1 (Figure 36). Oncoidal layers are commonly interbedded within shrub layers or between the bacterial shrub and intraclastic layers. Oncoids are more abundant upwards and are spherical to discoidal, commonly forming 2-5 m long lenses. Oncoidal layers commonly coarsen upward with individuals displaying diameters of 0.5-2 mm. The intraclastic

layers are 5-13 cm thick and are continuous for 40-70 m, pinching out distally. Bacterial shrub layers are 1-8 cm thick and are continuous for 60-120 m, becoming more dominant distally as intraclastic layers pinch out. Similar to Section-1, bacterial shrubs often encrust underlying intraclasts, suggesting a sudden shift in depositional environment. Within shrub layers are lenses 3-10 m long where rafts and grass molds are abundant, possibly due to pooling on the mound slope.

Section-3 a 1-2 m thick layer of intramicrites interbedded with bacterial shrubs overlying the previous two sections, composing the uppermost portion of the mound. Section-3 is heavily eroded in places and commonly covered by alluvium. However, in the proximal portion of Section-3, where it is thickest, an erosive boundary is present at the top of this section. At the distal end of this section, travertine gradually dips downward until it is obscured by alluvium.

The cyclic repetition of layers described for Sections-1 and 2 is likely due to the vent undergoing surges of hydraulic flow. The intraclastic layers contain the most angular and largest constituents, indicating a period of increased flow rate and erosion. Constituents at the top of intraclastic layers are commonly enveloped by bacterial shrub growth, indicating a waning of flow as bacterial growth becomes more dominate, trapping intraclast grains as water flow wanes. The bacterial shrub layers represent subaqueous deposition, although they may form with a water depth of only a few centimeters on the mound surface. Oncoids may occur as lenses located within bacterial shrub layers or at the transition of intraclastic and shrub layers. Oncoids represent periods in which bacterial growth was able to flourish, yet was kept in a mobile state. Oncoid

lenses between shrubs and intraclasts indicate gradual change in hydraulic flow. Oncoids occur in lenses, indicating that they likely formed within shallow depressions on the sloped surface of the mound. It is common to find sparse shrub horizons growing within the micritic layers, bacterial shrub growth smothered by the influx of sediment. Furthermore, when present, micritic layers gradate vertically into well rounded intraclasts, indicating a shift toward higher energy environments.

4.4 Proposed Depositional Succession of Mound-A

Based on facies and constituent relationships, Mound-A deposition can be divided into 6 stages (Figure 37). All travertine mounds within the study area cap the Chinle Formation, which is composed of cross-bedded conglomerates and sandstones. The Triassic Chinle Formation was shaped by the Pleistocene Little Colorado River during the time of spring emergence (Embid, 2009). The difference in elevation at which mounds cap the Chinle Formation can range up to 9 m. Therefore, these relationships show that there was some topographic relief at the time that travertine developed, and eventually the surrounding area gradually became inundated with water from the newly emerging spring systems. As the extensive low relief mounds were formed, there were breaks in the mound slope where higher water flow caused the precipitation of ray-crystal dams. However, the mound's development was dominated by laterally extensive bacterial shrub flats and water-rich paludal areas.

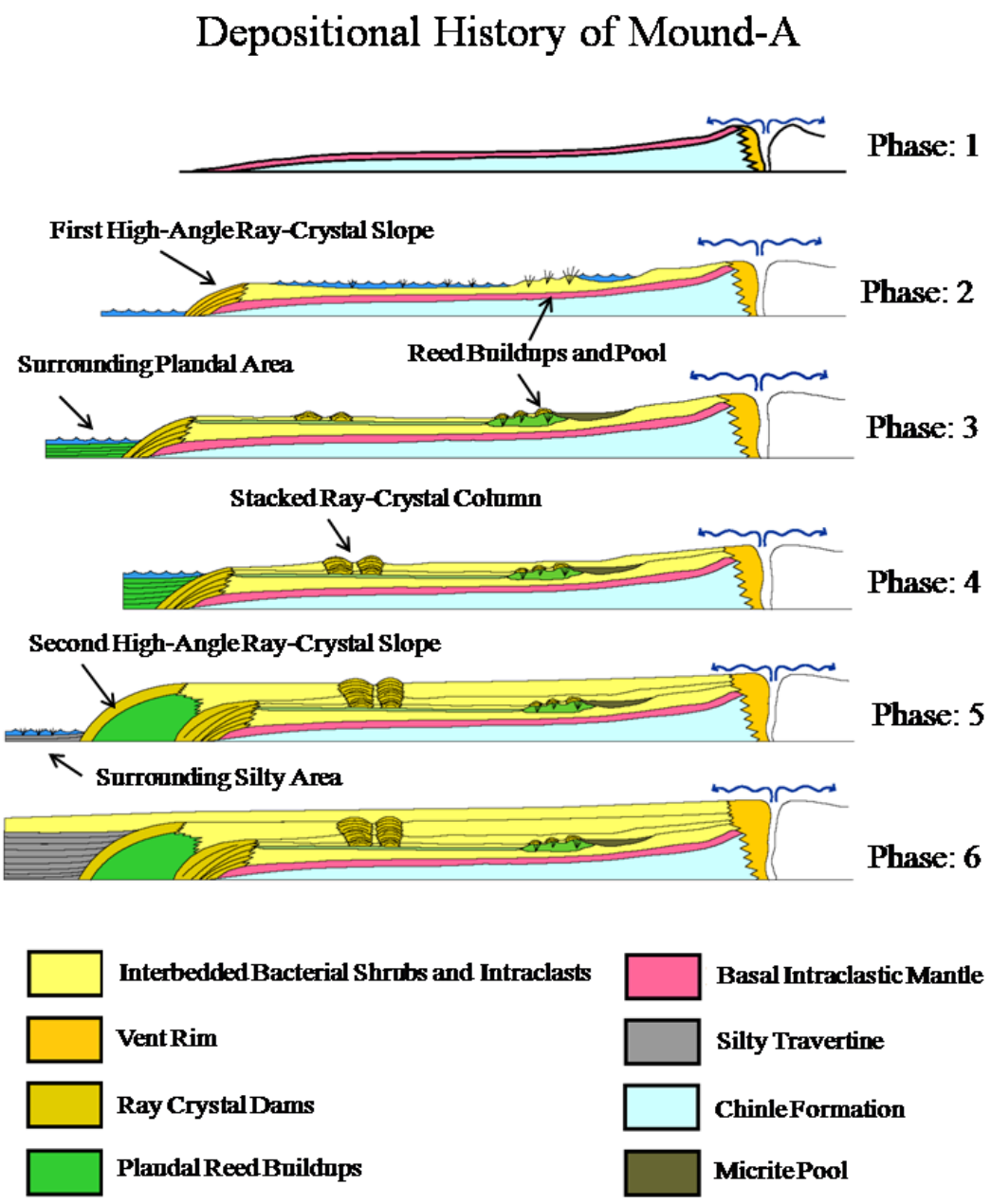

Figure 37: Depositional evolution over time of Mound-A. Phase–1: Initial spring emergence. Phase–2: Deposition of reed mounds with associated pools and formation of first distal edge smooth slope. Phase–3: Formation of ray-crystal dams on reed buildups and mound slope. Phase–4: Continued deposition of stacked smooth slope columns. Phase–5: Continued deposition of smooth slope columns and formation of second distal edge smooth slope. Phase–6: Filling of surrounding area and final deposition of travertine on mound slope of stacked ray-crystal columns.

4.4.1 Depositional Succession of Mound-A: Phase-1

The depositional evolution of Mound-A can be divided into six periods that reflect the temporal and spatial development of the mound spring system (Figure 37). The cross-bedded sandstone of the Chinle Formation underlies a sandy siltstone interbedded with poorly defined travertine. Therefore, it is likely that the silty travertine layer represents the initial state of mound formation onto the Chinle Formation. As the spring vent first established itself, undulatory lenses of silty travertine were precipitated by carbonate saturated water. The thin, poorly-defined, and silty nature of travertine in this period is likely due to a high volume of suspended sediment sourced from the establishment of a subsurface conduit for emerging spring water. Above the non-resistant calcareous silt layer is a dense basal intramicrite layer. The basal intramicrite layer is thicker, contains larger, more angular grains, and a significantly higher proportion of quartz grains in comparison to upper intraclastic layers of Mound-A. The shift from siltstone to intramicrite layers indicates a increase in the carbonate saturation of water expelled from the vent. This transition marks the beginning of travertine deposition and the initial stages of mound aggradation.

4.4.2 Depositional Succession of Mound-A: Phase-2

The broad slope of bacterial shrubs developed areas of paludal reeds and ray-crystal at sites of increased water flow. Deposition during Phase-1 created an appreciable difference in elevation between the developing travertine mound and the surrounding environment. However, the difference in elevation between the mound deposit and the

surrounding landscape was not great enough to create waterfalls. Therefore, water emptying into the surrounding area from the mound increased in flow rate, increasing precipitation, and causing the buildup of a smooth ray-crystal slope at the distal edge.

The base of the first distal edge smooth slope is laterally continuous with and located downstream from a series of encrusted reed buildups. Therefore, the distal edge slope likely began to form after or concurrently with the reed buildups (Figure 37). This was a period of bacterial growth in shallow water and encrustation of a macrophyte-rich, paludal spring system. Reed buildups blocked water flow, causing pooling on the upstream side. Organisms in travertine springs are quickly encrusted and higher taxa of plants are stabilized by rapid encrustation. Therefore, large buildups of encrusted reeds may have obstructed water flow, acting as an organic baffle and trapping constituents (Figure 38). Many constituents, such as oncoids, intraclasts, and phytoclasts, are encrusted by carbonate when trapped by reed buildups, further obstructing water flow. Once reed accumulations became large enough to sufficiently divert water, pooling occurred on the upstream side of the reeds. These pools were quiescent environments where fine micrite and rafts were deposited.

4.4.3 Depositional Succession of Mound-A: Phase-3

During Phase-3 the mound surface primarily consisted of bacterial shrub flats with localized areas of ray-crystal precipitation. Small ray-crystal dams began forming on the reed buildups deposited during Phase-2. Additionally, the stacked smooth slope

columns began forming on the mound surface. Furthermore, the paludal area surrounding the mound edge began to fill with reeds and bacterial shrubs.

The series of small ray-crystal dams that cap the crests of the reed buildups, indicate a shift towards higher energy water flow. The reed buildups continued to trap transported material and the adjacent pools filled with sediment. This caused water flowing over the obstructing reed buildups to precipitate ray-crystal dams due to increased hydraulic conditions (Figure 38). The bacterial shrubs laterally adjacent with the upstream side of the dams contain more rafts and grass molds than those associated with downstream bacterial shrubs, indicating that there was some shallow pooling behind the dams.

During this phase, ray-crystal dams first formed on the low-gradient mound slope and continued to aggrade, eventually forming the stacked smooth slopes seen in Phase-4 (Figure 37). Ray-crystals are indicative of sites characterized by high flow velocity and limited biogenic activity, typical of rapid precipitation on slopes. Therefore, the stacked smooth slopes represent a series of stacked concave downward laminae that formed where carbonate-rich waters flowed faster over a break in slope, prompting rapid degassing and precipitation of ray-crystals.

4.4.4 Depositional Succession of Mound-A: Phase-4

During this phase, alternating deposition of bacterial shrub and intraclastic layers dominated the slope with a localized buildup of stacked smooth columns. Also, the

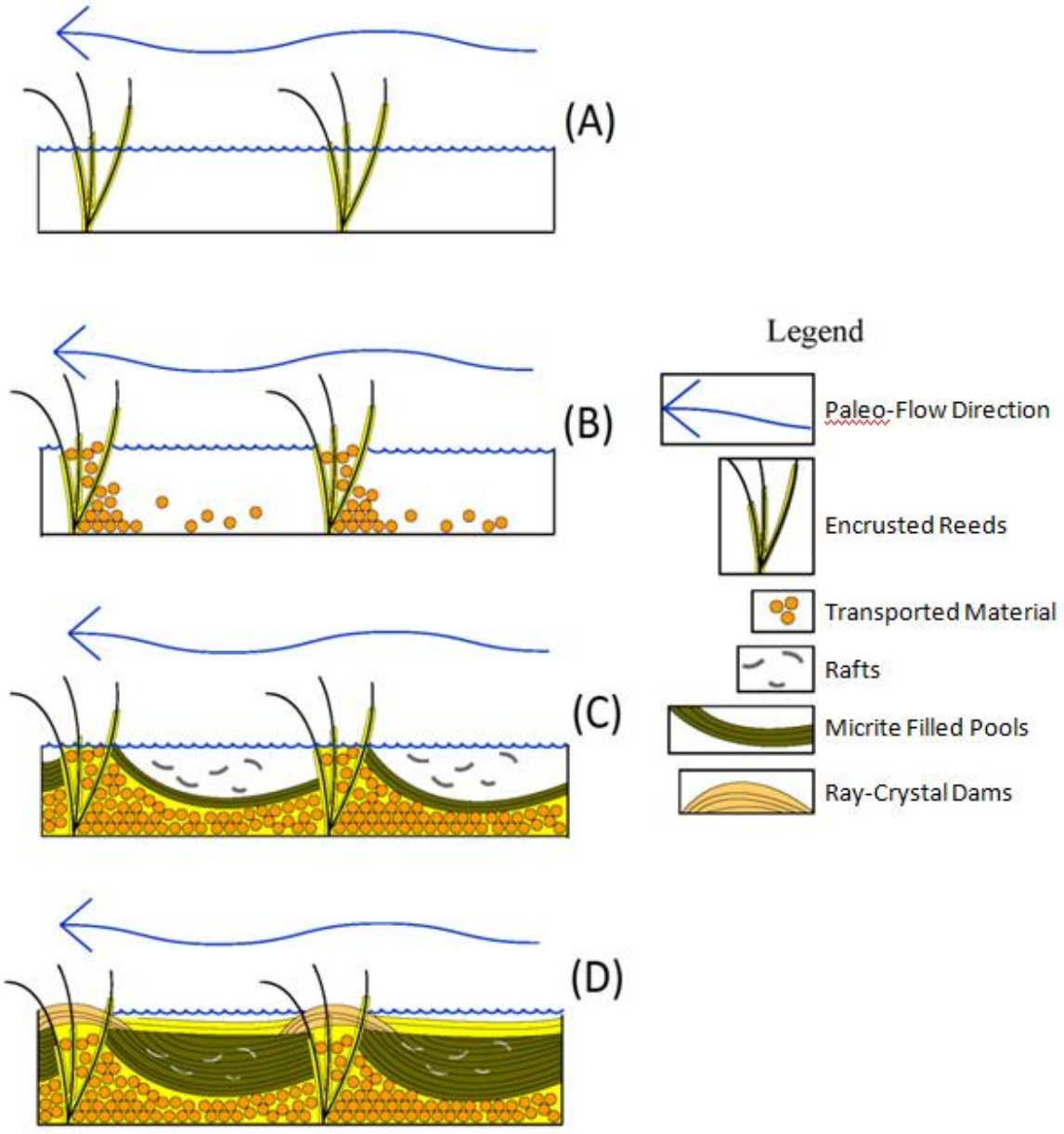

Figure 38: Diagram of initial growth of reed buildups as they trap sediment and obstruct flow. (A) Reeds are encrusted by carbonate. (B) Encrusted reeds trap oncoids and other transported material. (C) Accumulated material trapped by reeds eventually causing pooling on the upstream side of reeds. (D) Pools are filled with micrite and rafts, causing fast flowing water to flow over reeds resulting in precipitation of ray-crystal dams.

encrusted-reed buildups and filled pools deposited during Phase-3 were overlain by bacterial-shrub layers. At the edge of the mound, the distal edge smooth slope was still present, with surrounding paludal area continuing to fill.

The ray-crystal dams capping reed buildups persisted after the associated pools filled, becoming associated with the overlying sub-horizontal bacterial shrub and intraclastic layers (Figure 38). The interbedded-bacterial shrub and intraclastic layers above the ray-crystals conform to the undulatory surface created by the underlying series of dams. These layers eventually become sub-horizontal after 0.3 m of vertical accumulation, forming the gentle slope that characterizes the attitude of the rest of the mound layers. Therefore, as the mound aggraded through the deposition of interbedded-bacterial shrub and intraclastic deposits, the characteristic smooth mound slope began to form. Discharge channels are absent in the mound, and it is likely that emerging spring-water flowing over the mound surface exhibited laminar sheet-flow water conditions over the gently sloping mound surface. The rhythmic nature of interbedded-bacterial shrubs and intraclasts is likely due to fluctuations in discharge and/or a shift in flow path from the vent.

The initial break in slope that first formed the smooth slopes in Phase-3 caused the propagation of additional smooth slopes that persisted till Phase-5. This sloping deposit was likely the result of a small drop in elevation, yet was not too large a drop to form a rimstone dam or waterfall. Two stacked smooth columns were deposited contemporaneously with the interbedded bacterial shrub and intraclastic laminae forming the majority of the mound (Figure 37). The series of smooth slopes display a slight

progradation downstream. Layers adjacent to the stacked smooth slope thin and abut against the columns and are similar in lithology on either side of the deposit. These stacked ray-crystal columns were sites of increased water flow, further confirmed by the distribution of adjacent allochems. In relation to the stacked smooth slopes, intraclasts are more abundant downstream whereas rafts are more abundant upstream.

The area surrounding the mound where spring water drained was a paludal area rich in bacterial shrubs, reeds, grasses and micrite. Deposition waned on the distal smooth slope as the surrounding paludal area filled and aggraded with the mound. The adjacent paludal reed facies accumulated to approximately the same height as the first distal edge smooth slope, indicating the paludal environment was deposited contemporaneously with aggrading slope deposition. The abundant occurrence of reeds and grasses distal to the vent, suggests that waters at the distal end of the mound were habitable to a higher order of plants.

4.4.5 Depositional Succession of Mound-A: Phase-5

During this phase, the stacked smooth slope columns ceased deposition and a second distal slope developed. Laterally adjacent and associated with the second distal slope is the sub-horizontal bacterial shrub and intraclastic laminae that form the bulk of the mound (Figure 37). The first distal edge smooth slope that persisted until Phase-4 ceased deposition. The end of deposition of the first distal smooth slope is likely due to the accumulation of the surround paludal area outpacing slope deposition and/or because flow rate decreased, inhibiting deposition of the ray-crystal slope. As the mound grew in

size, another distal edge smooth slope formed on top of the surrounding paludal area deposited in Phase-4 (Figure 37). It is likely that after the first distal slope was abandoned a significant portion of the surrounding paludal area was eroded, until the formation of the second distal slope that caps the paludal deposit. The basal portion of the second distal edge smooth slope incorporates both gravel from the Chinle Formation and phytoclasts from the paludal facies. The formation of this second slope is likely similar in origin to the first, being due to an appreciable change in elevation from the paludal deposit and the surrounding area. Additionally, the initiation of the second distal edge smooth slope may also be due to an increase in discharge from the vent, increasing flow rate downstream.

The large distal edge smooth slope gradates upstream into sub-horizontal interbedded bacterial shrub laminae that are laterally continuous throughout the entire western roadcut exposure. Intraclasts interbedded with the bacterial shrub laminae thin distally and gradate into the second distal edge smooth slope. Therefore, the deposition of these interbedded layers represents a period of continued growth of mound height and propagation over time of the gentle mound slope. An abundance of rafts and grass molds indicates some small depressions on the gently sloping surface of the mound.

4.4.6 Depositional Succession of Mound-A: Phase-6

In Phase-6, 4.5 m of calcareous silt and gravel interbedded with travertine were deposited. These layers compose the final stage of growth and outer edges of mound, overlaying the second distal slope. This indicates that the surrounding area adjacent to the

distal slope was likely filled from eroded material transported by water emptying from the edges of the mound (Figure 37). There are undulatory horizons of carbonate-encrusted siliciclastic gravel, likely due to erosion of the Chinle Formation, which formed the paleo-surface of the surrounding area.

Overlying both the first distal edge smooth slope and the distal adjacent calcareous silt is heavily weathered, dense travertine. The heavily weathered travertine is laterally continuous proximally, making up the upper portion of the western roadcut. The upper portion is composed of interbedded-bacterial-shrubs with increasingly more interbedded-intraclastic and oncoidal layers. Oncoids indicate the presence of an agitated environment with microbial influence, whereas the increased proportion of intraclasts suggests higher flow rates as the mound grew. This layer features a 7 m long erosional boundary, representing a period of non-deposition. Therefore, the vent may have migrated or there was waning of flow, possibly caused by a falling hydraulic head during the final stages of mound growth.

CHAPTER 5: SUMMARY AND CONCLUSIONS

5.1 General-Mound Morphology and Geometry

Located in eastern Arizona, the Lyman Lake travertine complex consists of over 70 mounds scattered over a 33 km^2 area near the towns of Springerville and St. Johns, in Apache County. This study investigates the travertine deposits north of Lyman Lake, which can be divided into a travertine platform of coalesced mounds and southern individual mounds eroded by the Little Colorado River. The southern individual mounds are the erosional remnants of much larger deposits. For example, the Little Colorado River has segmented one mound into several individual deposits adjacent to the river. However, this study focuses on the individual mounds adjacent to Lyman Lake and specifically on one mound with a roadcut made to provide a service road to the Lyman Lake Dam.

The Lyman Lake travertine deposit is situated above the Springerville-St. Johns' CO_2 reservoir, a plunging anticline which focuses gas at the northwest end. The CO_2 reservoir contains two limestone members that are attacked by CO_2, yielding $CaCO_3$-rich groundwaters. The region contains deep seated faults that segment the CO_2 reservoir at variable depths. The potentiometric surface of the reservoir is uneven, with higher-pressure fluids forced along faults to higher elevations, allowing the migration of $CaCO_3$-saturated groundwater to the surface. The combination of faults and nature of the Springerville-St. John's Reservoir are fundamentally responsible for the deposition of these travertine deposits.

Travertine deposits within the study area cap the Chinle Formation. The travertines are primarily composed of interbedded bacterial shrub and intraclastic layers. Travertine mounds within the study area display a gently dipping, shield-like geometry with a central vent. These mound deposits are composed of sub-horizontal sheets of travertine, with a dip of just a few degrees, radially extending away from a vent and thinning distally. Vents from which subsurface were expelled to the surface, are preserved in many of the mounds. Mound vents present are partially preserved or filled with alluvium. Vents are commonly located in the center of the deposit, forming a slightly raised domal geometry with respect to the rest of the sub-horizontal mound. Internally, vents are composed of vertical walls that dip steeply outward into sub-horizontal bedding that extend over the entire mound.

5.2 Mound-A

This mound is located adjacent to the northwestern edge of Lyman Lake. The western edge of the mound was cut in order to build a service road that provides access to the Lyman Lake Dam. The mound is 350 m long and 150 m wide, situated adjacent to Lyman Lake. Similar to other mounds in the area, Mound-A is primarily composed of interbedded-bacterial shrub-and intraclastic layers. The cross-sectional view afforded by the road-cut displayed 7 facies likely deposited over 6 periods of deposition. This mound features morphological elements such as distal edge-smooth slopes and stacked-ray-crystal columns that laterally gradate with the sub-horizontal layers of bacterial shrubs and intraclasts. The orientation of phytoclastic material and imbrication of intraclasts indicates that water flowed in a west-northwestern direction away from the vent center.

However, due to the lack of discharge channels and the even thickness of shrub layers, it is likely that water flowed in laminar sheets over entire portions of the mound.

5.2.1 Mound Constituents

Mounds are primarily composed of interbedded layers of bacterial shrubs and intraclasts, with a wide range of other constituents such as rafts, reeds, grasses, oncoids, and ray-crystals. However, of the mounds that were studied, only Mound-A was heavily sampled and the constituents studied in detail, six common constituents were recognized.

1) Bacterial shrubs are the most abundant constituent composing mounds and are commonly interbedded with intraclasts. Bacterial shrubs occur as 3-50 cm thick accumulation of laminae that are laterally continuous for 10-70 m and the layers maintain an approximately constant thickness. Bacterial shrub layers are composed of laterally continuous and vertically repetitious couplets of arborescent laminae alternating with finely laminated micrite. Individual laminations, composed of individual bacterial shrubs, can be 0.2-2.5 cm thick. Bacterial shrubs are made up of upward radiating ‘branches’ that are composed of multiple ‘leaves’, forming an overall outward branching morphology of an individual bush. Due to the influence of bacteria during the formation of shrubs, extensive microporosity is present due to the decay of encrusted bacterial cell. Bacterial shrub layers are composed of multiple shrubs stacked in the layer. Shrubs within a single layer are typically of the same height, whereas there may be significant variation of shrub height between separate layers. Shrubs may nucleate from horizons of oncoids or intraclastic layers. Individual intraclasts are commonly found suspended by overlying

bacterial shrub growth at the interface between layers. Bacterial shrubs are often present in micritic layers in an incipient form, likely smothered by the influx of sediment. The presence of bacterial shrubs indicates deposition in a shallow, subaqueous environment. Chafetz and Folk (1984) observed that bacterial shrubs are a common constituent within the H_2S-rich hot spring deposits of Tivoli, Italy. Some spar cement surrounding bacterial shrubs was composed of sheaths of gothic-arch calcite, a unique crystal form where the internal crystal lattice is arched by the presence of sulfur.

2) Intraclastic layers are commonly interbedded with bacterial-shrub layers and occasionally with oncoidal or micritic layers. Intraclastic layers can be 3-40 cm thick, with platy individual grains ranging in size from 0.2-70 mm long. Intraclastic layers occur in laterally extensive lenses approximately 10-70 m long**,** pinching out distally. Intraclastic layers display an upward trend towards thicker layers with larger grain size and an increased association with oncoidal layers. However, individual layers are commonly fining upward in grain size. In addition, oncoidal layers underlying intraclasts form a gradational boundary. Intraclastic platy fragments, 2-7 cm long, are common on the distal side of dams.

3) Rafts occur in patches or lenses, being either suspended in micrite or surrounded by bacterial shrub growth. Rafts vary in length and thickness, yet individual patches of rafts are very well sorted, displaying almost identical sizes. Large rafts 4-9 cm long oriented sub-horizontally are only found suspended in micrite within pool deposits created by the damming effects of reed buildups. Chaotically oriented, smaller rafts 0.5-4 cm long are found in bacterial shrub layers, commonly in association with grass molds.

Variations in raft length are due to differing hydraulic conditions breaking rafts into differing sizes. The deposition of rafts commonly results in the creation of shelter porosity beneath them, yielding fenestral porosity that can only be filled by secondary cementation. Due to pooling, rafts are common on the upstream side of smooth sloping dams.

4) Oncoids are a common constituent, being bacterially-mediated coated grains that are composed of a nucleus surrounded by cortices composed of bacterial shrubs that are radially oriented away from the nucleus. Oncoids range in size from 1-15 mm, occurring in lenses 0.5-10 m long and 3-8 cm thick between or above bacterial-shrub layers. They may also grade into intraclastic layers and are commonly coarsening upward. Oncoids may have a spherical to oblate shape and display a range of growth forms, ranging from an incipient stage with thin cortices to a well-developed gravel-sized individual with thick cortices. The nuclei of oncoids in the study area commonly consist of poorly defined intraclasts, rafts, clumps of micrite, or calcite crystals. Oncoids are the result of bacterial growth occurring in a mobile form in an environment that is periodically agitated. Therefore, oncoids display a similar microporosity to that of bacterial shrubs, due to the decay of encrusted bacterial cells. In the upper section of the outcrop, oncoids become more abundant, likely indicating an increase in flow strength.

5) Reed and grass in a travertine system commonly produce moldic porosity, caused by the decay of encrusted plants. Reed molds can be 4-15 cm long and 0.5-2 cm in diameter, whereas grass molds can be 1-3 cm long and 1-4 mm in diameter. Reeds and grass are commonly associated with each other, occurring in clusters or lenses 2-4 m

long. Reeds may occur as sparse individuals or abundant clustering of material that may obstruct water flow. The encrustation of reeds and grasses may entrap other constituents. Grass molds are commonly associated with bacterial shrub growth and rafts, commonly occurring in clusters or lenses. Reed molds are commonly associated with bacterial shrub growth, rafts, and phytoclastic material. Reeds are commonly vertically oriented or tilted downslope, whereas phytoclastic-reed molds are commonly sub-horizontal with the long axis oriented with paleo-flow direction.

6) Ray-crystal shrubs are not a common component, yet form major morphological features of the mound. In outcrop, ray-crystals compose three morphological features: the vent, stacked smooth slope dams and distal-edge high-angle-smooth slopes. The stacked smooth slopes can be 1-2 m tall, consisting of a succession of stacked layers of crystalline crusts 8-20 cm long and 1-6 cm thick composed of laminae 0.05-3 cm thick. Stacked smooth slopes display a marked break in slope compared to laterally adjacent beds. Distal edge smooth slopes are composed of 0.05-5 cm thick laminae of ray-crystal crusts that abruptly dip downward. These large deposits can be 2-6 m long and 0.5-1.5 m thick. Ray crystal crusts are composed of layers of calcite crystals that are oriented perpendicular to the depositional surface, forming dense crystal aggregates. Individual ray-crystal fans may amalgamate together into layers termed crystalline crusts. Amalgamated crusts are more common on higher gradient slopes, whereas individual fans are more common on more gentle slopes. Ray crystals are 1-5 mm high, displaying a fan-shaped, radiating pattern. The fine laminations are growth lines that are concave downward, extending away from the fan base

Interbedded shrubs and intraclasts form the gently sloping surface of the mound, resulting in the characteristic pancake-like morphology of mounds within the field area. The outcrop along the road-cut can be divided into two sections of interbedded-intraclastic and shrub layers, each associated with a distal edge-smooth-sloping feature. Overlying the first two sections is a third section of interbedded intraclasts and shrubs that gradually dip distally. Intraclastic layers display lateral thinning, yet extend farther than oncoidal beds. Therefore, the distal portion of the slope has very few intraclastic layers and even less oncoidal layers. These sections represent periods of mound growth.

Within Mound-A there are repeated sequences of constituents that represent the waxing and waning of flow strength. Each constituent requires specific hydraulic conditions to form, allowing an interpretation of the paleo-conditions required for deposition of constituents. Repeated vertical sequences occur as layers of shrubs, oncoids, intraclasts then micrite. However, oncoidal and micritic layers may not be present. Furthermore, the frequency and thickness of oncoidal and intraclastic layers increase upward in the measured sections. The bacterial shrub layers represent subaqueous deposition, although they may form with a water depth of only a few centimeters on the mound surface. Intraclastic layers contain the most angular and largest constituents, indicating a period of increased flow rate and erosion. However, constituents at the top of intraclastic layers are commonly enveloped by bacterial shrub growth, indicating a sudden waning of flow as bacterial growth becomes more dominate, trapping intraclasts. Oncoids may occur as lenses located within shrub layers or between shrub and intraclastic layers. Oncoids occur periods of slow hydraulic flow in which

bacterial growth was able to flourish, yet was kept in a mobile state. When occurring between bacterial shrub and intraclastic layers, oncoids represent a gradual shift in hydraulic flow. Oncoids occur in lenses, indicating that they likely formed within shallow depressions on the sloped surface of the mound. It is common to find incipient shrub horizons growing within the bottom portion of micritic layers, indicating that bacterial shrub growth was being smothered by the influx of intraclastic particles.

5.2.2 Depositional Facies and Morphological Elements

The road-cut through the western edge of Mound-A allows for a good cross-sectional study. The mound is composed of gently sloping, laterally-continuous-interbedded shrub and intraclastic layers overlying and associated with a range of morphological features such as stacked-smooth-slope columns, reed buildups, and distal-edge high-angle-smooth slopes.

The reed buildups and associated pools form a layer that ranges from 0.1-0.3 m thick and is 5 m long. In association with the encrusted-reed buildups are a series pools filled with micrite and paper-thin rafts on the upstream side of the reed accumulations, extending 15 m upstream. This paludal layer consists of five-reed accumulations, decreasing in size downslope. The reed buildups are composed of encrusted *in situ* plants that trap phytoclasts, oncoids, and intraclasts. Ray-crystal dams 5-10 cm thick form on top of the encrusted-reed buildups and are associated with laterally-adjacent bacterial-shrub and intraclasts. The reed buildups have a similar relationship to terrace-pools, where pools occur on the upstream side as flow is obstructed and slowed. Rafts and fine

micrite are a common component of depressional pools, due to the quiescent hydraulic conditions allowing the deposition of these allochems. The pools associated with reed buildups contain the largest rafts observed in the mound, ranging from 4-9 cm long.

The stacked smooth slope deposits are spaced 8 m apart, and are composed of ray-crystal layers building on top of each other. The first ray-crystal slope column is composed of stacked ray-crystals 1.5-2 m high, composed of individual ray-crystal layers 3-6 cm thick and 12-20 cm wide. Beds adjacent to the columns are composed of interbedded intraclasts and bacterial shrubs which thin towards the stacked slopes. Layers adjacent to the column cannot be traced through the dam surface, yet are very similar in lithology and thickness on either side. Therefore, it is likely that the ray-crystal slope grew contemporaneously with the formation of adjacent sediment. Small rafts are abundant behind the slope and intraclasts are more abundant downslope. The proximal side of the column typically has more rafts and thicker sequences, indicating some pooling behind the stacked slope. Large intraclasts are present on the downstream side that are angular to platy in micritic deposits. Therefore, given the presence of intraclasts, the stacked slopes were the result of a long-lived break in slope where flow rate increased.

There are two large sloping deposits located in the distal portion of the western road-cut. These sloping deposits are concave downward structures that display a marked break in slope, where sub-horizontal beds rapidly change attitude to steeply dipping to the distal end of the mound. The first sloping deposit is located 15 m proximally and 2.5 m below the second slope. The distal edge smooth sloping deposits are 0.5-1.5 m thick,

abruptly dipping down at an angle of 30-45°. Both distal-edge-smooth-slope deposits are composed of ray-crystal laminae. The proximal slope is composed of multiple layers which display identical attitude with the overall change in slope of the deposit. However, the distal-sloping deposit is composed of multiple scalloped laminae with a concave downward shape that eventually gradate upslope into planar laminae. Both distal edge smooth slopes gradate with laterally continuous, sub-horizontal interbedded intraclastic and shrub layers. Therefore, the interbedded intraclasts and shrubs associated with the higher distal slope overlie those associated with the proximal slope.

Bibliography

Aldrich, M. J., and Laughlin, A. W., 1984, A model for the tectonic development of the southeastern Colorado Plateau boundary: Journal of Geophysical Research, Solid Earth, v. 89, p. 10207-10218.

Allen, C.C., and Albert, F.G., 2000, Microscopic Physical Biomarkers in Carbonate Hot Springs: Implications in the Search for Life on Mars: Icarus , v. 147, p. 49-67.

Allis, R.G, Chidsey, T., Gwynn, W., Morgan, C., White, S.P., Adams, M., and Moore, J., 2001, Natural CO_2 reservoirs on the Colorado Plateau and Southern Rocky Mountains: candidates for CO_2 sequestration: Proceedings of First National Conference on Carbon Sequestration, p. 1144-1163.

Arenas, C., Gutierrez, F., Osacar, C., and Sancho, C., 2000, Sedimentology and geochemistry of fluvio-lacustrine tufa deposits controlled by evaporate solution subsidence in the central Ebro Depression, NE Spain: Sedimentology, v. 47, p. 883-909.

Cather, S.M., Chamberlin, R.M., and Ratte, J.C., 1994, Tertiary stratigraphy and nomenclature for western New Mexico and eastern Arizona: in Chamberlin, R.M., Kues, B.S., Cather, S.M., Barker, J.M., and McIntosh, W.C., eds, NMGS Guidebook, 45th Field Conference, Mogollon Slope, West Central New Mexico and East Central Arizona, p. 259-266.

Cather, S.M., and McIntosh, W.C., 1994, The Plio-Pleistocene Quemado Formation of West-Central New Mexico: in Chamberlin, R.M., Kues, B.S., Cather, S.M., Barker, J.M., and McIntosh, W.C., eds., NMGS Guidebook, 45th Field Conference, Mogollon Slope, West Central New Mexico and East Central Arizona, p. 279-281.

Carthew, K.D., and Drysdale, R.D., 2003, Late Holocene fluvial change in a tufa-depositing stream: Davys Creek, New South Wales, Australia: Australian Geographic, v. 34, p. 123-139.

Chafetz, H.S., and Folk, R.L., 1984, Travertines: depositional morphology and the bacterially constructed constituents: Journal of Sedimentary Petrology, v. 54(1), p. 289-316.

Chafetz, H.S., Rush, P.F., and Utech, N.M., 1991, Microenvironmental controls on mineralogy and habit of $CaCO_3$ precipitates: an example from an active travertine system: Sedimentology, v. 38, p. 107-126.

Chafetz, H.S., and Lawrence, J.R., 1994, Stable isotopic variability within modern travertines: Geographie physique et Quaternaire, v. 48, p. 257-273.

Chafetz, H.S., and Guidry, S.A., 1999, Bacterial shrubs, crystal shrubs, and ray-crystal shrubs: bacterial vs. abiotic precipitation: Sedimentary Geology, v.126, p. 57-74.

Chafetz, H.S., 2013, Porosity in bacterialy induced carbonates: Focus on Micropores: American Association of Petroleum Geologists Bulletin, v. 97, p. 2103-2111.

Chafetz, H.S., and Guidry, S.A., 2003, Deposition and diagenesis of Mammoth Hot Springs travertine, Yellowstone National Park, Wyoming, U.S.A.: Canadian Journal of Earth Sciences, v. 40, p. 1514-1529.

Chen, J., Zhang, D.D., Wang, S., Xiao, T., and Rongui, H., 2004, Factors controlling tufa deposition in natural waters at waterfall sites: Sedimentary Geology, v. 166, p. 353-366.

Condit, C.D., Crumpler, L.S., Aubele, J.C., and Elston, W.E., 1989, Patterns of volcanism along the southern margin of the Colorado Plateau; the Springerville Field: Journal of Geophysical Research: Solid Earth and Planets, v. 94(6), p. 7975-7986.

Crossey, L.J., Karlstrom, K.E., Springer, A.E., Newell, D., Hilton, D.R., and Fischer, T., 2009, Degassing of mantle-derived CO_2 and He from springs in the southern Colorado plateau region-Neotectonic connections and implications for groundwater systems: Geological Society of America Bulletin, v. 121(7), p. 1034-1053.

Crumpler, L.S., Aubele, J.C., and Condit, C.D., 1994, Volcanoes and neotectonic characteristics of the Springerville Volcanic Field, Arizona: in Chamberlin, R.M., Kues, B.S., Cather, S.M., Barker, J.M., Mcintosh, W.C., (Eds), NMGS Guidebook, 45th Field Conference, Mogollon Slope, West Central New Mexico And East Central Arizona, p. 147-164.

Drysdale, R.N., Taylor, M.P., and Ihlenfeld, C., 2003, Factors controlling the chemical evolution of travertine-depositing rivers of the Barkly karst, northern Australia: Hydrological Process, v. 16, p. 2941-2962.

Dunham, R.J., 1962, Classification of carbonate rocks according to depositional texture: W.E. Ham (ed.), Classification of Carbonate Rocks. Memoir of the American Association of Petroleum Geologists, p. 108-121.

Embid, E.H., 2009, U-Series dating, geochemistry, and geomorphic studies of travertines and springs of the Springerville Area, east-central Arizona, and tectonic implications: Geological Society Of America, Abstracts With Programs, v. 41(7), p. 441.

Emig, W.H., 1917, The travertine deposits of the Arbuckle Mountains Oklahoma, with reference to the plant agencies concerned in their formation: Bulletin of the Oklahoma Geological Survey, v. 29, p. 9-75.

Faulds, J.E., Feuerbach, D.L., Miller, C.F., and Smith, E.I., 2001, Cenozoic evolution of the northern Colorado River extensional corridor, southern Nevada and northwestern Arizona: Utah Geological Association Publication, v. 30, p. 239-272.

Florsheim, J.L., Ustin, S.L., Tang, Y., Di, B., Huang, C., Qiao, X., Peng, H., Zhang, M., and Cai, Y., 2013, Basin-scale and travertine dam-scale controls on fluvial travertine, Jiuzhaigou, southwestern China: Geomorphology, v. 180-181, p. 267-280.

Ford, T. D., and Pedley, H. M., 1992, Tufa deposits of the world: Journal of the Speleological Society of Japan, v. 17, p. 46-63.

Ford, T.D., and Pedley, T.D., 1996, A review of tufa and travertine deposits of the world. Earth-Science Reviews, v. 41, p. 117-175.

Fouke, B.W., Farmer, J.D., Des Marias, D.J., Pratt, L., Sturchio, N.C., Burns, P.C., and Discipulo, M.K., 2000, Depositional facies and aqueous-solid geochemistry of travertine-depositing hot springs (Angel Terrace, Mammoth Hot Springs, Yellowstone National Park, U.S.A): Journal of Sedimentary Research, v. 70, p. 565-585.

Fouke, B.W., Bonheyo, G.T., Sanzenbacher, B., and Frias-Lopez, J., 2003, Partitioning of bacterial communities between travertine depositional facies at Mammoth Hot Springs, Yellowstone National Park, U.S.A.: Canadian Journal of Earth Science, v. 40, p. 1531-1548.

Folk, R. L., 1959, Practical petrographic classification of limestones: Bullletin of the American Association of Petroleum Geologists, v. 43, p. 1-38.

Folk, R.L., 1993, SEM imaging of bacteria and nannobacteria in carbonate sediments and rocks: Journal of Sedimentary Petrology, v. 63(5), p. 990-999.

Folk, R.L., 1994, Interaction between bacteria, nannobacteria, and mineral precipitation in hot springs of Central Italy: Geographie Physique et Quaternaire, v. 48, p. 233- 246.

Folk, R.L., and Chafetz, H.S., 1983, Pisoliths in Quaternary travertines of Tivoli, Italy: T.M. Peryt (ed.), Coated Grains, Berlin (Springer-Verlag), p. 474-487.

Folk, R.L., Chafetz, H.S., and Tiezzi, P.A., 1985, Bizarre forms of depositional and diagenetic calcite in hot-spring travertines, central Italy: The Society of Economic Paleontologists and Mineralogists, Carbonate Cements, Special Publication #36, p. 349-369.

Gilfillan, S.M.V., Ballentine, C.J., Holland, G., Blagburn, D., Lollar, B.S., Stevens, S., Schoell, M., Cassidy, M., 2008, The noble gas geochemistry of natural CO_2 gas reservoirs from the Colorado Plateau and Rocky Mountain Provinces, USA: Geochimica et Cosmochimica Acta, v. 72, p. 1174-1198.

Guo, X., and Chafetz, H.S., 2012, Large tufa mounds, Searles Lake, California: Sedimentology, v. 59, p. 1509-1535.

Guo, L., Riding, R., 1998, Hot-Spring travertine facies and sequences, Late Pleistocene, Rapolano Terme, Italy: Sedimentology, v. 45, p. 163-180.

Hammer, Ø., Dysthe, D.K., and Jamtveit, B., 2010, Travertine terracing: patterns and mechanisms: Geological Society of London Special Publications, v. 336, p. 345-355.

Hancock, P.L., Chalmers, R.M.L., Altunel, E., and Cakir, Z., 1999, Travitonics: using travertines in active fault studies: Journal of Structural Geology, v. 21, p. 903-916.

Jones, B., and Renaut, R.W., 1995, Noncrystallographic calcite dendrites from hot-spring deposits at Lake Bogoria, Kenya: Journal of Sedimentary Research, v. 65, p. 154-169.

Jones, B., and Renaut, R.W., 2010, Calcareous spring deposits in continental settings. Developments in Sedimentology, v. 61, p. 177-224.

Karlstrom, K.E., Crow, R.S., Peters, L., McIntosh, W., Raucci, J., Crossey, L.J., Umhoefer, P., and Dunbar, N., 2007, $^{40}Ar/^{39}Ar$ and field studies of Quaternary basalts in Grand Canyon and model for carving Grand Canyon: Quantifying the interaction of river incision and normal faulting across the western edge of the Colorado Plateau: Geological Society of America Bulletin, v. 119, p. 1283-1312.

Kerr, R.C., and Turner, J.S., 1996, Crystallization and gravitationally controlled ponding during the formation of mound springs, terraces, and "black smoker" flanges: Journal of Geophysical Research, v. 101, p. 25125-25137.

Kitano, Y., 1963, Geochemistry of calcareous deposits found in hot springs: Journal of Earth Science, Nagoya University, v. 11, p. 68-100.

Kosun, E., Sarigul, A., and Varol, B., 2005, Sedimentological investigation of Antalya tufas: Ozkul, M., Yagiz, S., Jones, B., (Eds), Proceedings of the 1st International Symposium on Travertine. Kozan Ofset Matbaacilik San. Ve Tic,. Ltd. Sti. Ankara, p. 50-61.

Linares, R., and Rodriguez, A., 2011, IAG Planetary Geomorpholgy Working Group. http://www.psi.edu/pgwg/images/jul11image.html

McKee, E.D., 1954, Stratigraphy and history of the Moenkopi Formation of Triassic age: Geological Society of America Memoirs, v. 61, p. 1-126.

Moore, J., Adams, M., Allis, R., Lutz, S., and Rauzi, S., 2003, CO_2 mobility in natural reservoirs beneath the Colorado Plateau and southern Rocky Mountains: an example from the Springerville-St. Johns Field, Arizona and New Mexico: Second Annual Conference On Carbon Sequestration, p. 1-22.

Moore, J., Adams, M., Allis, R., Lutz, S., and Rauzi, S., 2005, Mineralogical and geochemical consequences of the long-term presence of CO_2 in natural reservoirs: an example from the Springerville-St. Johns field, Arizona, and New Mexico, USA: Geochemical Aspects Of CO_2 Sequestration, Chemical Geology, v. 217, p. 365-385.

Mudd, G.M., 1999, Mound springs of the Great Artesian Basin in south Australia: a case study from Olympic Dam: Environmental Geology, v. 39, p. 463-476.

Ordonez, S., Gonzalezz, J.A., and Garcia del Cura, M.A., 1986, Petrographie et morphologie des edifices tuffeux quaternaires due centre: Espagne, Mediterranee, v. 1-2, p. 52-60.

Ozkul, M., Varol, B., and Alcicek, M.C., 2002, Depositional environments and petrography of the Denizli travertines: Bulletin of the Mineral Research and Exploration Institute of Turkey, v. 125, p. 13-29.

Pedley, H. M., 1990, Classification and environmental models of cool freshwater tufas: Sedimentary Geology, v. 68, p. 143-154.

Pedley, H.M., 1992, Freshwater (phytoherm) reefs: the role of biofilms and their bearing on marine reef cementation: Sedimentary Geolology, v. 79, p. 255-274.

Pentecost, A., 1985, Association of cyanobacteria with tufa deposits: identity, enumeration and nature of the sheath material revealed by histochemistry: Geomicrobiology Journal, v. 4, p. 285-298.

Pentecost, A., 1991, Springs that turn life to stone: New Scientist, p. 42-44.

Pentecost, A., and Viles, H.A., 1994, A review and reassessment of travertine classification: Geographie physique et Quaternaire, v. 48, p. 305-314.

Pentecost, A., 1995, The microbial ecology of some Italian hot-spring travertines: Microbios, v. 81, p. 45-58.

Pentecost, A., 2010, Travertine, Netherlands, Springer Publishers, 445 p.

Piperov. N., Kamenskiy, I.L., and Tolstikhin, I.N., 1988, Noble gas isotopes in Bulgarian hot springs: Geochemistry International, v. 25, p. 43-51.

Potochnik, A.R., 1989, Depositional style and tectonic implications of the Mogollon Rim Formation (Eocene), East-Central Arizona: New Mexico Geological Survey Guidebook, 40th Field Conference, Southeastern Colorado Plateau, p. 107-118.

Rauzi, S.L., 1999, Carbon dioxide in the St. Johns-Springerville area, Apache County, Arizona: Arizona Geological Survey Open-File Report, v. 99-2, p. 1-22.

Renaut, R.W., Morley, C.K., and Jones, B., 2002, Fossil hot-spring travertine in the Turkana Basin, northern Kenya: structure, facies, and genesis: Renaut, R.W., Ashley, G.M., (Eds), Sedimentation in Continental Rifts, Society for Sedimentary Geology Special Publication, v. 73, p. 123-141.

Riding, R., 2000, Microbial carbonates: the geological record of calcified bacterial-algal mats and biofilms: Sedimentology, v. 47, p. 179-214.

Sant'Anna, L.G., Riccomini, C., Rodrigues-Francisco, B.H., Sial, A.N., Carvalho, M.D., and Moura, C.A.V., 2004, The Paleocene travertine system of the Itaborai basin, southeastern Brazil: Journal of South American Earth Sciences, v. 18, p. 11-25.

Sirrine, G.K., 1958, Geology of the Springerville-Saint John's area, Apache County, Arizona: PhD Thesis, University Of Texas, Austin, 248 p.

Stone, C., 1979, An overview of the geothermal potential of the Springerville area, Arizona: Arizona Geological Survey Open-File Report, v. 79, p. 1-25.

Tucker, M. E., and Wright, V. P., 1990, Carbonate mineralogy and chemistry. Carbonate Sedimentology, p. 284-313.

Veysey, J., Fouke, B.W., Kandianis, M.T., Schickel, T.J., Johnson, R.W., and Goldenfeld, N., 2008, Reconstruction of water temperature, Ph, and flux of ancient hot springs from travertine depositional facies: Journal of Sedimentary Research, v. 78, p. 69-76.